AN ABSTRACT OF THE THESIS OF

YUN-GANG LIU for the degree of DOCTOR OF PHILOSOPHY

in CHEMISTRY presented on May 4, 1989

Title: A CHEMICAL AND PETROGRAPHIC STUDY OF REFRACTORY INCLUSIONS FROM KABA (CV3) CHONDRITE

Abstract approved: Redacted for Privacy

Roman A. Schmitt

Refractory inclusions from Kaba (CV3) chondrite were studied by instrumental neutron activation analysis (INAA) and electron probe microanalysis (EPMA). The inclusions observed cover a wide range of chemical patterns, mineral assemblages and textures, indicating the complexity of early solar nebular conditions. The elemental abundances normalized by C1 chondritic abundances vary smoothly as a function of their volatilities, suggesting these inclusions were formed by condensation/evaporization processes in the primeval solar nebula.

The average REE pattern of Group III inclusions has an enrichment of 31xC1 with approximately equal depletions of Eu and Yb (Eu/Eu^{*}=0.33, Yb/Yb^{*}=0.29). Group III inclusions are irregularly-shaped aggregates of rounded or sub-rounded melilite-rich nodules rimmed with mono-mineralic layers of high-Al phase, Ti-Al pyroxene and hedenbergite.

KI53 is an irregular aggregate. It shows a strongly fractionated REE pattern, but differs from typical the Allende Group II pattern by exhibiting normal Eu and Yb abundances.

KI77 and KI88 inclusions consist of anorthite, diopside and enstatite, with Si-rich phase in fine-grained areas. Their element patterns suggest they were condensed from a gaseous environment rich in moderately volatile elements.

The lower enrichment of Al, Ti and Ca is interpreted by the partial vaporization of the inclusion by a transient event in an oxidizing environment near the nebular midplane. This process caused the partial loss of Al, Ti, Ca and more volatile elements. The rim is the resultant vaporization residue. This model combines the modification of refractory elemental pattern and the rim formation in one event. The partial evaporization of a precursor inclusion with an unfractionated REE pattern would form a rim where Yb and Eu are strongly depleted in different degrees, and the interior is not effected. A Group III pattern would be observed to be the summation of two components, rim and interior.

The similarities between Kaba and Allende in whole-rock composition and their inclusion mineralogies and textures suggest they were formed in a generally similar nebular region. Kaba inclusions are less altered by secondary reactions with a gas phase at lower temperature, therefore informations of early solar nebular conditions are better preserved.

A CHEMICAL AND PETROGRAPHIC STUDY OF REFRACTORY INCLUSIONS FROM KABA (CV3) CHONDRITE

BY
YUN-GANG LIU

A THESIS

submitted to

Oregon State University

in partial fulfillment of
the requirements for the
degree of

Doctor of Philosophy

Completed May 4, 1989

Commencement June, 1990

APPROVED:

Redacted for Privacy

Professor of Chemistry in Charge of Major

Redacted for Privacy

Head of Department of Chemistry

Redacted for Privacy

Dean of Graduate School

Date Thesis Presented May 4, 1989

ACKNOWLEDGEMENTS

I wish to express my gratitude to my major professor, Dr. Roman A. Schmitt, for his guidance and encouragement, and particularly my gratitude to Dr. Chih H. Wang for his constant encouragement and very helpful advice. Dr. Scott S. Hughes is greatly acknowledged for his valuable suggestions, discussions, and assistance which significantly improved the quality of this work. I am also gratful to Dr. John A. Wood of the Harvard-Smithsonian Center for Astrophysics, where I did the petrographic study.

Technical support and assistance for the neutron activations were provided by T. V. Anderson, A. D. Hall, D. S. Pratt, V. H. Golightly, M. R. Conrady and Robert Walker of the Radiation Center, Oregon State University. Dr. Akihiko Hashimoto, Dr. D. A. Kring and B. A. Holmén of Harvard-Smithsonian Center for Astrophysics are acknowledged for their assistance and discussions on the petrographic study.

The Kaba meteorite specimen was made available through the courtesy of Dr. A. Graham of the British Museum of Natural History.

This study was financially supported by the National Aeronautics and Space Administration Grant NAG 9-63 to Dr. R. A. Schmitt.

TABLE OF CONTENTS

LIST OF FIGURES

LIST OF TABLES

LIST OF APPENDIX TABLES

A CHEMICAL AND PETROGRAPHIC STUDY OF REFRACTORY INCLUSIONS FROM KABA (CV3) CHONDRITE

1. INTRODUCTION

1.1 Kaba as a Member of CV3 Chondrites

On April 15, 1857, a stony meteorite, approximately 3 kg, fell in the neighborhood of the village Kaba of Bihar County, Hungary, and has been kept in the College of the Reformed Church at Debreczen, Hungary since its recovery. Small samples were later forwarded to a couple of museums. The largest collection outside of Hungary is in the British Museum (two specimens, 104.5 g total), from where 1.4 g were provided for this study.

Kaba was classified as a CV3 chondrite (Van Schmus, 1969; Van Schmus and Hayes,1974). CV3 chondrites are rich in refractory inclusions. Interest in the inclusions was prompted by the observation of Marvin et al. (1970) on the Allende, a CV3 meteorite, that the mineral assemblage is remarkably similar to that postulated for an early high temperature condensate from a gas of solar composition, so that a record of the early history of solar nebular was preserved. Allende is the only CV chondrite which has been extensively studied. In the study of CV chondrites McSween (1977) found that metamorphism has apparently effected several CV meteorite. Fine-grained olivine inclusions and Ca-Al rich inclusions in Allende may have undergone partial Fe/Mg exchange with the matrix. The fine-grained amoeboid inclusions in Allende are markedly enriched in Fe relative to amoeboid inclusions in other CV members Bali, Grosnaja,

Kaba and Mokoia. The compositions of Allende coarse-grained chondrules have not been altered to any great extent. The contents of primordial noble gasses also may correlate with the metamorphic effect. Among the CV3 chondrites Allende and Coolidge are the most depleted in the rare gas isotopes ^{36}Ar, ^{84}Kr and ^{132}Xe, while the corresponding gas contents are considerably larger in Efremovka and Leoville with Kaba and Mokoia in between (McSween, 1977).

In the study of matrix minerals in CV3 chondrites, Peck (1983 and 1984) found that the olivine in Allende, Grosnaja and Vigarano has a limited range of composition and a distinct composition (Fo_{53}, Fo_{50} and Fo_{48}, respectively) which appear to be approaching equilibrium. Olivine in Kaba and Mokoia is less equilibrated and exhibits broader compositional ranges. Furthermore, the ratios of clinopyroxene to feldspathoids + phyllosilicates systematically increase with the degree of equilibration of matrix olivine in these five chondrites. These results suggest the degree of equilibration decreases in the order of Allende, Grosnaja, Vigarano, Mokoia and Kaba. Also from oxygen isotopic compositional study, Clayton and Mayeda (1984) found that the ^{18}O contents decrease in the order of Mokoia, Grosnaja, Allende and Vigarano.

The above observations suggest that Allende may have experienced more metamorphic effects. Other CV3 chondrites, such as Kaba and Mokoia, may be more primitive in terms of their chemical and mineralogical properties, and therefore potentially more informative about early solar system processes.

Due to the small sample size and the difficulty in their acquisition, only a few studies on Kaba has been reported. The first detailed mineralogical and chemical study of Kaba was reported by the Hungarian scientists Sztrokáy et al. (1961). The whole rock composition was chemically analyzed. The thin-section observations of chondrules and matrix were described. A greyish-white spot of 2-3 mm wide and 12-18 mm long was investigated by microscope and X-ray analyses. This spot contains Mg-Al spinel accompanied by enstatite. Fegley and Post (1985) believed this spot first described by Török in 1858 may be the first report of refractory inclusion in meteorites. Schmitt et al. (1972, 1974) have reported the bulk composition and the composition of chondrules in a wide spectrum of stony meteorites, including Kaba and Mokoia. The studies of matrices by Peck (1983, 1984) have been cited above. Fegley and Post (1985) first reported a detailed petrographic and mineralogical study on a Ca-Al-rich inclusion (CAI) in Kaba. This fine-grained CAI contains abundant small, rounded and spinel-rich objects rimmed with Ti-Al-pyroxene, anorthite, diopside and hedenbergite. The spinel-rich nodules have important morphological and mineralogical similarities to the spinel-cored objects in Allende, Mokoia and other carbonaceous and ordinary chondrites. These nodules are interpreted as fractionated distillation residues of primitive dust. The preservation of distinct diopside-hedenbergite rims on the spinel-rich bodies and the small grain size of CAI matrix suggest that the CAIs accreted in a cool environment and experienced subsequently a relatively cool thermal history in the Kaba parent body.

1.2 Classification of Refractory Inclusions

CV3 chondrites contain chondrules, olivine-rich and Ca-Al-rich inclusions and matrix in which the chondrules, aggregates and their fragments are embedded. Inclusions have been classified in various ways (Clarke et al., 1970; Gray et al., 1973; Blander and Fuchs, 1975). However, the most widely used classifications are those based on chemical composition (Martin and Mason, 1974; Mason and Taylor, 1982), and on texture and mineralogy (Grossman, 1975; Grossman and Steele, 1976; MacPherson and Grossman, 1984). A new classification system was proposed by Kornacki et al. (1983) and Kornacki and Wood (1984) on the basis of the size and abundance of three fundamental constituents: concentric objects, chaotic material and inclusion matrix. It is worthwhile to review these classification systems in order to understand their different nomenclatures in describing the same type of inclusion.

Martin and Mason (1974), and Mason and Taylor (1982) recognized six distinct groups of Allende inclusions by their characteristic REE patterns as well as other refractory elements and mineralogical and textural parameters. Group I CAIs are coarsed-grained chondrules consisting largely of melilite and fassaite with minor amount of spinel and anorthite. They have unfractionated chondrite-normalized REE pattern at 10-15 times C1 abundance with a slightly positive Eu anomaly. Group II inclusions are mostly fine-grained aggregates with melilite, fassaite and spinel, minor nepheline and sodalite, and accessory perovskite and hibonite. Group II inclusions show strongly

fractionated REE pattern: La-Sm abundances 10-50 x chondrite, a negative Eu anomaly, rapid decline of the heavier REE except for a positive Tm anomaly (Tm ~ Sm), and Yb ~ Eu. Group III inclusions are characterized by an unfractionated REE pattern at 10-40 times Cl, except for negative Eu and Yb anomalies of about equal magnitude. Major minerals are melilite, fassaite and spinel with a variety of textures from coarse-grained chondrule-like objects to fine-grained aggregates. Group IV inclusions are Mg-rich chondrules and aggregates, largely of olivine and clinopyroxene, with low and relatively unfractionated REE pattern, 2-4 x chondrite. Group V inclusions show an unfractionated REE pattern. They are practically indistinguishable from Group I inclusions in major-element chemistry, mineralogical composition and texture. Group VI inclusions exhibit flat REE patterns except for positive Eu and Yb anomalies. They have a wide range in chemical and mineralogical compositions and in texture, from melilite-rich chondrules to aggregates. Many unique REE patterns different from the above six groups have been reported, e.g. the inclusion with ultra-refractory component (Boynton et al., 1980) and the inclusion with a negative Ce anomaly (Conard, 1976).

Grossman et al. (Grossman, 1975; Grossman and Steele, 1976; MacPherson and Grossman, 1984) divided Ca-Al-rich inclusions, including both chondrules and aggregates, into coarse- and fine-grained inclusions by texture and mineralogy. The coarse-grained inclusions are further divided into Type A (melilite-rich), Type B (fassaite-rich) and intermediate Type I (anorthite-rich). Type A has two subtypes: "compact" and "fluffy". Compact Type A inclusions are

chondrules. Fluffy Type A inclusions are aggregates of nodules with Wark-Lovering type rim sequence. Of the primary phases for both subtypes, melilite is the most abundant, >75% by volume. Other minerals are spinel (5-20%), hibonite (~5%) and perovskite (1-3%). Type B inclusions contain 30-60% fassaite, 15-30% spinel, 5-25% plagioclase and 5-20% melilite.

In the study of Allende and Mokoia, Kornacki et al. found that inclusions are aggregates containing varying proportions of distinct constituents, termed concentric objects, chaotic materials and inclusion matrix. A classification system was proposed based on the abundances of these three fundamental constituents. Olivine-rich inclusions occur in two textural varieties: unrimmed olivine aggregates (Type 1A) and rimmed olivine aggregates (Type 1B). Ca-Al-rich inclusions are classified, according to the size and abundance of their constituent concentric objects, into unrimmed complex CAIs (Type 2), rimmed complex CAIs (Type 3), and simple CAIs (Type 4). They have their subtypes based on their mineralogy.

A summary of these classification schemes can be found in Kornacki and Wood (1984). The complexity of classification and the complexity of their chemistries, mineralogies and textures of inclusions, suggest these inclusions experienced very complex histories. Though the parallelism between petrographic Types and chemical Groups exist in a general way, these correspondences do not always apply. In this study a combination of chemical and petrographic classifications, similar to the approach of Wark (1985), will be used to specify both Group and Type of an inclusion.

1.3 Condensation from Solar Nebula

The early history of the solar nebula can be inferred by detailed studies of chondrites (Wood, 1988). In the formation of chondritic components in the solar nebula, high temperature vaporization and condensation played a major role. The condensation temperatures of minerals from a cooling nebular gas of solar composition under equilibrium condition can be calculated from thermodynamic data. These calculations have been done for major elements by Grossman (1972), for trace elements by Wai and Wasson (1977), Fegley and Palme (1985) and Kornacki and Fegley (1986). A more comprehensive compilation can be found in Wasson's book (1985). The condensation temperatures apply equally well for vaporization under equilibrium conditions. The actual nebular process might be more complex: equilibrium may not be maintained all the time, multistage vaporization and condensation may be involved, the gas phase may not be of solar composition, etc.. However, the condensation sequence provides a first-order basis for the understanding of the thermal history recorded by chondritic components.

2. EXPERIMENTAL

2.1 Sample Preparation

Two chips of Kaba meteorite, numbered BM 33969a, 1.4 g total, were obtained from Dr. Andrew Graham, British Museum of Natural History. Sixty three inclusions (designated as KI), as well as four chondrules (KC) and two matrix samples (KM) were hand-picked under a binocular microscope with stainless dental tools. KIs and KCs were separated from meteorite matrix as completely as possible. Due to the irregular shape and small size, absolute matrix-free inclusions were hard to obtain. Matrix samples are the milligram-size fragments free of chondrules and large (comparing with overall sample size) inclusions examined under a binocular microscope, but tiny grey inclusions cannot be avoided. Two 100-mg samples of whole rock (KW) also were prepared for analysis.

Also two Mokoia matrix (MM), two whole rock (MW), and three Allende matrix samples were prepared for element analysis and for comparison with Kaba.

2.2 Neutron Activation Analysis

Samples were subjected to instrumental neutron activation analysis (INAA) for major, minor and trace elements at the Radiation Center, Oregon State University. The basic features of neutron activation analysis have been described by Laul (1979). An improved procedure was used by counting activated specimens with both Ge(Li) (100 cm^3 volume with 1.79 keV resolution and 19.3% efficiency for the

1.33 MeV ^{60}Co gamma ray) and 5mm thick planar intrinsic Ge (640 eV resolution for the 122 keV gamma ray) detectors. The optimized activation and counting schedule is summarized in Table 2.1. This procedure includes a short activation for short half-life radionuclides (Irradiation I) and a long activation for intermediate and long half-life radionuclides (Irradiation II), and two and five sequential countings, respectively. The radionuclides were counted at proper decay times and on appropriate detectors according to their half-lives and gamma ray energies. The USGS standard BHVO, Geological Survey of Japan standard JB-1 and the Smithsonian Institution Allende standard were used as standards in the INAA procedure.

INAA data for whole rock and matrix are presented in Appendix Table I and for inclusions in Appendix Table II. The element abundances of KI53, KI77 and the average of Group III and Group IV inclusions are listed in Table 2.2.

2.3 Electron Microprobe Study

Seventeen inclusions with high Ca and Al abundances and high enrichments of refractory elements were further studied with EPMA (electron probe microanalysis) at Dr. John A. Wood's laboratory, Harvard-Smithsonian Center for Astrophysics. Fourteen inclusions with lower enrichments of refractory elements and flat REE pattern (1-5.5 x chondritic) were randomly chosen for the same study. Two of them were later found to be chondrules.

Samples were mounted on glass slides with Crystalbond. The exposed surfaces were polished sequentially with 6, 1 and finally

Table 2.1 Irradiation and counting scheme of instrumental neutron activation analysis

Irradiation	Nuclide	Half-life	E_γ(keV)	Ge(Li)	LEPD	Decay Time	Counting Time (sec)
I. Thermal neutron flux 9×10^{12} n/sec·cm^2 10 min.	^{51}Ti	5.76 min	320.1	X		Count 1 10 min	300
	^{27}Mg	9.46 min	1014.4	X			
	^{52}V	3.75 min	1434.1	X			
	^{28}Al	2.24 min	1779.0	X			
	^{49}Ca	8.72 min	3084.4	X			
	^{165}Dy	2.35 h	94.7		X	Count 2 2 h	1000
	^{56}Mn	2.58 h	846.8	X			
	^{24}Na	15.0 h	1368.5	X			
	^{42}K	12.4 h	1524.6	X			
II. Thermal neutron flux 3×10^{12} n/sec·cm^2 14 h	^{165}Dy	2.35 h	94.7		X	Count 1 2 h	1800
	^{152m}Eu	9.32 h	121.8		X		
	^{56}Mn	2.58 h	846.8	X			
	^{24}Na	15.0 h	1368.5	X			
	^{42}K	12.4 h	1524.6	X			
	^{166}Ho	26.8 h	80.6		X	Count 2 8 h	8000
	^{69m}Zn	13.8 h	438.6	X			
	^{76}As	26.3 h	559.1	X			
	^{72}Ga	14.1 h	834.0	X			
	^{153}Sm	46.7 h	103.2		X	Count 3 40 h	14000
	^{198}Au	2.70 d	411.8	X			
	^{82}Br	35.3 h	776.5	X			
	^{140}La	40.3 h	1596.5	X			
	^{147}Nd	11.1 d	91.1		X	Count 4 7 d	40000
	^{191}Os	15.4 d	129.4		X		
	^{186}Re	3.78 d	137.2		X		
	^{177}Lu	6.7 d	208.4		X		
	^{175}Yb	4.2 d	396.3	X			
	^{170}Tm	129 d	84.3		X	Count 5 30 d	40000-80000
	^{233}Pa(Th)	27.0 d	98.4		X		
	^{181}Hf	42.4 d	133.0		X		
	^{141}Ce	32.5 d	145.4		X		
	^{75}Se	120 d	264.4	X			
	^{192}Ir	73.8 d	316.5	X			
	^{51}Cr	27.7 d	320.4	X			
	^{103}Ru	39.25 d	497.1	X			
	^{58}Co(Ni)	70.9 d	810.8	X			
	^{160}Tb	72.1 d	879.3	X			
	^{46}Sc	83.8 d	889.2	X			
	^{59}Fe	44.5 d	1099.3	X			
	^{60}Co	5.27 y	1173.2	X			

Table 2.2 The element abundances of quasi-Group II KI53 and average of Group III and Group IV inclusions from Kaba and respective data from Allende[a]

	Kaba				Allende		
	Quasi-Group II		Group III	Group IV	Group II	Group III	Group IV Aggregates
	KI53	KI77					
Ti(%)	0.40	0.34	0.33	0.17	0.39	0.80	0.12
Al	8.8	9.6	13.4	2.24	15.6	22.7	3.1
Fe	10.6	0.81	8.9	12.9	5.8	4.1	13.2
Mg	10.2	6.6	8.2	16.6	6.7	7.2	18.8
Ca	7.3	8.8	8.6	1.8	8.7	14.4	2.54
Na	0.72	0.47	0.41	0.38	2.94	1.23	1.13
K(%)	0.076	---	0.041	0.031	0.21	0.047	0.098
Sc(ppm)	14.7	16.9	177	17.5	29.4	111	22.4
V	500	250	960	110	55	180	---
Cr	1220	3100	780	1900	1140	620	1580
Mn	1030	1080	920	1140	490	70	940
La	4.0	2.8	8.3	1.1	6.6	6.1	1.13
Ce	7.9	7.9	18	---	17.3	13.9	3.2
Nd	---	---	16.4	---	13.8	11.0	1.9
Sm	2.00	1.82	4.4	0.47	3.93	3.44	0.66
Eu	0.65	0.68	0.55	0.20	0.32	0.53	0.23
Dy	1.1	1.2	7.8	0.78	1.78	6.5	0.73
Ho	0.15	0.20	1.8	0.22	0.16	1.8	0.15
Tm	0.40	0.19	---	---	0.75	0.75	---
Yb	2.3	2.6	1.4	0.77	0.79	1.55	0.62
Lu	0.10	0.11	0.58	0.095	0.02	0.71	0.09
Hf	0.36	---	3.4	---	<0.28	2.4	0.39
Co	170	19	190	300	34	36	100
Ni	4230	290	6280	7010	280	163	3050
Zn	280	105	210	120	812	1169	443
Ga	3.4	0.58	3.3	4.2	---	---	---
As	1.0	---	1.7	1.7	1.27	---	3.0
Br	---	---	6.1	1.8	17.6	---	1.0
Ru	---	---	15.8	---	0.49	12.9	2.3
Re	---	---	1.10	0.066	0.013	1.09	---
Os	---	---	20.2	1.5	0.202	9.9	1.49
Ir	0.17	---	20.0	1.36	0.141	10.6	1.11
Au(ppm)	0.024	---	0.064	0.104	0.024	0.095	0.193

[a] Allende data are from Wark (1983).

0.25 um diamond paste. The JEOL 733 instrument with a 15 kV and 20 nA beam was used for EPMA and backscattered electron microscopy (BSE) study to establish petrographic characteristics.

The EPMA data are presented in Appendix Table III through VIII. These data are grouped according to the chemical Groups and the petrographic Types of these inclusions.

3. ELEMENTAL ABUNDANCES OF WHOLE-ROCK AND MATRIX

The average element abundances of Kaba and Mokoia whole rocks and matrices and Allende matrix are listed in Table 3.1. The whole rock data for Allende are taken from Jarosewich et al. (1987).

The Cl-normarized elemental abundances of whole-rocks of Kaba and Allende are plotted in Figure 3.1 for lithophile elements, and Figure 3.2 for siderophile and other elements which are not expected to condense as silicates. The whole-rock data for Allende are taken from Jarosewich et al. (1987). Elements are ordered from left to right according to increasing volatilities, i.e., decreasing nebular condensation temperatures (Grossman, 1972; Wai and Wasson, 1977; Fegley and Palme, 1985; Kornacki and Fegley, 1986). Some changes have been made in the order that differ from the calculated sequence. The revised order and the reasoning can be found in Kornacki and Fegley (1986) and Kallemeyn and Wasson (1981). The relative volatilities of Al, Ti and Ca are discussed in Chapter 11. The whole-rock elemental concentrations of Mokoia generally agree with the data of Kallemeyn and Wasson (1981). The whole-rock composition of Kaba is very similar to that of Allende. Relative to Cl, the refractory elements are slightly enriched and volatile elements are depleted. The major elements of the three chondritic matrices are consistent with that reported by McSween and Richardson (1977). In the matrices of all three chondrites the abundances of refractory elements are generally slightly lower than those in whole-rocks, and the abundances for volatile elements are about equal. The Na and K in Allende matrix are lower than observed in Kaba and Mokoia matrices and in Allende whole-

Table 3.1 Element abundances in whole rocks and matrices of Kaba, Mokoia and Allende

	Kaba		Mokoia		Allende	
	Whole Rock	Matrix	Whole Rock	Matrix	Whole Rock[a]	Matrix
Ti(%)	0.090	0.058	0.087	0.079	0.090	0.053
Al	1.43	1.20	1.49	1.38	1.74	1.32
Fe	23.2	25.4	23.3	24.0	23.6	27.1
Mg	13.3	12.8	12.8	9.8	14.8	12.2
Ca	1.52	1.24	1.58	1.44	1.84	1.33
Na	0.35	0.36	0.38	0.35	0.34	0.17
K(%)	0.031	0.034	0.032	0.029	0.033	0.018
Sc(ppm)	8.8	7.6	9.5	8.2	11	8.8
V	75	61	81	75	92	69
Cr	3010	3240	2970	3220	3600	2710
Mn	1360	1540	1340	1440	1470	1560
La	0.44	0.35	0.65	0.38	0.52	0.68
Ce	1.3	---	1.2	1.0	1.33	---
Sm	0.235	0.211	0.256	0.248	0.34	0.260
Eu	0.098	0.094	0.108	0.117	0.11	0.107
Dy	0.46	0.37	0.54	0.35	0.42	0.31
Ho	---	0.072	0.068	0.062	0.10	---
Yb	0.30	0.27	0.33	0.25	0.30	0.39
Lu	0.026	0.030	0.030	0.036	0.052	0.024
Hf	0.18	0.13	0.16	---	0.21	---
Co	630	610	630	630	600	630
Ni	13600	13700	13600	16100	14200	13100
Zn	140	150	170	150	110	180
Ga	6.4	6.8	6.3	7.5	6	6.3
As	2.1	2.0	2.2	2.2	1.9	1.8
Se	11.2	8.0	9.8	13.5	10.5	9.3
Br	1.8	1.8	2.1	1.7	1.5	2.8
Ru	0.77	0.80	0.92	0.70	0.85	0.57
Re	0.045	---	0.063	0.030	0.063	0.061
Os	0.53	0.41	0.51	0.57	0.75	0.78
Ir	0.50	0.39	0.57	0.60	0.74	0.54
Au(ppm)	0.175	0.135	0.150	0.153	0.15	0.175

[a] Data taken from Jarosewich et al. (1987).

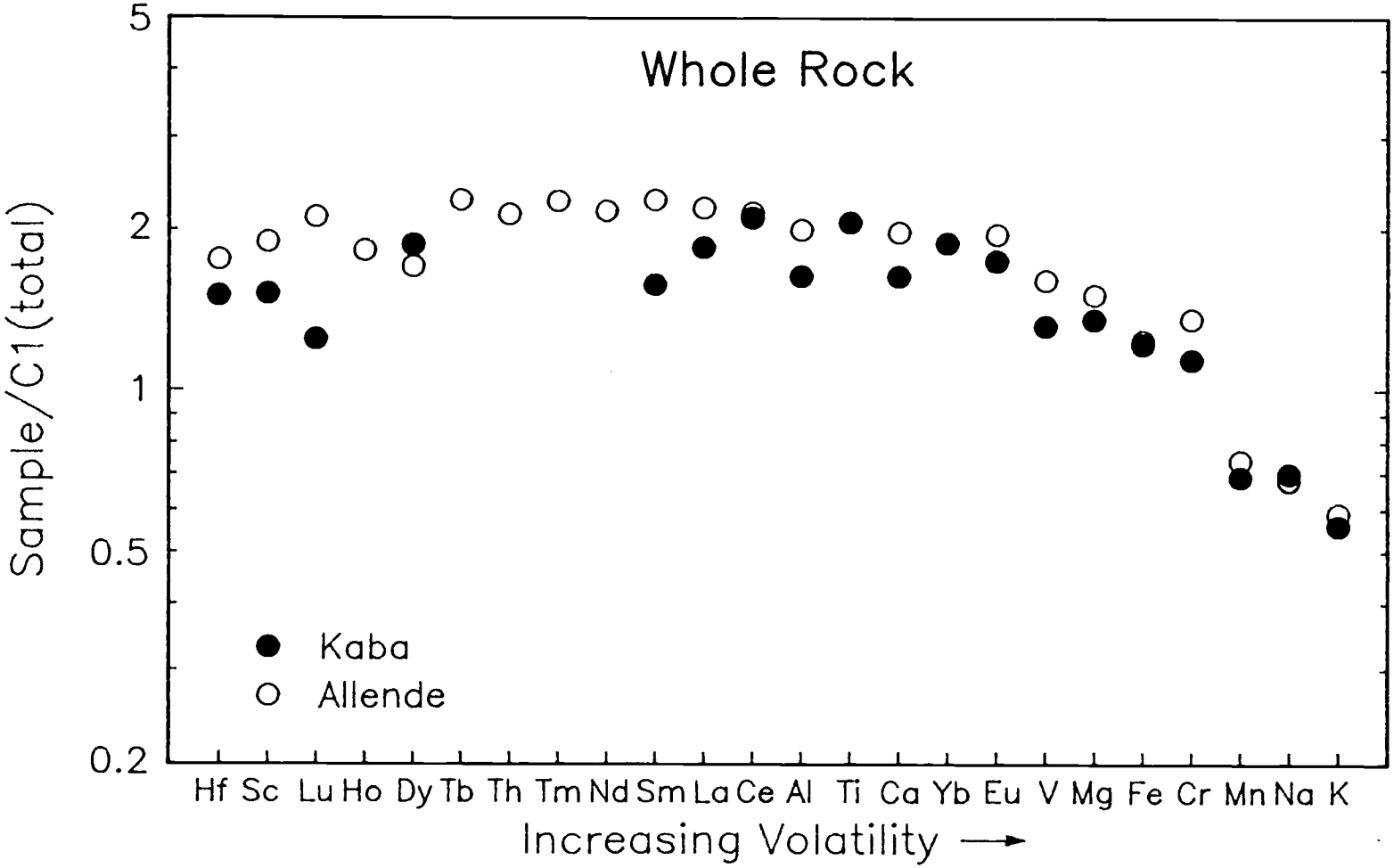

Fifure 3.1 The C1-normalized abundances of lithophile elements in whole rocks of Kaba and Allende. Allende data are taken from Jarosewich et al. (1987).

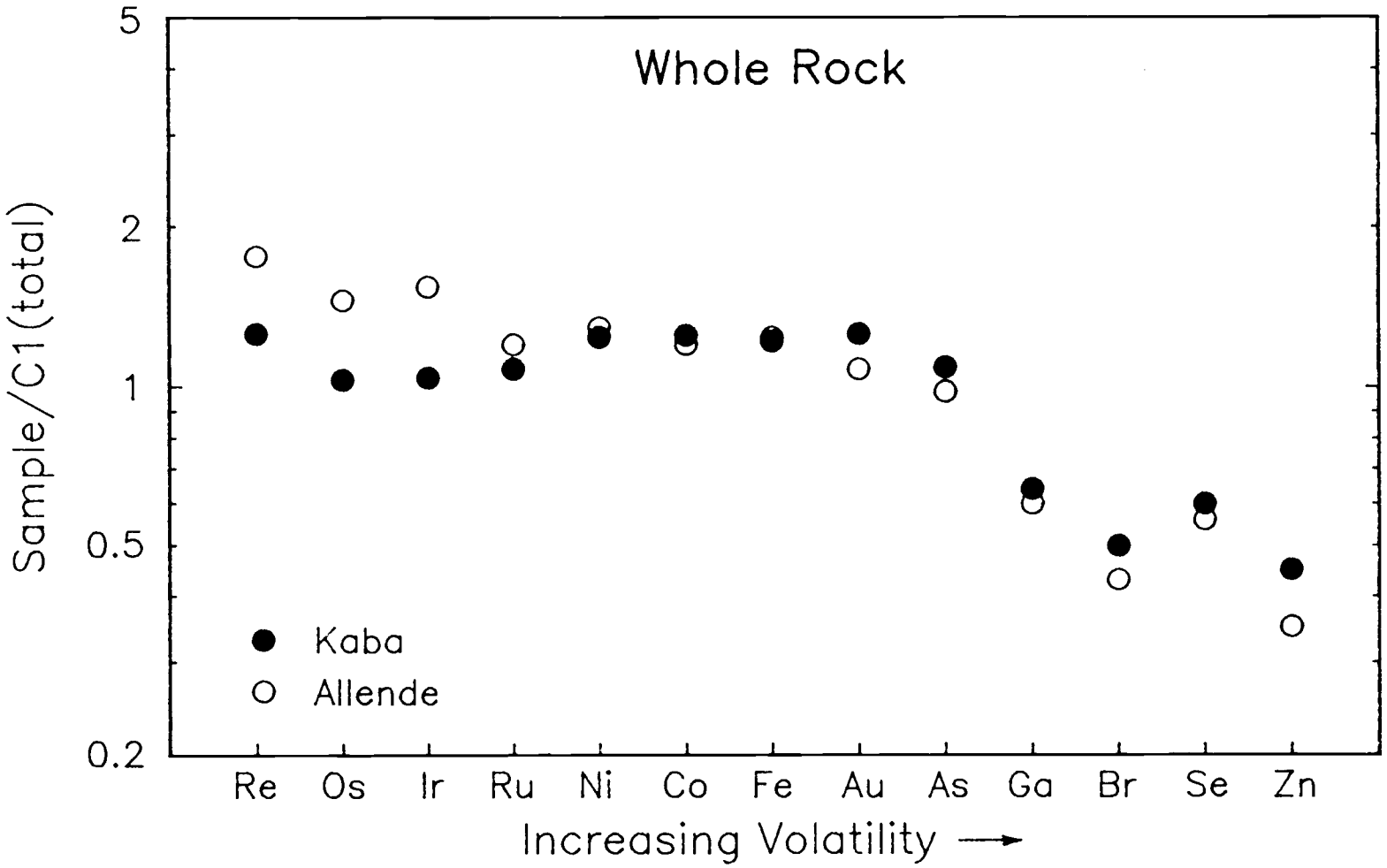

Figure 3.2 The Cl-normalized abundances of siderophile and other non-lithophile elements in whole rocks of Kaba and Allende. Allende data are taken from Jarosewich et al. (1987).

rock, but agree with McSween and Richardson (1977). This may possibly be due to the inhomogeneity of these two elements in the matrix.

4. GROUP III INCLUSIONS

4.1 Elemental Chemistry

Seven inclusions (KI60, KI62, KI73, KI74, KI75, KI86 and KI92) have unfractionated REE pattern (14-44 x Cl) with negative Eu and Yb anomalies. The ranges of Eu/Eu^* and Yb/Yb^* are 0.28-0.36 and 0.21-0.33, respectively. The average elemental abundances of these seven samples are plotted in Figures 4.1, 4.2 and 4.3 for the REE, lithophile and siderophile element patterns, respectively.

Group III inclusions in Allende have been reported by Mason and Martin (1977), Mason and Taylor (1982), Inclusion O by Tanaka and Masuda (1973), B-30 by Gray et al. (1973) and Conard (1976), 7R-44A by Nagasawa et al. (1977), and CG2 and FG13 by Grossman and Ganapathy (1975,1976). These data have been compiled by Wark (1984) and Kornacki and Fegley (1986).

Kaba and Allende have several features in common. First, the refractory lithophile and siderophile elements are equally enriched relative to Cl chondrites, 31 x Cl for Kaba and 27 x Cl for Allende. Second, enrichment factors decrease with volatility from Yb and Eu for lithophiles and Ni for siderophiles. The corresponding cut-off temperatures are between 1532 and 1398°K (Ce-Eu) (Kornacki and Fegley, 1986) for the lithophile elements and 1642 to 1446°K (Ru-Ni) (Fegley and Palme, 1985) for siderophile elements. This range could be narrowed if more elements had been determined. Third, the volatile elements are depleted relative to Cl from Mg for lithophiles and from Ni for siderophiles, at the level of 0.6 x Cl for Kaba and

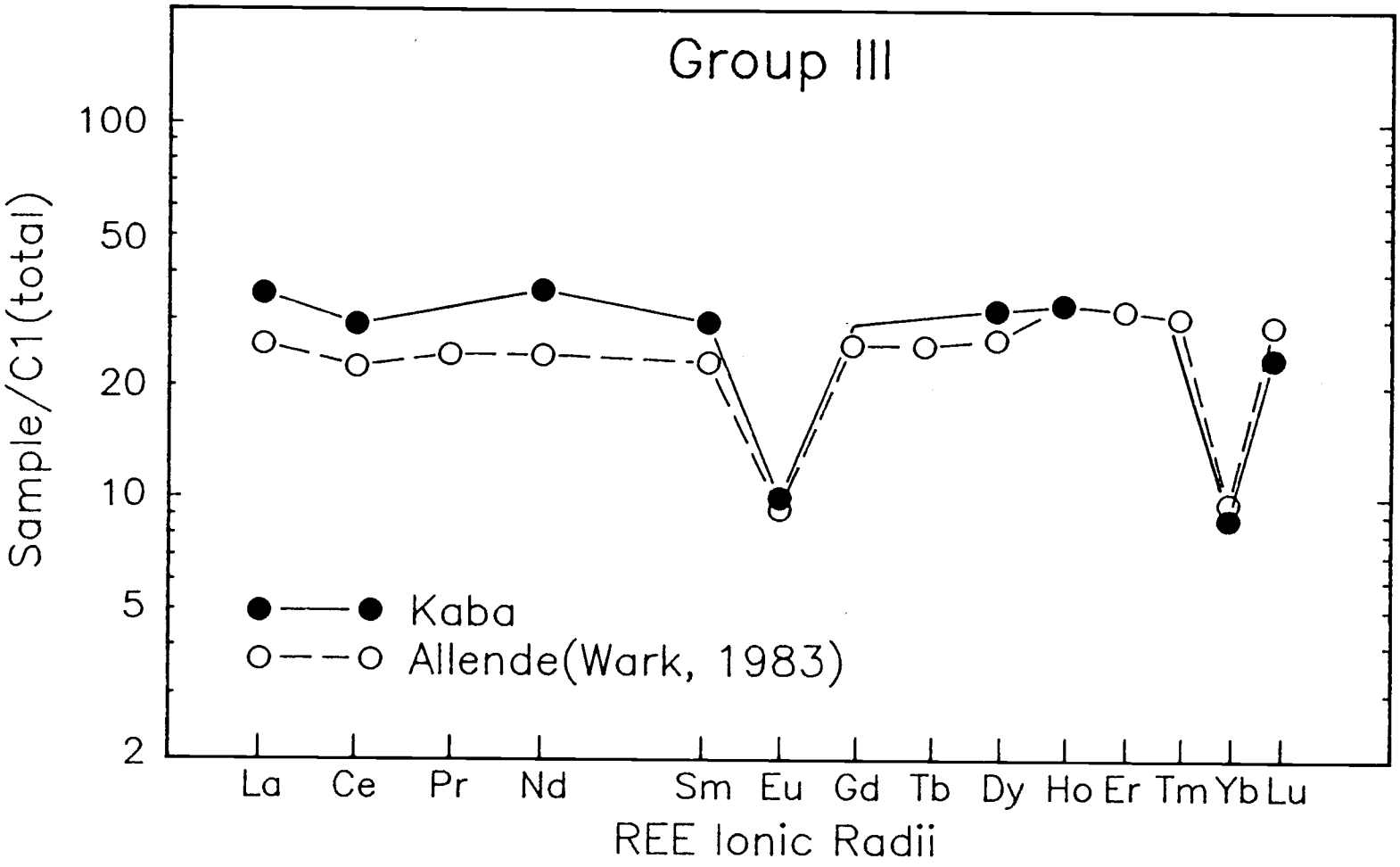

Figure 4.1 The average Group III patterns of Kaba and Allende. Allende data are taken from Wark (1983).

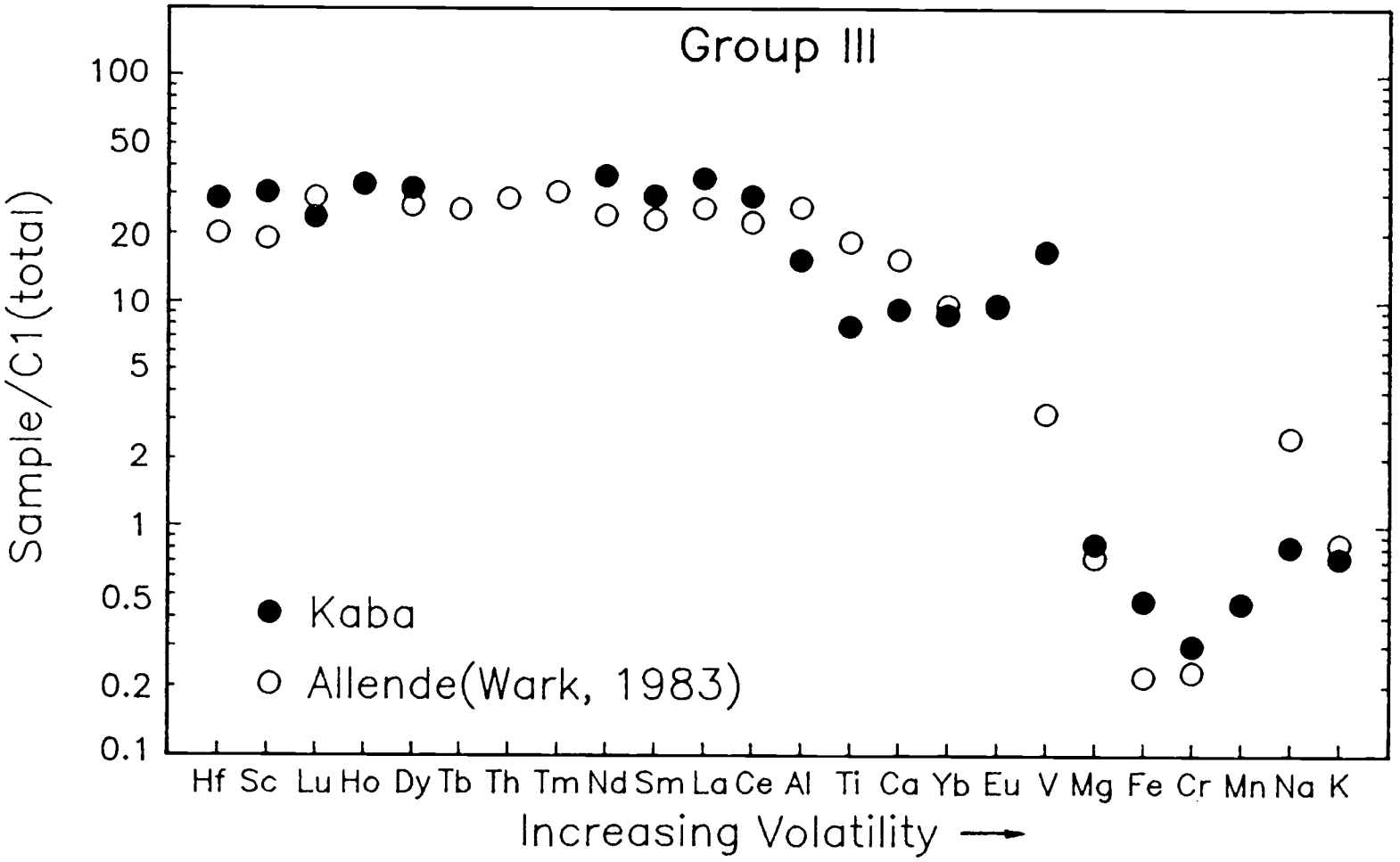

Figure 4.2 The C1-normalized average abundances of lithophile elements in Group III inclusions. Allende data are taken from Wark (1983).

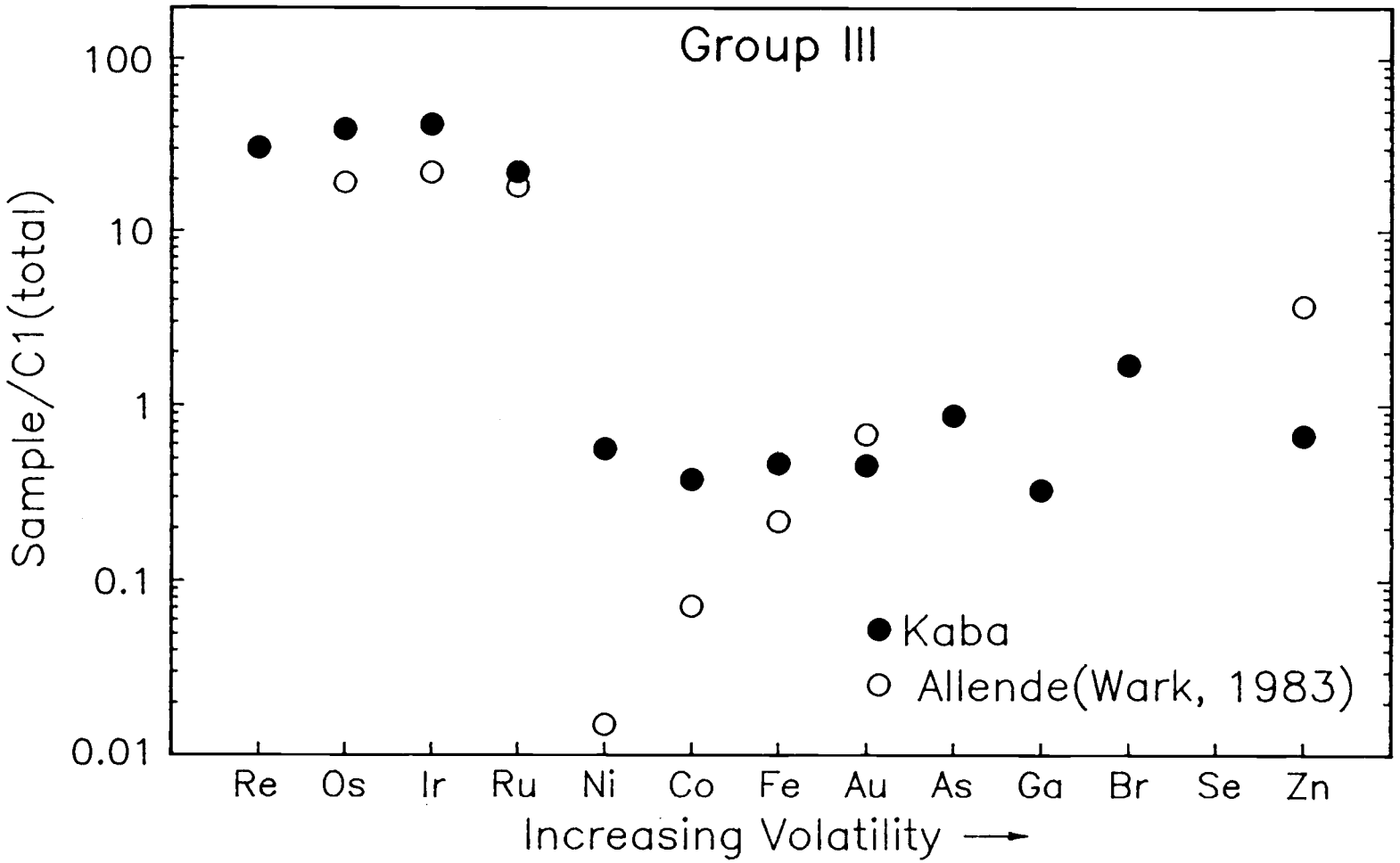

Figure 4.3 The C1-normalized average abundances of siderophile and other non-lithophile elements in Group III inclusions. Allende data are taken from Wark (1983).

more scattered for Allende, possibly due to the fewer measurements for some elements. Mg, Cr, Ni, Co, Fe, Au and As are also depleted relative to their whole-rock abundances. Fourth, Eu and Yb are depleted by nearly equal fractions relative to other REE. Eu/Eu^* and Yb/Yb^* are 0.33 and 0.29 for Kaba and 0.42 and 0.39 for Allende, respectively. The Al, Ca and Ti are more depleted in Kaba than are other refractory trace elements. Na is lower in Kaba Group III inclusions than in Allende fine-grained Group III inclusions. These observations need to be explored further.

The uniform enrichment of refractory elements implies that they were totally condensed from gas phase, where their relative abundances were the same as solar composition (Grossman and Ganapathy, 1976). The relatively lower enrichment of Al, Ca and Ti in Kaba Group III inclusions could be due to the incomplete condensation of the elements when these inclusions formed. This will be further discussed in Chapter 11. The major elements Fe and Mg are also depleted in Group III inclusions, indicating that the major Fe, Mg-containing minerals were formed later at a lower temperature.

The REE patterns have been discussed by several workers. Thermodynamic calculations by Boynton (1975) and Davis and Grossman (1979) were done mainly for the Group II inclusions, and they are also applicable to Group III pattern. At first sight, the Group III REE patterns may be interpreted by the total condensation of most REE while Eu and Yb are volatile enough to have only been partially condensed. However, detailed examination of the REE volatilities reveals that Yb is only slightly more volatile than the LREE, and Eu

is much more volatile than Yb under solar nebular oxygen fugacity conditions. But the above simple model of Group III pattern formation suggests equal volatilities for Yb and Eu because they are equally depleted. Several alternative suggestions have been proposed. Boynton (1975) showed that the early nebular condensates have a preference for the light REE relative to the heavy REE. This preference will tend to exhibit an enhanced volatility of Yb relative to La. Davis and Grossman (1979) suggested that the condensation took place in a highly reduced region of the nebula so that the Yb volatility increased. Boynton (1983) argued that one would expect that the reducing environment has a similar effect on Sm. But the Sm depletion is not observed, suggesting that only slightly more reducing conditions can be tolerated. It is very unlikely that Yb would have a volatility almost equal to that of Eu. Therefore Boynton further suggested that Eu and Yb are sufficiently more volatile than the other REE so that they will not have condensed significantly when the remaining REE have totally condensed. At this time, if the condensed grains are partially separated from the gas (e.g. by settling to the median plane of the nebula) and condensation continues, Eu and Yb at this second stage can condense totally and maintain their solar proportions. As an alternative mechanism, Davis and Grossman (1979) suggested that Eu and Yb were added with later volatile rich components. Similarly, Liu and Schmitt (1988) proposed a two-component model, one a pure Group III end member in which Eu and Yb are variably yet highly depleted, the other with an unfractionated flat REE pattern.

Boynton and Wark (1984, 1985, 1987) have analyzed the REE and other elements in the rim and interior for several CAI grains. The absolute REE abundances are higher in the rims than in the interiors. The two most volatile REE, Eu and Yb, are depleted in the rim patterns relative to the interior patterns. They suggested that the CAI rims formed by a rapid heating process acting on a precursor CAI, leaving the rim as a refractory residue. The heating event which produced this evaporation must have been very intense and of short duration. Further discussion of Group III pattern formation is found in Chapter 11.

KI31 also has a Group III pattern except that Sc is less enriched than REE. KI31 was destroyed during the preparation of a slide for electron microprobe study, and therefore no EPMA and BSE information are avaible for understanding the Sc depletion.

4.2 Textural Features

All these inclusions share important textural and structural features : they are irregularly-shaped aggregates consisting of rounded or sub-rounded nodules except that KI60 is a single rounded object. These nodules are rich in gehlenitic melilite and spinel, and the nodules in most inclusions are rimmed. Within this group, however, there are three variants differing in structure and texture.

One variant is KI60, which is a single rounded body with a diameter of approximate 0.3 mm (Fig. 4.4a). The interior of the body consists of the intergrown melilite and spinel. Cavities and cracks can be seen. One cavity is filled with plagioclase. The rounded

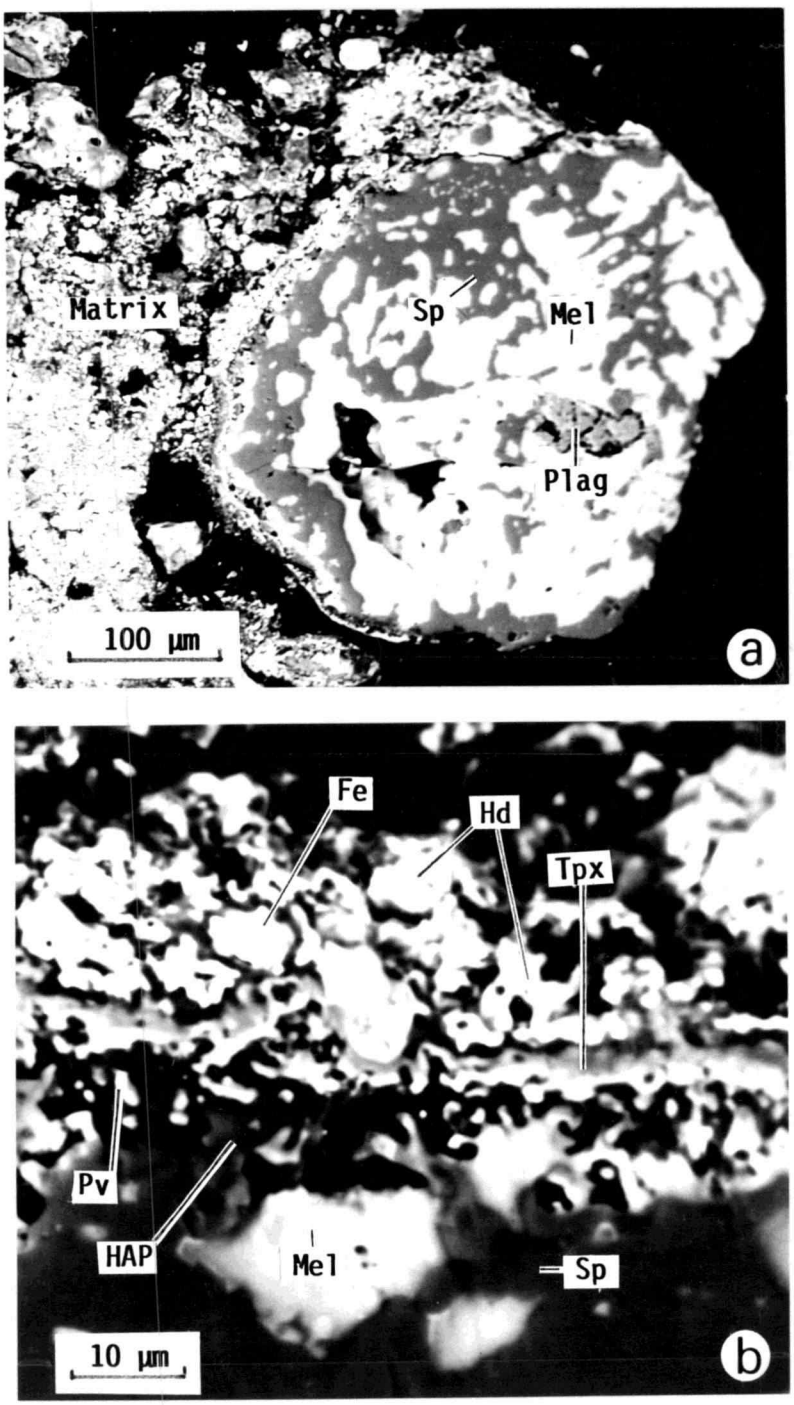

Figure 4.4 BSE images of KI60 (a) and its rim (b). Abbreviations: Mel — melilite, Sp — spinel, Plag — plagioclase, HAP — high-Al phase, Pv — perovskite, Tpx — Ti-Al-pyroxene, Hd — hedenbergite, Fe — Fe-rich phase.

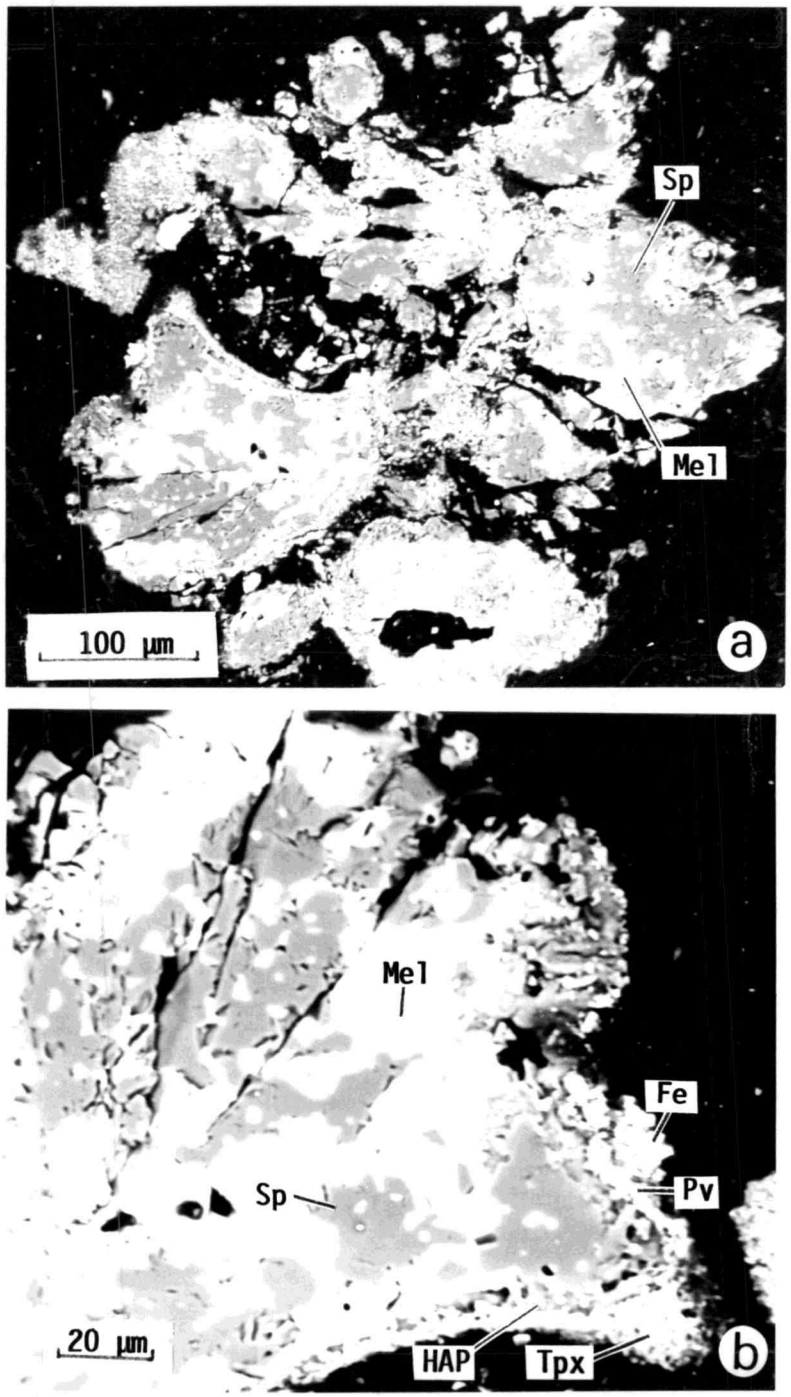

Figure 4.5 BSE images of KI62 (a) and a representative nodule (b). Abbreviations: Mel — melilite, Sp — spinel, Tpx — Ti-Al-pyroxene, HAP — high-Al phase, Pv — perovskite, Fe — Fe-rich phase.

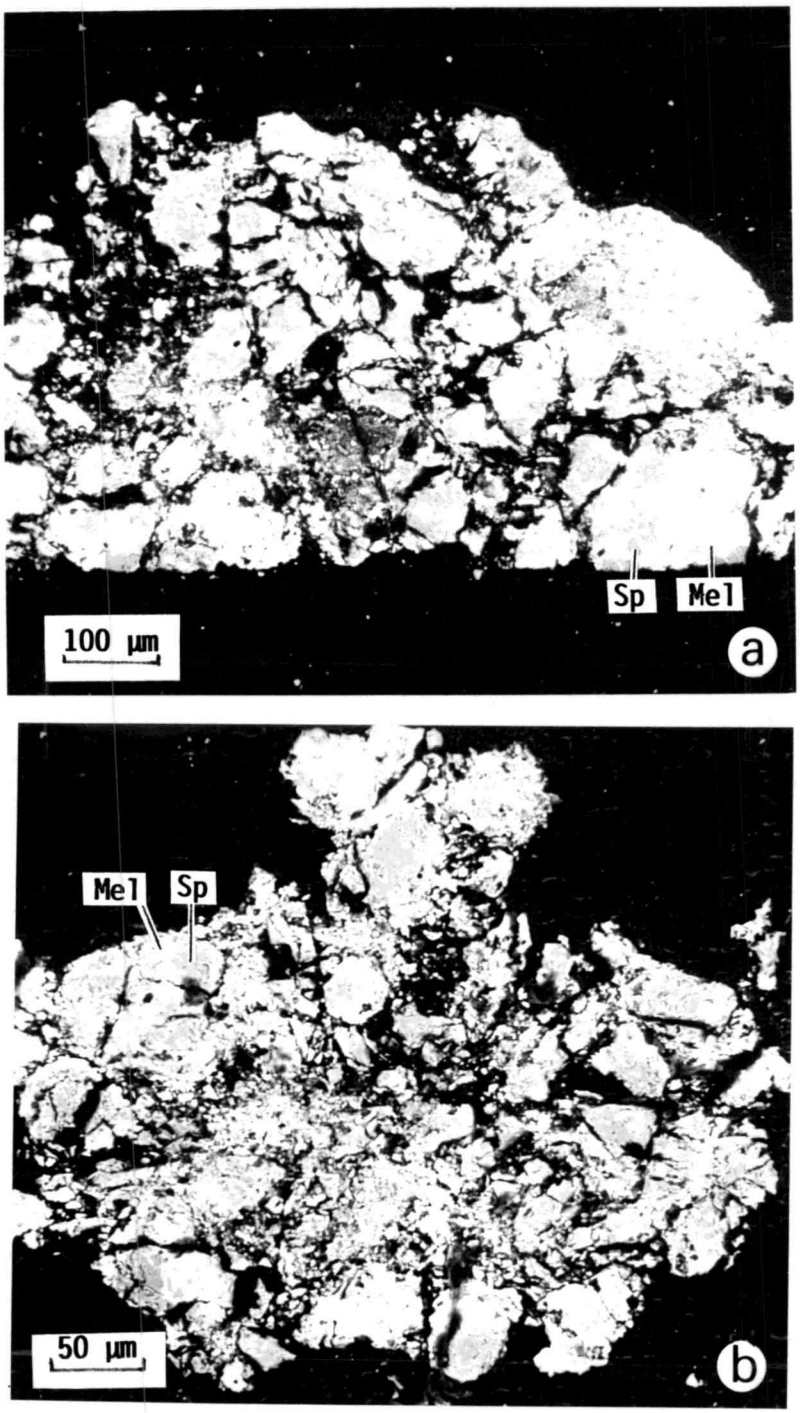

Figure 4.6 BSE images of KI73 (a) and KI75 (b).
Abbreviations: Mel — melilite, Sp — spinel.

melilite-spinel body is rimmed by a sequence of thin, mineralogically distinct layers. The rim is not complete; part of it was possibly lost during the extraction of the inclusion. The rim layers are better seen in the higher magnification BSE photograph in Fig. 4.4b. The rim sequence of mineral layers, from melilite-spinel core outward, consists of high-Al phase (HAP), Ti-Al pyroxene and hedenbergite of various thicknesses with some small perovskite blebs (1-2 um) scatterd along the boundary of melilite-spinel core and rim. A few Fe-Ni grains are attached to the hedenbergite layer. The thickness of the entire rim sequence is 10-20 um. Following the classification used by Kornacki and Wood (1985) and Fegley and Post (1985), we refer to Al-bearing clinopyroxene which contains <1 wt.% TiO_2 as Al-diopside, and that which contains >1 wt.% TiO_2 as Ti-Al-pyroxene (Tpx).

The inclusions of the second variant are irregularly shaped aggregates consisting of rounded or sub-rounded nodules of variable size. These nodules are individually rimmed by a sequence of mineral layers similar to that described for KI60. Inclusions KI62, KI74, KI86 and KI92 are of this variant. The BSE image of KI62 is shown in Fig.4.5a. The overall size of this aggregate is 0.4 mm. The sizes of individual nodules range from 50 to 200 um. Nodules consist of an intergrowth of melilite and spinel of variable proportion. These nodules are surrounded, completely or incompletely, by their own rims. There are cavities of variable size and shape and fractures on these nodules. Between the nodules are void space and fragments of nodules. A BSE picture of one of the nodules with higher

magnification is shown in Fig.4.5b. Cavities and fractures can be seen. There is no sign of alteration within cavities and fractures. The nodules are rimmed by the layers of HAP, Tpx and diopside. Attached to the Tpx and diopside are grains of hedenbergite. The thickness of the entire rim sequence varies between 10-30 um. Perovskite grains (1-2 um) are scattered in the HAP and Tpx layers. A few Fe grains are attached to the Tpx or hedenbergite layers.

The third variant is characterized by either the absence of rims on nodules or underdeveloped rims. KI73 and KI75 are of this catagory (Figs.4.6a and b). Their overall dimensions are 0.5 mm. Some nodules are rounded or sub-rounded in the size of 50-100 um. Most grains are fragments of irregular shape and in variable size. Rims can be seen in some grains but they incomplete and very thin.

The representative EPMA data of minerals in Kaba Group III inclusions are listed in Table 4.1.

4.3 Mineral Chemistry

Melilite

Melilite for all Group III inclusions shows a limited compositional range, Ak2.5-14.3%. The average for each inclusion ranges from Ak5.8% for KI62 to 10.7% for KI73. The overall average for all Group III inclusions is Ak7.9%. Thirty nine melilite analyses were made for KI60. The histogram of Ak mole percent is shown in Fig.4.7. The Ak% ranges from 2.5% to 14%, with an average of 7.2%. The minor element contents of melilite from all Group III inclusions are low.

Table 4.1 Representative EPMA data of minerals in Kaba Group III inclusions (wt. %)

	Melilite	Spinel		Anorthite	High-Al Phase	Ti-Al-pyroxene	Hedenbergite
		Interior	Edge				
SiO_2	23.53	0.10	0.11	41.20	22.82	35.84	47.11
MgO	1.14	28.20	26.29	3.01	15.86	12.60	0.66
Al_2O_3	34.01	71.22	69.04	37.32	44.00	18.26	0.23
CaO	41.36	0.18	0.08	16.45	4.77	25.64	22.93
FeO	0.00	0.01	1.16	0.90	5.56	0.32	27.73
TiO_2	0.01	0.29	0.29	0.02	2.18	5.48	0.10
Na_2O	0.00	0.03	0.00	1.03	1.18	0.02	0.06
K_2O	0.02	0.00	0.00	0.04	0.29	0.01	0.00
V_2O_3	0.03	0.60	0.60	0.06	0.35	0.30	0.06
Cr_2O_3	0.08	0.11	0.07	0.01	0.03	0.38	0.07
MnO	0.12	0.01	0.02	0.00	0.10	0.02	0.31
NiO	0.00	0.00	0.00	0.04	0.02	0.12	0.04
ZnO	0.06	0.14	0.00	0.13	0.00	0.00	0.08
Total	100.36	100.89	97.64	100.21	97.16	98.99	99.37

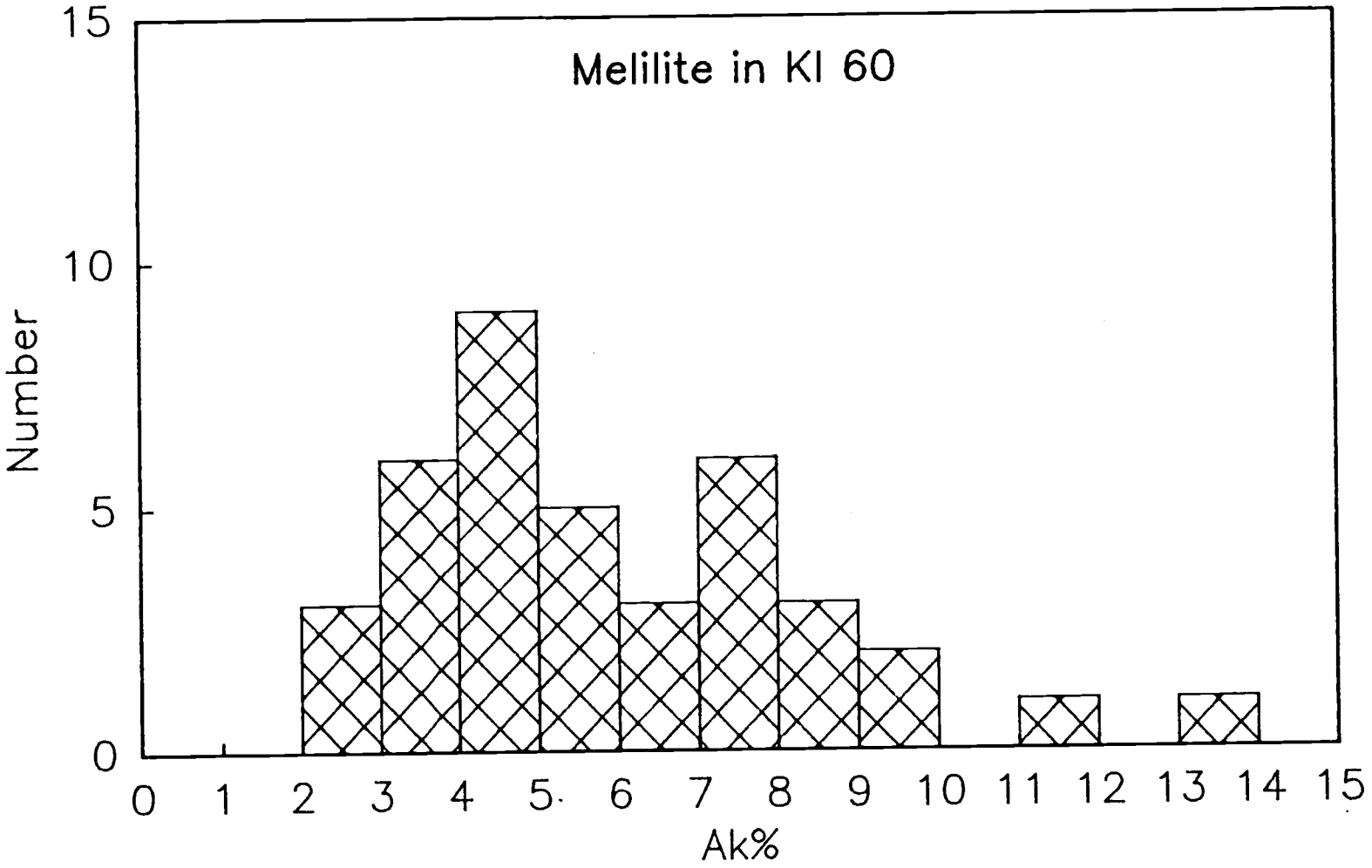

Figure 4.7 The histogram of Ak% in melilite of KI60.

The melilite compositions of Allende coarse-grained Type A inclusions range from Ak6 to Ak58 and peak at 15-20 (Grossman, 1975). Melilite from "fluffy" Type A CAIs (FTA) has a composition range of Ak 0-33 (MacPherson and Grossman, 1984). The melilite in Kaba Group III inclusions tend to be lower in Ak than in Allende Type A and FTA inclusions, and also lower than that reported in Mokoia Type B inclusions (Cohen et al., 1983). The melilite in spinel-rich inclusions studied by Fegley and Post (1985) has a composition of Ak 10-30 with a mean Ak 18, which is also higher than that in Kaba Group III inclusions.

Spinel

The representative analyses of spinel are listed in Table 4.3.2. The major component in all spinel is $MgAl_2O_4$. The spinel at the outermost edge of the melilite-spinel core may contain higher iron, e.g. 1% FeO as illustrated by the last three analyses in Table 4.3.2. In Allende FTAs, Fe-rich spinel (several percent FeO or more) occurs in the Wark-Lovering rim sequence and within or near zones of intense alteration in inclusion interiors, and suggests that Fe was introduced into the spinel during alteration (MacPherson and Grossman, 1984). In Kaba inclusions higher Fe contents are found in spinel only at the outermost edge of the core at several points. The Fe contents (~1-3% FeO) are much lower than in Allende FTAs, suggesting a lower degree of alteration. The spinels in Kaba spinel-rich inclusions also show low Fe content, ~0.04-0.93% FeO with a mean value of 0.26% (Fegley and Post, 1985). Vanadium contents in all

inclusions are at the level of ~0.55% V_2O_3. This value is lower than 1.5% in spinel from Allende FTAs (MacPherson and Grossman, 1984). Spinel in Allende coarse-grained inclusions usually contain less V (0.5%). In Kaba V contents remain at the same level in spinels in the interior and at the edge, and there is no correlation observed between V and Fe. El Goresy et al. (1980) reported the positive correlation between V and Fe in spinel from Allende inclusions. Allen et al. (1978) found in the Allende CG-11 inclusion that spinels in the interior are Fe-poor (0-0.17% FeO), whereas those in the rim are Fe-rich (6.3-6.8% FeO). In addition, they stated that spinels in the interior are generally richer in V (0.25-1.20% V_2O_3) than those in the rim (0.37-0.43% V_2O_3). But the overlap of their V data do not support their statment. There is no correlation of Fe with V in spinels from Allende FTA inclusions (MacPherson and Grossman, 1984).

Minerals in Rim Sequence

1. High-Al phase: The innermost rim surrounding the melilite-spinel core is a layer of high-Al phase (HAP) and voids. This layer is dark on BSE image. They are Al-Mg-rich silicates with varying amount of Ca and Fe. They also contain a considerable amount of alkali elements, e.g. Na may be up to ~2.5%. High-Al phase materials are common in the rims of CAIs. The composition of similar materials have been reported by Wark and Lovering (1977) as an unknown phase in the rim of Allende coarse-grained CAIs; by Cohen et al. (1983) as a high-aluminum phyllosilicate (HAP); and by Fegley and Post (1985) as a high-aluminum phase (also HAP) in a spinel-rich CAI from Kaba. In

this work this unidentified mineral phase is referred as a high-Al phase (HAP). The compositions of the HAP in Kaba Group III inclusions show in general higher Al content while the HAP from KI94 has a quite similar composition as reported for Allende, Mokoia and Kaba. The component mineral(s) of these materials have not been unambiguously identified because the grains are too small to be removed for X-ray diffraction study. Cohen et al. (1983) suggested on the basis of crystal chemistry and X-ray diffraction studies that the high-aluminous phyllosilicate may be either an Al-serpentine or a mixed-layer phyllosilicate or a very fine-grained mixture of more than one mineral, and that the structural formula of low-aluminous phyllosilicate (LAP) is almost identical to the idealized formula of trioctahedral montmorillonite. Based on the compositions and the interlayer spacing, Tomeoka and Buseck (1986) claimed that they identified HAP as a high-Al saponite and LAP as saponite in Mokoia inclusions. In the study of the alteration of Al-rich inclusions in Allende amoeboid olivine aggregates, Hashimoto and Grossman (1987) suggested that this material is a mixture of Na-rich phlogopite and chlorite or Al-rich serpentine.

2. Ti-Al-pyroxene, diopside and hedenbergite: In Allende CAI rims the Ti-Al-pyroxene grades into Al-diopside outward (Wark and Lovering, 1977). In Kaba inclusions, the Ti-Al-pyroxene contains various amount of Al and Ti. Due to the small thickness of the Tpx layer, it was impossible to observe the compositional grading. Hedenbergite forms a distinct layer.

5. QUASI-GROUP II INCLUSION KI53

5.1 Elemental Chemistry

KI53 has a strongly fractionated REE pattern (Fig. 5.1). The constant LREE abundances (13 x C1) and the rapid decline of HREE with the positive Tm anomaly (or normal Tm relative to the LREE) shows that the REE pattern of KI53 is similar to a typical Allende Group II pattern. But it differs in that the KI53 REE pattern shows no Eu and Yb negative anomalies. A plot of lithophile elements (Fig. 5.2) also shows that the most-refractory elements are depleted. The ultrarefractory siderophile element Ir is also severely depleted (0.35xC1). A large number of Allende Group II inclusions have been reported. Their element abundances have been summarized by Wark (1983) and Kornacki and Fegley (1986).In addition to higher Eu and Yb abundances, V is also much higher than observed in Allende Group II inclusions, and is only slightly depleted than are the moderately refractory elements such as La and Sm. A comparison with the average Allende Group II pattern suggests that KI53 formed at a lower temperature relative to the Allende Group II inclusions based on the relatively less depletions of Eu, Yb and V. Na and K are believed to be introduced in the low temperature alteration after the primary formation of the inclusion. The Na and K contents are considerably lower than observed in Allende , indicating a lesser degree of secondary alteration. It is of some interest that Eu and Yb abundances are nearly equal in Group II patterns.

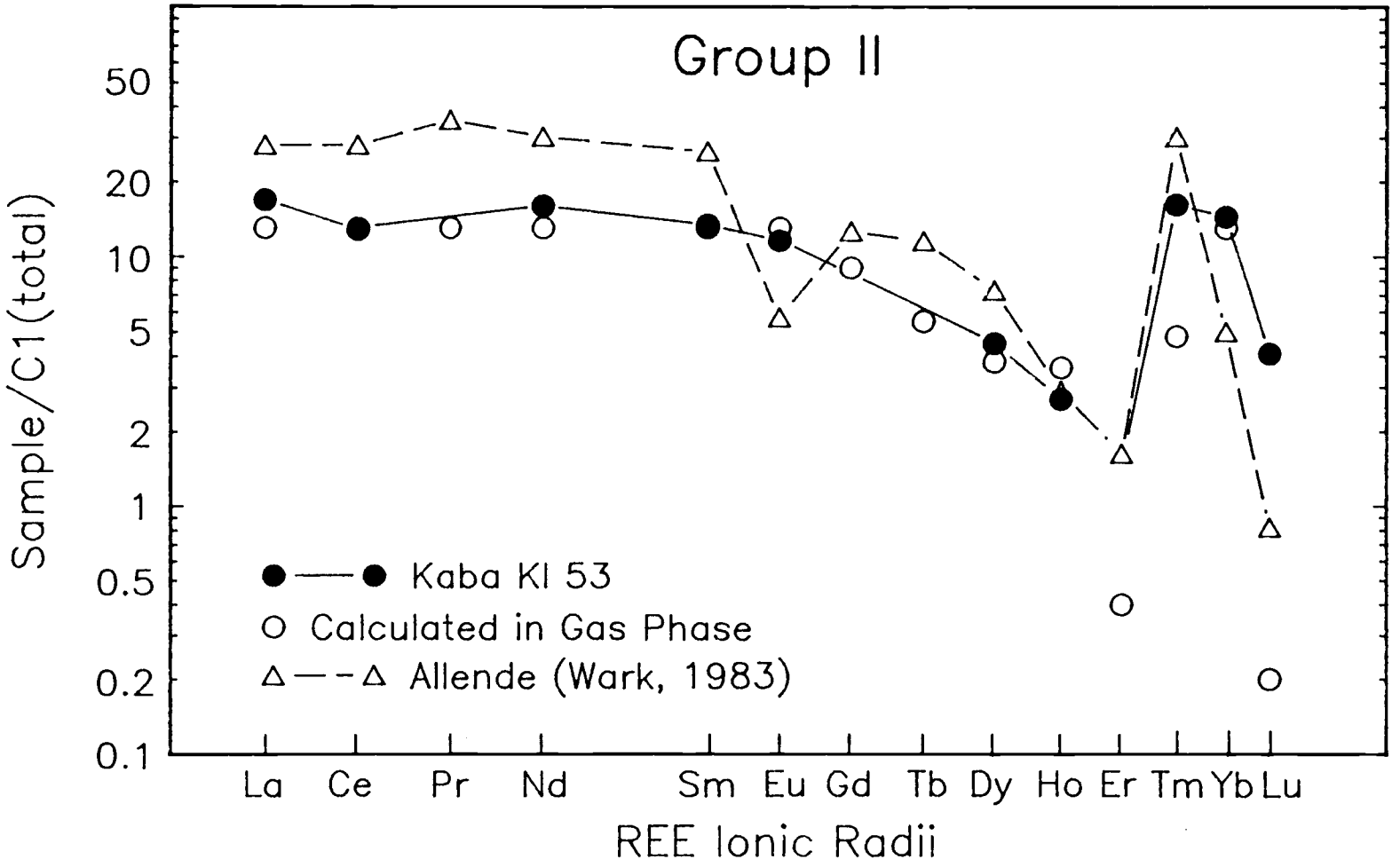

Figure 5.1 The Cl-normalized REE patterns of Kaba KI53, Allende Group II (Wark, 1983) and the calculated REE abundances (normalized to La=13xCl) remaining in the gaseous phase after 0.007% of total has been condensed.

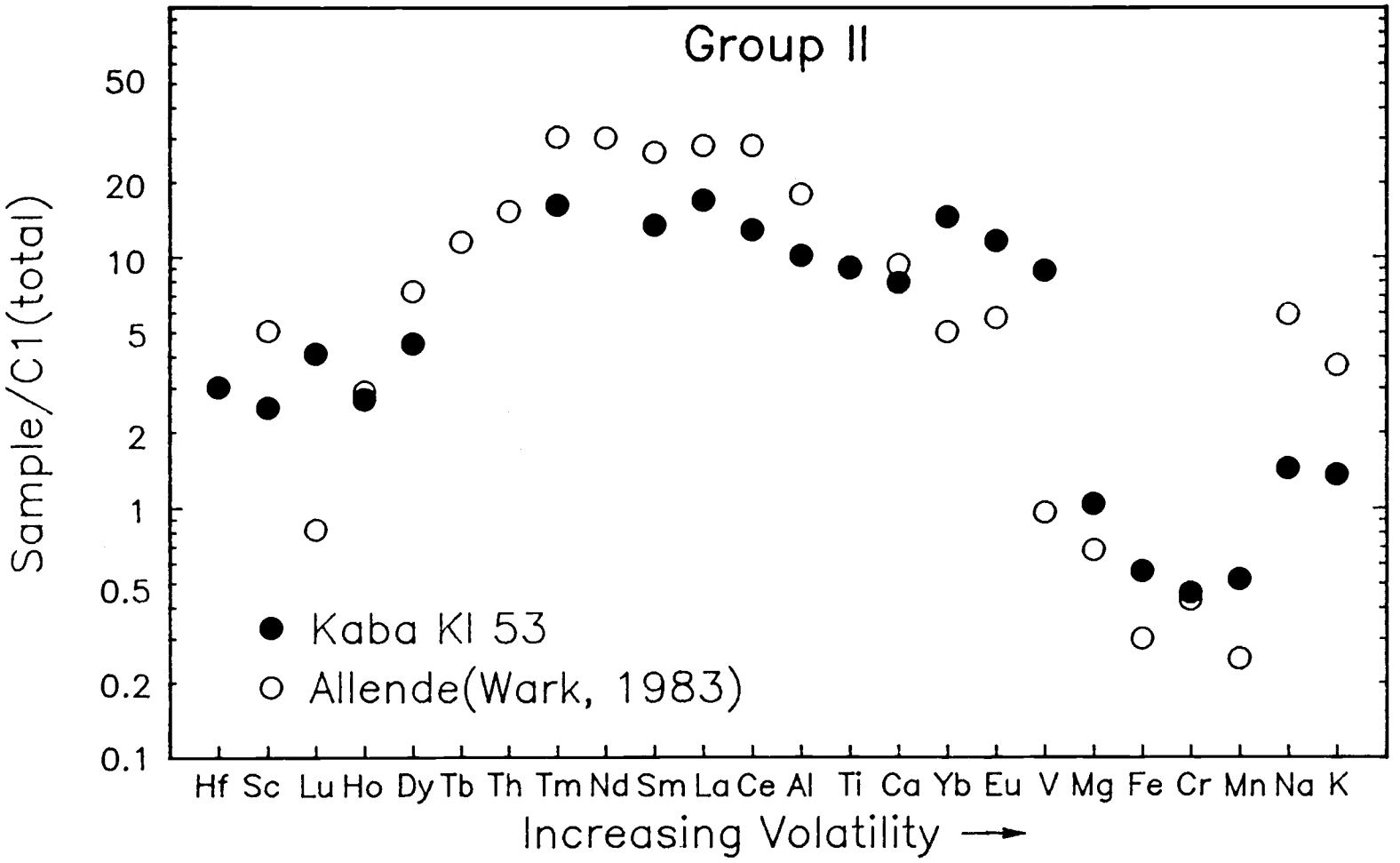

Figure 5.2 The C1-normalized abundances of lithophile elements in Kaba KI53 and Allende Group II inclusions (Wark, 1983).

A similar REE and lithophile patterns of A2 have been reported by Conard (1976). Her A2 inclusion shows no Eu and Yb anomalies and higher abundances of moderately volatile elements Sr and V. A2 is a Ca-Al-rich chondrule with melilite, fassite, anorthite and spinel (Gray et al., 1973). The Allende FUN inclusion EK1-4-1 (Nagasawa et al., 1982) also shows a REE pattern which is strongly fractionated and is similar to the Group II pattern but Eu and Yb are not depleted. In this respect, it is similar to KI53. But Ir and Sc are not depleted in EK1-4-1 which is different from KI53.

The REE patterns like these correspond to the relative REE abundances in the gaseous phase during gas-solid fractionation in the solar nebular environment (Boynton, 1975). Following Boynton's procedure, the calculated relative abundances (normalized to La 13 x C1) remaining in the gaseous phase after 0.007% of total La has been condensed is plotted in Fig. 5.1. The formation of a homogeneous solid with REE activity coefficient ratios of unity is assumed in the calculation. The calculated relative abundances match the observed pattern very well except that the calculated Er and Lu are more depleted. The good match is strong evidence for formation of KI53 in a solar nebular volume where the ultra-refractory elements had been partially condensed and removed (probably to the nebular midplane), similar to the Allende Group II formation. The KI53 inclusion was formed in this remaining gaseous phase by the condensation of essentially all the refractory elements, including Eu, Yb and V. The typical Allende Group II inclusions must have formed at a higher

temperature leaving a significant fraction of moderately volitile elements such Eu, Yb and V, in the gas phase.

5.2 Petrographic Study

KI53 is an irregularly-shaped aggregate with an overall size of 0.5 mm (Fig. 5.3). It consists of numerous facies of different sizes. The larger ones are rounded or sub-rounded objects with the sizes of 25-40 um (Figs. 5.4a, b and c). Some smaller objects, ~10 um, have similar rounded or sub-rounded shapes. These objects, large or small, have a common feature, that is, they are lined at the edge by a band of Tpx or diopside of varying thickness. This Tpx or diopside band may not be complete. Some irregular-shaped objects are also surrounded by a band of Tpx or diopside. The cracks and cavities are common on all these objects. Most small sized objects are in irregular shape and they are the fragments of the objects described above identified by the similar mineral assemblage and by the lining of Tpx or diopside at a portion of the curved edge (Fig. 5.4d)

The object in Fig. 5.4a has a mineral assembldge of melilite, spinel and patched HAP in the core and is surrounded by diopside with irregular thickness and discontinued in some places. Perovskite blebs (1-2 um) are scattered both in the core and on the edge. Hedenbergite grains can be found only on the edge. The melilite (at the center and lower-right quarter) grades from light to darker patches, indicating an increasing degree of alteration (analyses 1 to 3 of melilite in Appendix Table IV). The increasing degree of darkness corresponds to decreasing Ca and increasing Mg, suggesting that Mg is replacing Ca

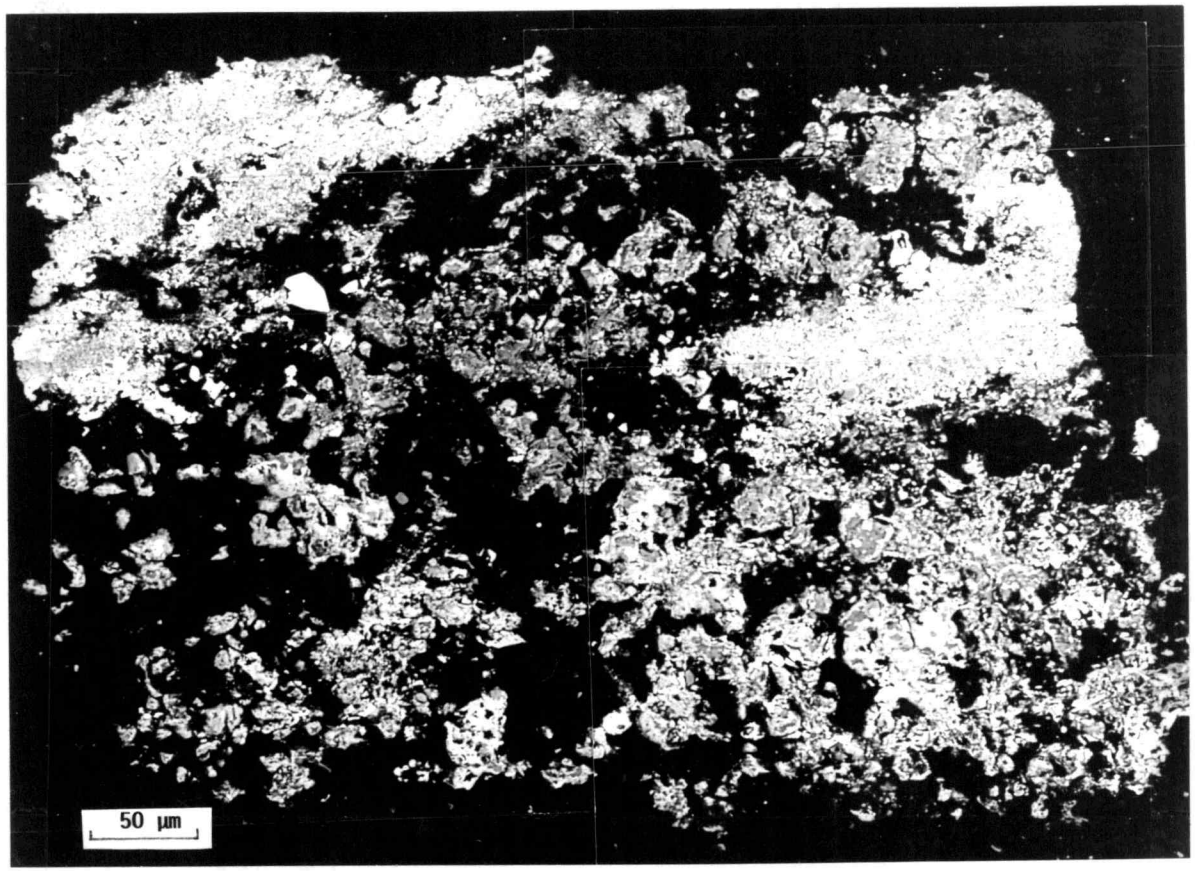

Figure 5.3 BSE images of KI53.

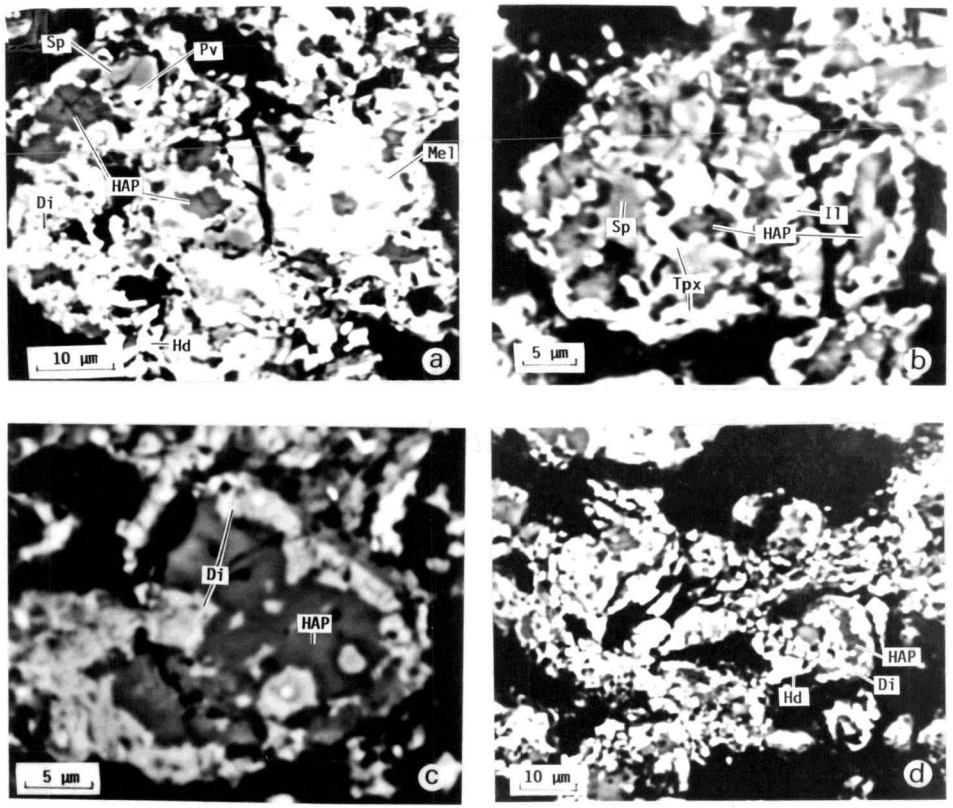

Figure 5.4 BSE images of individual nodules in KI53.
Abbreviations: Mel — melilite, Sp — spinel, Di — Al-diopside, Hd — hedenbergite, Pv — perovskite, HAP — high-Al phase, Tpx — Ti-Al-pyroxene, Il — ilmenite.

Table 5.1 Representative EPMA data of minerals in KI53 (wt. %)

	Melilite	Spinel	High-Al Phase	Ti-Al-pyroxene	Hedenbergite
SiO_2	23.12	1.33	24.76	47.07	47.83
MgO	1.32	25.17	13.35	16.86	1.96
Al_2O_3	32.78	71.21	32.29	11.18	0.67
CaO	42.18	0.59	5.09	22.18	22.65
FeO	0.50	1.44	5.16	0.72	26.88
TiO_2	0.07	0.16	1.52	1.73	0.05
Na_2O	0.06	0.03	0.26	0.08	0.11
K_2O	0.01	0.00	0.34	0.06	0.00
V_2O_3	0.09	0.34	0.23	0.25	0.06
Cr_2O_3	0.02	0.19	0.07	0.00	0.00
MnO	0.11	0.00	0.06	0.00	0.67
NiO	0.02	0.00	0.17	0.05	0.06
ZnO	0.00	0.00	0.07	0.15	0.18
Total	100.27	100.44	83.36	100.33	101.12

as the first step of melilite alteration. The object on Fig. 5.4b has a mineral assemblage of spinel, Tpx and HAP, lined by Tpx and diopside on the edge. Ilmenite grains can be found in the core and at the edge. No melilite and perovskite can be found. Only HAP and Tpx/diopside are found in the object of Fig.5.4c. These three objects represent an increasing degree of alteration, very similar to the alteration described by Hashimoto and Grossman (1987). In this alteration sequence, melilite is altered first by replacement of Ca by Mg, then breaks down to form HAP. Perovskite is altered to ilmenite, and finally spinel and ilmenite all break down into fine-grained HAP.

6. ANORTHITE-RICH INCLUSIONS KI77 AND KI88

6.1 Elemental Chemistry

KI77 and KI88 have unique mineral and petrographic features, which are discussed in the next section. Their REE pattern (Fig. 6.1) and lithophile pattern (Fig. 6.2) are very similar to those of KI53. The most refractory elements are depleted relative to moderately refractory elements. The moderately volatile elements, except the most volatile element V in this group, have similar abundances as moderately refractory elements. They differ from typical Allende Group II pattern in their normal Eu and Yb and less depleted V abundances. From the available data we believe that KI88 has a similar element pattern as KI77 does.

6.2 Petrographic Study

KI77 and KI88 have a size of 400 um and 600 um at the longest dimension, respectively. These two inclusions have very similar mineralogies as well as chemistries. Their textures appear to be igneous, consisting chiefly of anorthite (~50%), diopside (~20%), enstatite (~10%) and fine-grained areas (~20%) of diopside, anorthite, Si-rich phase, and tiny (~1 um) Fe-rich blebs (Fig. 6.4). Representative EPMA are presented in Table 6.1. The composition of anorthite has an average of An94. The Na content is higher in the fine-grained area (analyses 4 and 5 in Appendix Table V). Enstatite is enclosed by anorthite and is almost pure (En>99%). Diopside contains <5% Al_2O_3, 0.8-2.2% TiO_2 and 0.7-2.2% Cr_2O_3. The Al content

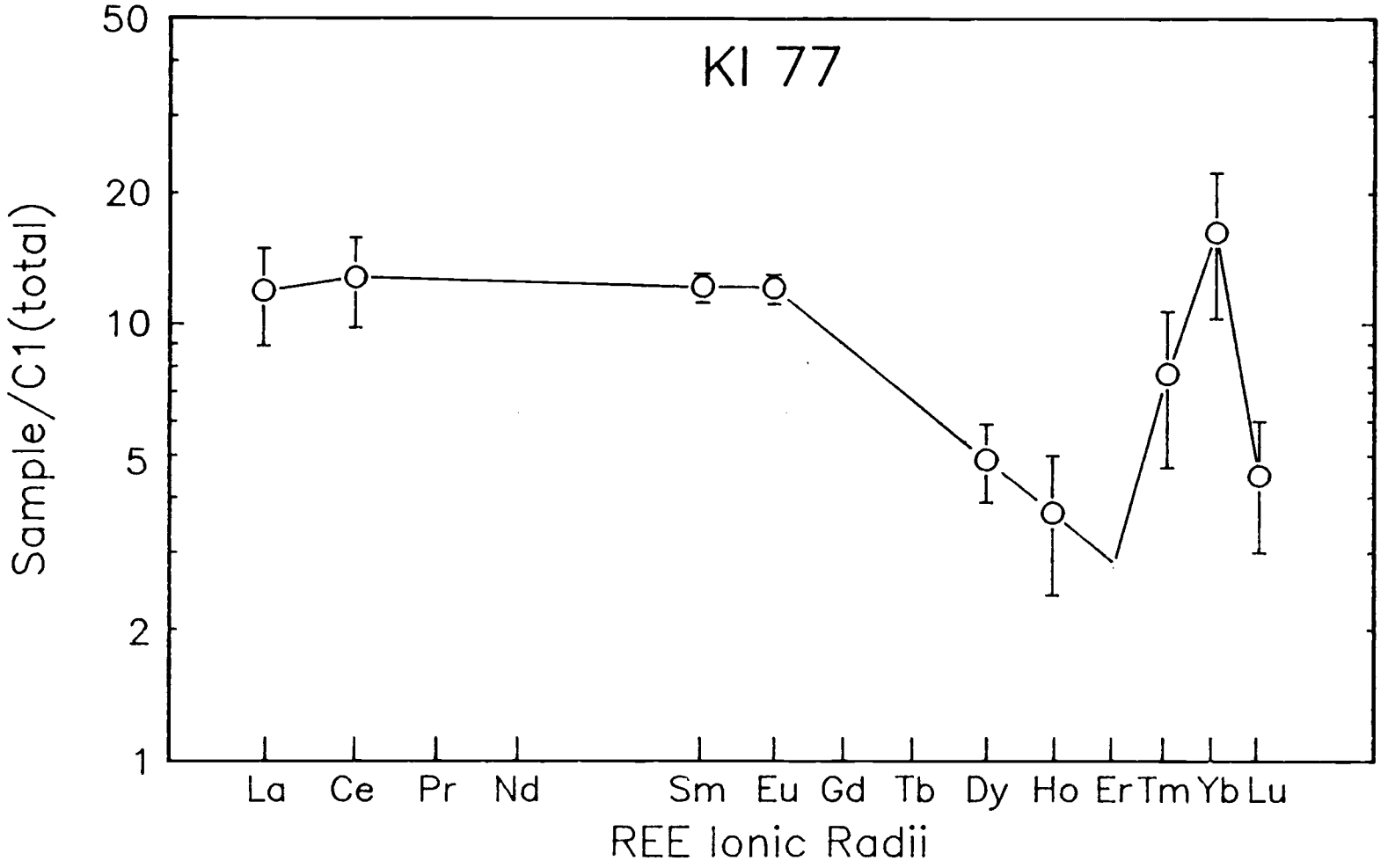

Figure 6.1 The C1-normalized REE pattern of KI77.

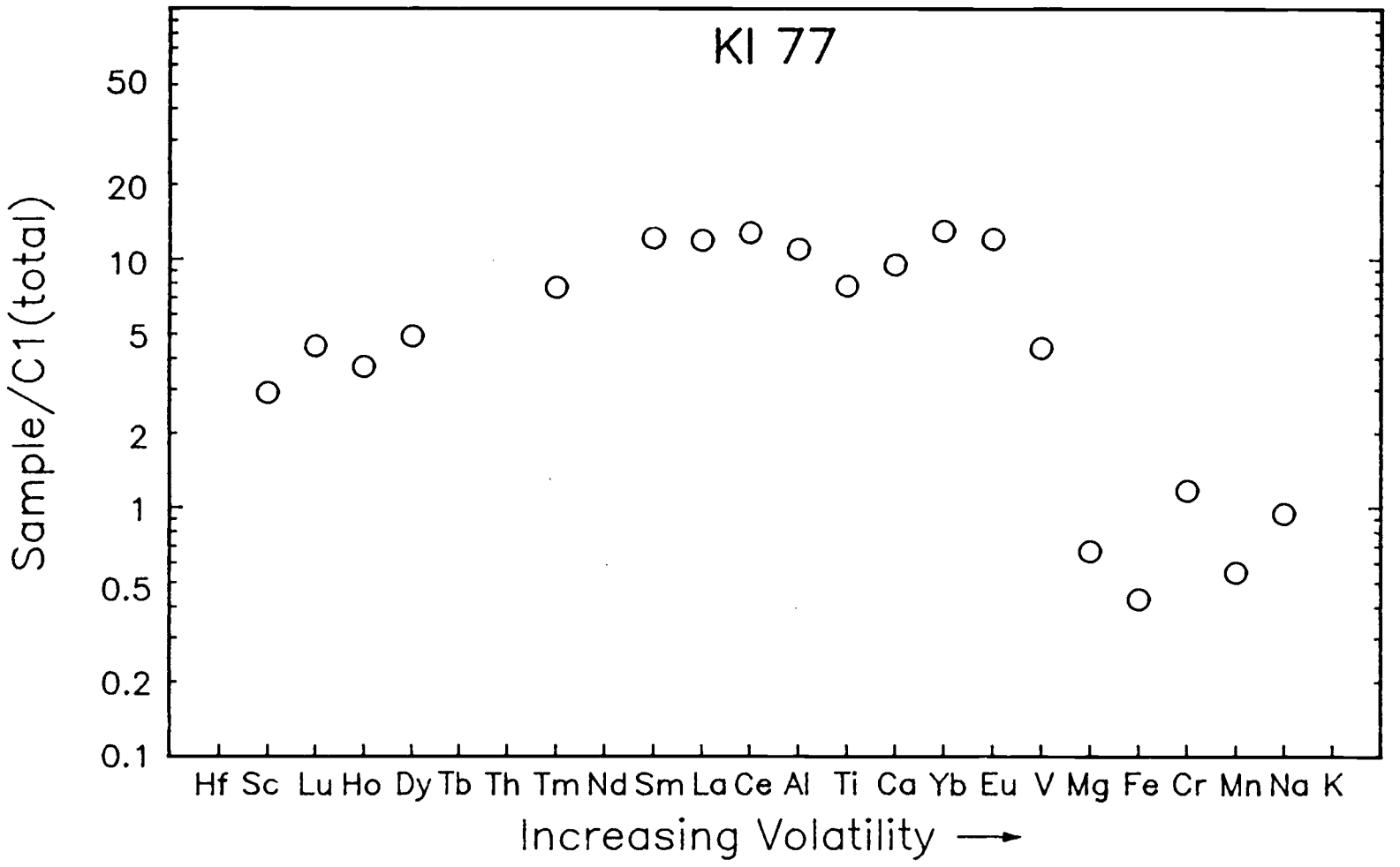

Figure 6.2 The C1-normalized abundances of lithophile elements in KI77.

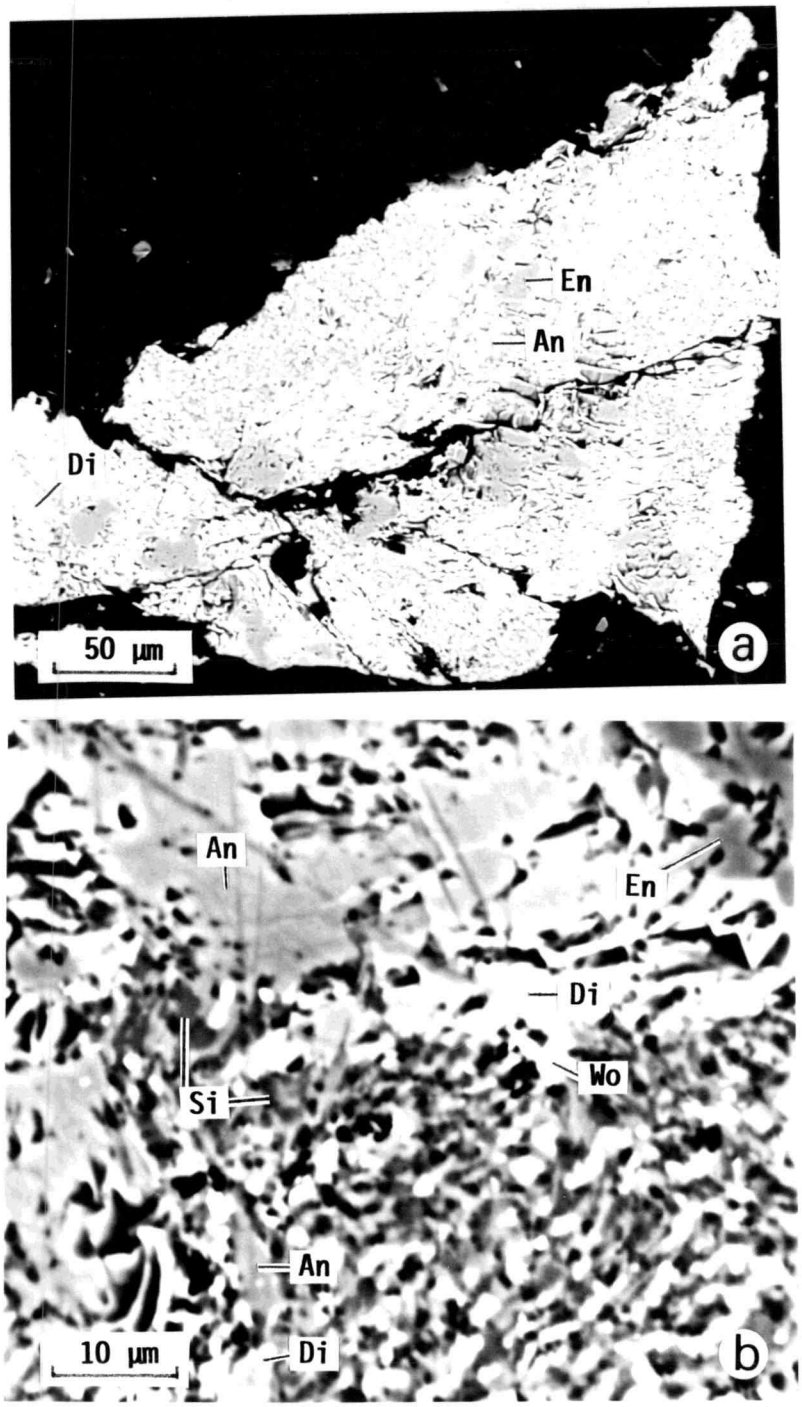

Figure 6.3 BSE images of KI77 (a) and its fine-grained area (b). Abbreviations: An — anorthite, En — enstatite, Di — diopside, Wo — wollastonite, Si — Si-rich phase.

is lower than in diopside in the Group III rims and in KI53. The mineralogy of the Si-rich phase in fine-grained areas is not identified (analyses 1 and 2 in Appendix Table V). Spinel and melilite are absent. This overall mineralogy differs from plagioclase-rich Type C CAIs and CA chondrules (Wark, 1987). Wark subdivided Type C inclusions into two groups, the Ti-Al-pyroxene(Tpx)-rich group (Type C CAIs) and Tpx-poor group (Type C CA). Type C CAIs are composed of 30-60 vol % anorthite and up to 35 vol % each of Tpx, melilite and spinel. CA chondrules contain more sodic plagioclase, pyroxene, olivine, and spinel. The major element composition of KI77 is similar to Wark's CA (1987). But the olivine and spinel which CA contains are absent in KI77 and KI88. This mineral assemblage is also not found in the condensation sequence (Grossman, 1972). According to condensation calculation, anorthite would be formed in the nebula at 1362°K by the reaction of previously condensed spinel and diopside. At 1349°K previously condensed forsterite begins to react with gas to form enstatite. The ratio of enstatite to forsterite gradually increases with falling temperature. There is still a considerable fraction of forsterite remaining at 1200°K. Calculations for non-classic solar nebular composition (Wood and Hashimoto, 1988) also predicted the coexistence of forsterite with anorthite, diopside and enstatite. Forsterite was not found in KI77 and KI88.

Comparing the mineral assemblages and major element abundances of KI77 and KI88 with those of Group III inclusions, we observe that inclusions contain less Al and higher Si, suggesting that these

Table 6.1 Representative EPMA data of minerals in KI77 (wt. %)

	Anorthite	Enstatite	Diopside	Si-rich phase
SiO_2	45.52	57.33	54.81	74.81
MgO	0.65	38.13	21.73	0.33
Al_2O_3	33.86	2.57	2.16	15.23
CaO	20.30	1.70	20.81	8.01
FeO	0.07	0.56	0.40	0.34
TiO_2	0.04	0.37	1.00	0.30
Na_2O	0.52	0.01	0.00	0.60
K_2O	0.01	0.03	0.02	0.02
V_2O_3	0.05	0.15	0.17	0.03
Cr_2O_3	0.05	0.89	0.78	0.05
MnO	0.04	0.18	0.22	0.00
NiO	0.15	0.17	0.07	0.13
ZnO	0.13	0.10	0.00	0.11
Total	101.38	102.19	102.18	99.97

inclusions condensed from a gas enriched in elements of moderate volatility either as liquids or as solids which were remelted later. A magmatic origin is excluded by considerations of elemental abundances vs. volatility shown on Fig. 6.2. If we plot KI77 on a compositional trajectory diagram of nebular condensates and residues of Fig.15 in Wark (1987), KI77 is far from solid condensates and evaporative residues paths. It falls on the liquid condensate line of 1 atm., implying a liquid condensate origin. The nebular pressure required to condense liquids from gas of solar composition is unusually high. As an alternative, the liquids may condense under a higher dust/gas ratio, which has a similar effect by increasing the total pressure to 1 atm. as proposed by Wark (1987). It is concluded that KI77 and KI88 were probably formed as liquid condensates.

Plagioclase-rich inclusions and chondrules have attracted increasing interests not only because they provide evidence of a new kind of high temperature process (Wark, 1987), but also provide important clues regarding the relationship between the CAIs and ferromagnesian chondrules (Kring and Holmén, 1988; Sheng et al., 1988). Compositionally they are intermediate between CAIs and ferromagnesian chondrules.

7. INCLUSION WITH SUPER-REFRACTORY COMPONENT: KI4

KI4 shows an enrichment of HREE relative to LREE (Lu 12xCl to La 5xCl) (Fig. 7.1). The abundances of refractory lithophile elements show a gradual decrease with an increase of volatility (Fig. 7.2). The abundances of siderophile elements also show a systematic decrease from Os (0.78xCl) to Au (0.28xCl), but the enrichment relative to Cl is more than one order of magnitude lower than that of lithophiles. The correlation between the elemental abundances and their volatility suggests that this pattern is a result of condensation or vaporization.

KI4 is a fragment of 500 um at its longest dimension and has a yellowish color. The BSE image (Fig.7.3) shows that the predominant mineral is enstatite. There are two major cracks which divide the inclusion into three areas. The Area 1 on the left is composed of enstatite with Fe-rich spots. The Area 2 on the upper-right are dominated by the fine-grained Al-Mg-rich material (HAP) with enstatite, anorthite and Fe-rich phase. The Area 3 on the lower-right is composed of enstatite, diopside and HAP with abundant olivine grains which are rich in Fe.

The EPMA data of minerals are presented in Appendix Table VI. The enstatite in Areas 2 and 3 contains more Fe and Al (analyses 2 and 3) than in Area 1 (analysis 1). Also Cr and Mn are higher in analyses 2 and 3 than in 1. There are anorthite grains in Area 2 and along the boundary of Areas 1 and 3. They are surrounded by HAP. In Area 2 enstatite and anorthite are islands surrounded by HAP. In Area 3, HAP is along the boundary of Areas 1 and 3. This texture suggests

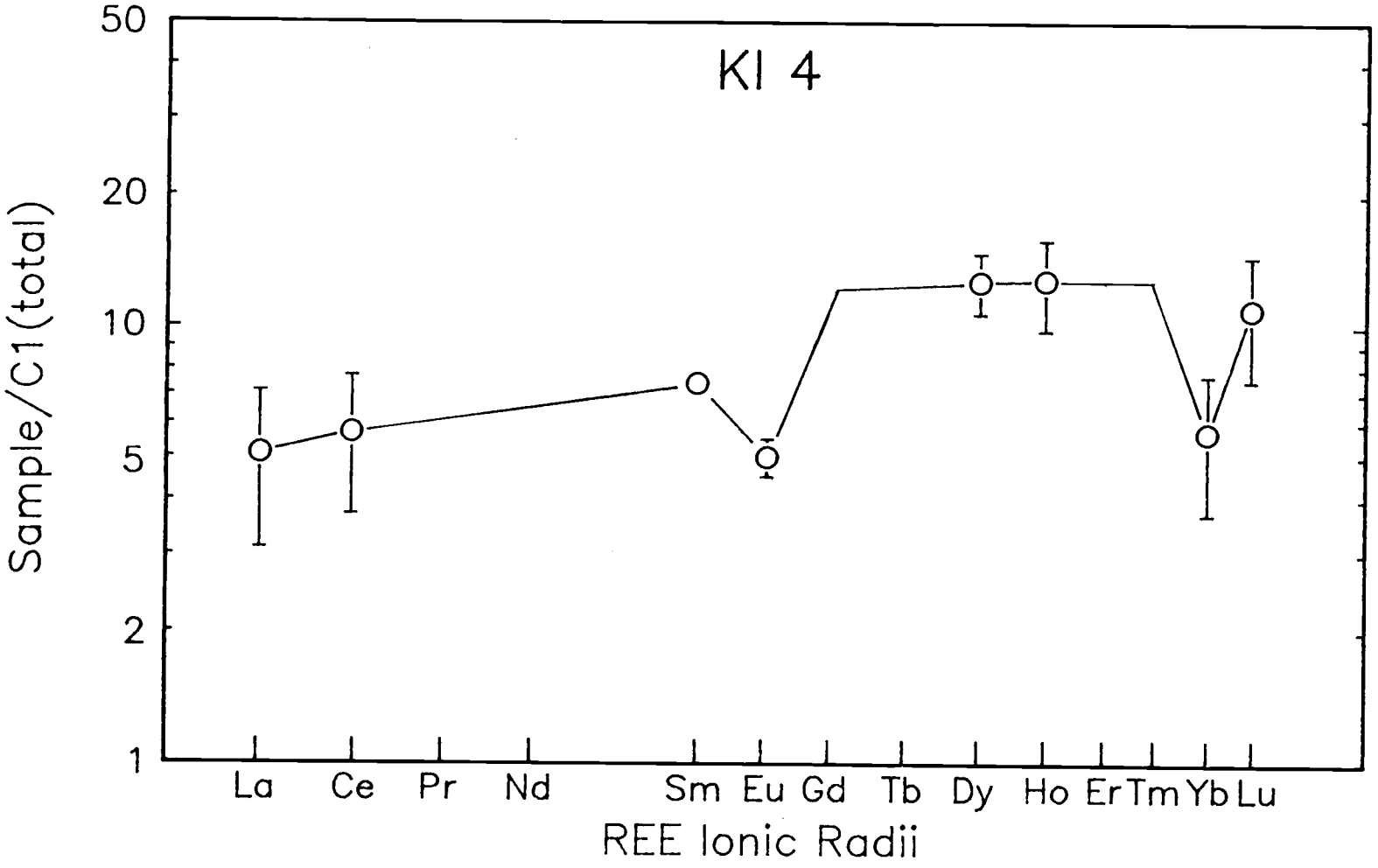

Figure 7.1 The C1-normalized REE pattern of KI4.

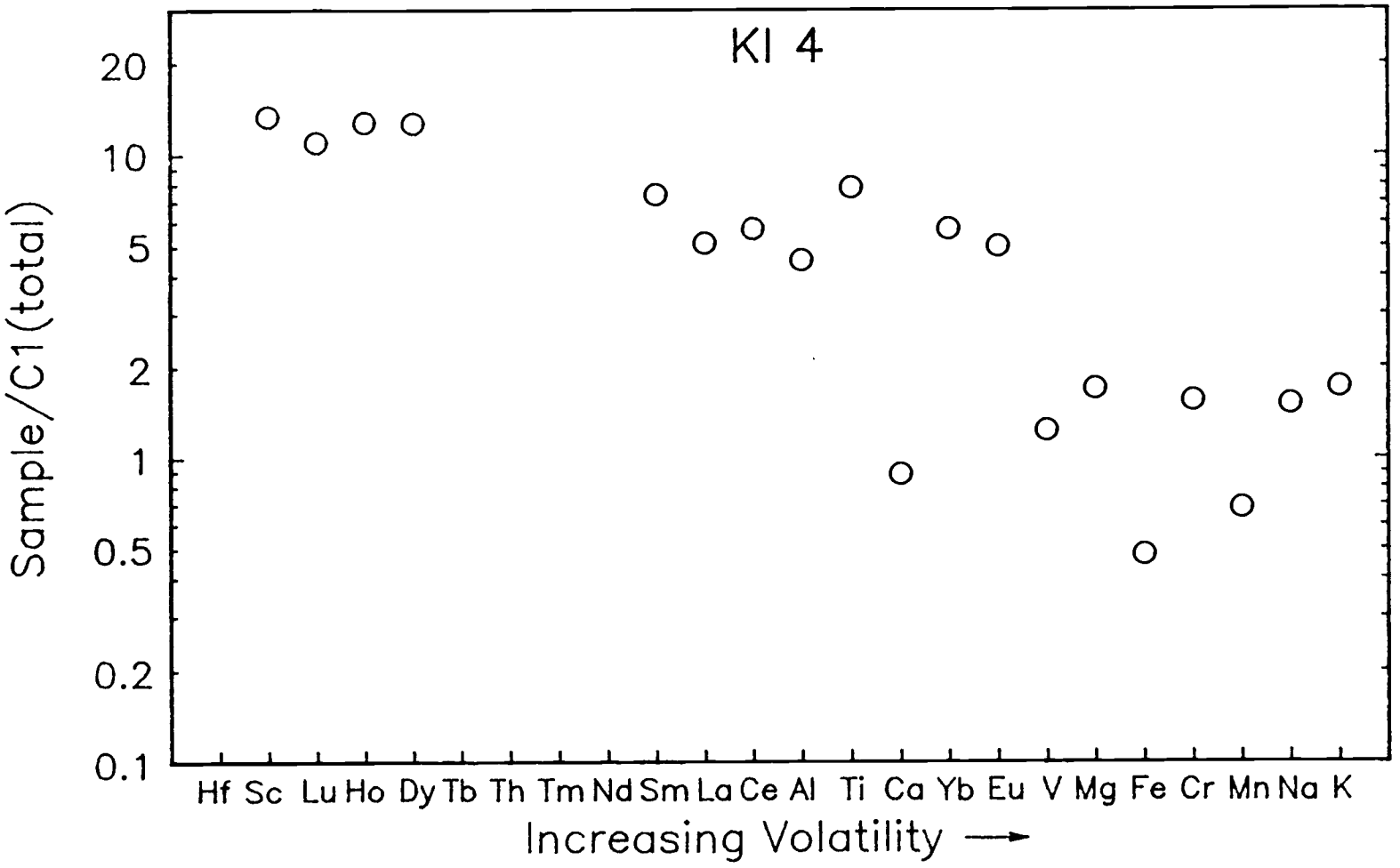

Figure 7.2 The C1-normalized abundances of lithophile elements in KI4.

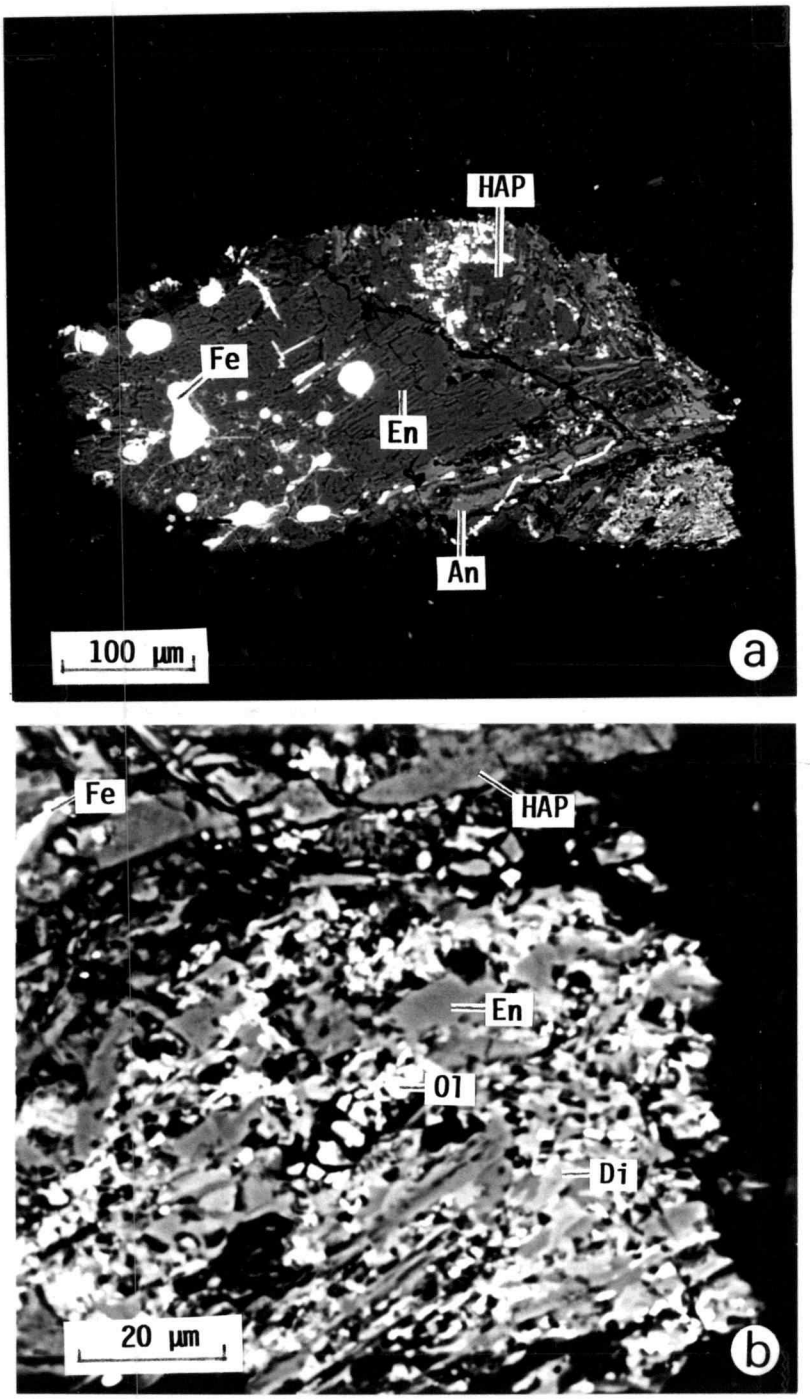

Figure 7.3 BSE images of KI4 (a) and its lower-right part (b). Abbreviations: En — enstatite, An — anorthite, HAP — high-Al phase, Fe — Fe-rich phase, Di — diopside, Ol — olivine.

that anorthite is being alterated to HAP. Diopside is abundant in Area 3. It contains considerable amount of Fe (6-11%) and Al (~5%). Olivine in Area 3 is also rich in Fe.

The higher enrichment of ultra-refractory elements relative to the more volatile elements suggests that KI4 contains an ultra-refractory component which is a high-temperature product either by condensation or as the residue of evaporization. This pattern was predicted by Boynton (1975) and classified as Group 0 by Wark (1983)

There are a few ultra-refractory inclusions that have been reported: MH-115 and SH-2 from Murchison (Boynton et al., 1980; Ekambaram et al., 1984), an object from Ornans (Palme et al., 1982) and the core of 3643 from Allende (Wark, 1986). MH-115 is composed of spinel and hibonite, and refractory element enrichments range from ~100xCl for Lu down to ~30xCl for La. Iridium is similarly enriched as Lu. SH-2 is also a spinel-hibonite aggregate with Lu 1000xCl and La 110xCl. Other ultra-refractory lithophile and siderophile elements are enriched to the similar magnitude as is Lu. The tiny 1 ug object from Ornans consisting of a metal Fremdling in an unknown host material has enrichments ranging from 15,000xCl for Re, Os and Ir, 10,000xCl for Lu and Hf, to 3,920xCl for Ru and <30 for Sm. The core for the Allende CAI 3643 is composed of hibonite, melilite and metal nuggets. The core is highly enriched in the ultra-refractory lithophiles (~200xCl) and siderophile elements (e.g. Os, 350xCl), and displays a steep fractionation of moderately refractory metals, whose abundances decrease with increasing volatility down to 20xCl for Rh.

Comparing KI4 with reported ultra-refractory inclusions, I note that KI4 shows a much lower enrichment for refractory elements and contains no high-temperature condensation mineral. The predominant mineral of KI4 is enstatite which is consistent with the low Al and Ca in bulk analysis. In Grossman's condensation sequence, enstatite is condensed at 1349°K, a temperature compatible for the condensation of essentially all refractory elements. This seems to contradict the observed enrichments of the super-refractory elements. A possible formation scenario may be that the super-refractory elements condensed at a high temperature first, followed by transport of the condensed materials into another nebular volume where the temperature was lower and where enstatite condensed, so that the refractory element pattern was preserved but the enrichment factor was considerably lowered by the dilution of enstatite. The primary ultra-refractory component which served as a carrier of the super-refractory elements was either altered at the lower temperature or not shown on the BSE picture due to its small size. Diopside, anorthite (plagioclase) and Al-Mg-rich material are the possible alteration products we have seen in many cases.

8. A COMPOUND INCLUSION: KI94

The REE of KI94 shows an irregular pattern; e.g., the LREE are enriched to ~15xCl. Tb, Dy and Tm are highly enriched to ~50xCl and Eu and Yb in the middle to ~25xCl. Fig. 8.1 shows the enrichment in the order of increasing volatilities for lithophile elements. For super-refractory elements, the enrichment seems to increase with increasing volatility. The enrichment reaches the highest value at ~50xCl for very-refractory elements, then decreases rapidly to ~15xCl. The enrichment for moderately-refractory elements remains quite constant at ~15xCl, except for the positive anomalies of Eu and Yb. Volatile elements are depleted severely. It is plausible that this pattern can be interpreted by superposing a strongly fractionated pattern on a Group VI pattern. The fractionated pattern peaks at very-refractory elements and is depleted for both ultra- and moderately-refractory elements.

KI94 has an overall size of ~400 um at longest dimension. The BSE image (Fig. 8.2) suggests that KI94 consists of two components, one is a spherule containing melilite and spinel, the other contains only melilite. Both are surrounded by a rim on upper and right sides; the other sides are broken. The spherule is generally defined by a circle of spinel, and some spinel grains scatter around the boundary. Perovskite blebs are abundant in melilite. The EPMA data are summarized in Table 8.1. The composition of melilite ranges from Ak8.2 to 24.8 with the average of 13.4. Fig. 8.3 shows the melilite composition across the inclusion along the line A-B-C-D. There is no systematic variation between the melilite inside and outside the

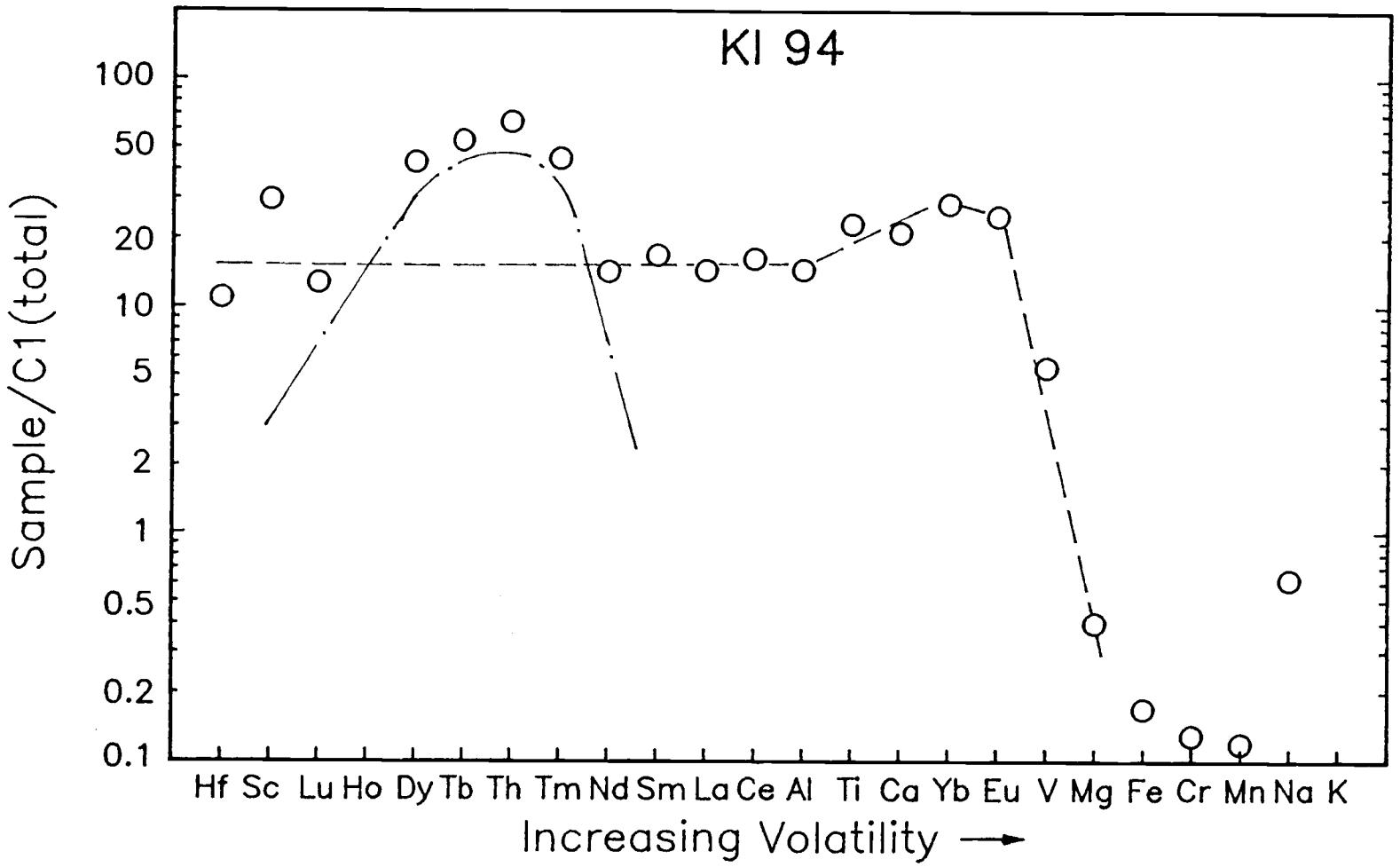

Figure 8.1 The Cl-normalized abundances of lithophile elements in KI94.

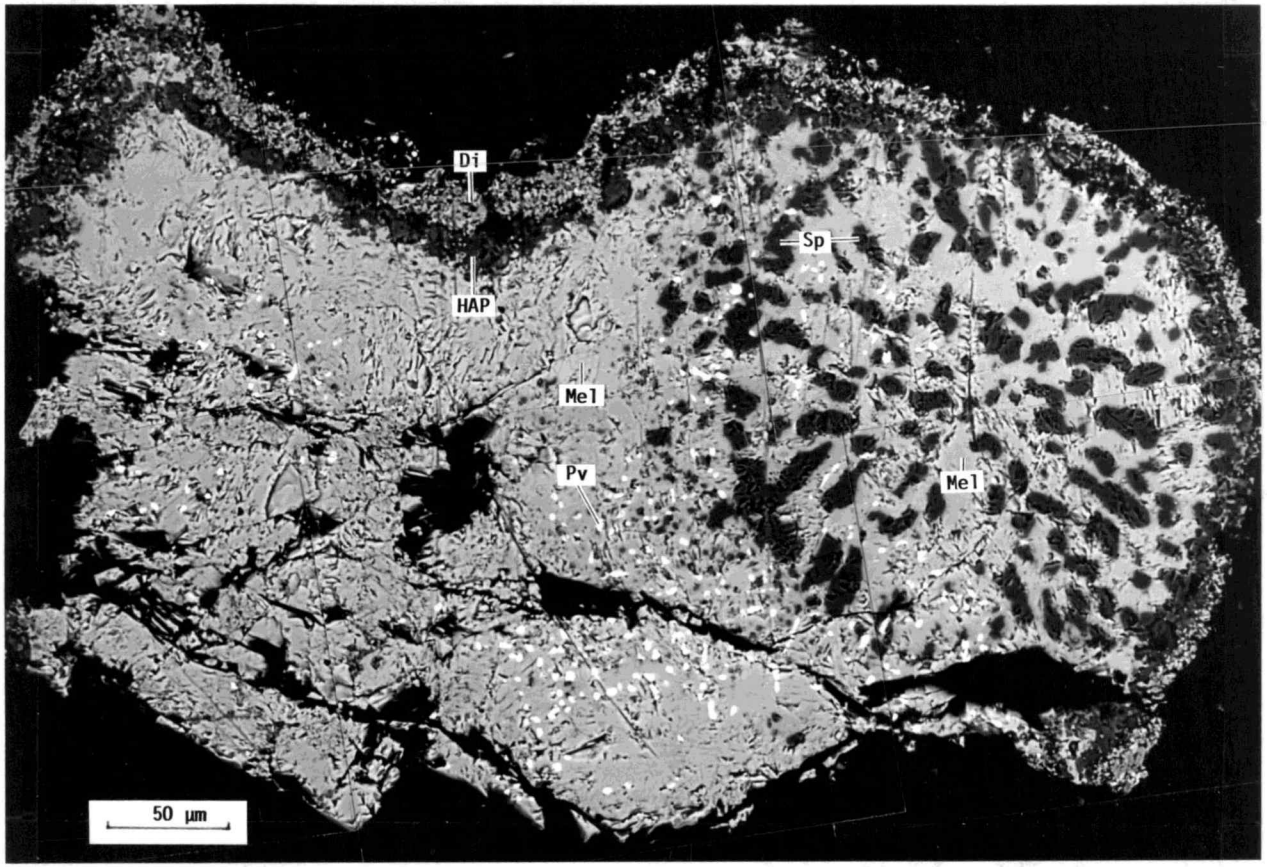

Figure 8.2 BSE image of KI94.
Abbreviations: Mel — melilite, Sp — spinel, Pv — perovskite, Di — Al-diopside, HAP — high-Al phase.

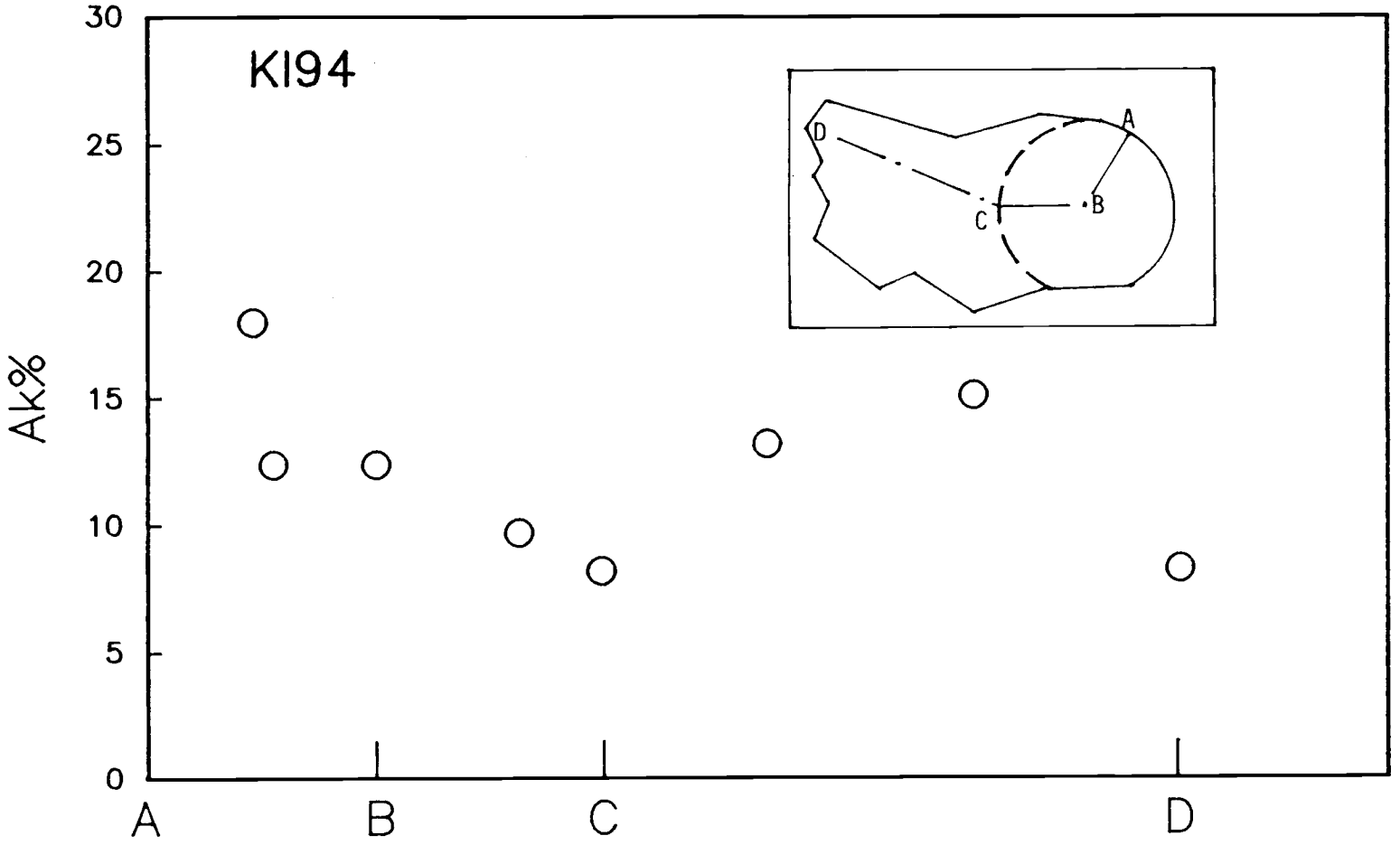

Figure 8.3 The Ak% of melilite along the line A-B-C-D in KI94

Table 8.1 Representative EPMA data of minerals in KI94

	Melilite		Spinel		High-Al	Ti-Al-
	in spherule	out spherule	interior	along rim	Phase	pyroxene
SiO_2	23.56	24.27	0.05	0.39	23.14	40.92
MgO	1.70	1.84	28.23	27.07	14.77	10.78
Al_2O_3	31.46	32.88	70.63	70.63	26.57	13.51
CaO	42.75	41.00	0.23	0.31	1.81	24.72
FeO	0.02	0.02	0.01	0.96	5.51	2.95
TiO_2	0.02	0.04	0.19	0.06	0.03	3.46
Na_2O	0.03	0.01	0.01	0.02	2.13	0.07
K_2O	0.02	0.00	0.00	0.00	0.55	0.00
V_2O_3	0.08	0.03	0.57	0.41	0.09	0.46
Cr_2O_3	0.00	0.00	0.08	0.22	0.00	0.05
MnO	0.00	0.04	0.00	0.00	0.06	0.03
NiO	0.03	0.09	0.00	0.02	0.12	0.01
ZnO	0.00	0.11	0.07	0.00	0.14	0.00
Total	99.69	100.33	100.08	100.09	74.90	96.95

spherule. The Fe contents in the spinel along the rim are higher (0.26-1.4%, average 0.76% FeO) than in interior (0-0.09%, average 0.05% FeO). The spinel, where the spherule borders pure melilite, contains normal low Fe, suggesting that these two parts joined first. Iron was added to spinel later as a secondary alteration so that only the spinel along the rim contains higher Fe.

The texture and the refractory element pattern both suggest a compound inclusion. It seems these two components were formed in separate nebular regions. One was formed in a nebular region where the super-refractory elements had already been depleted, and the condensation was ended before the condensation of moderately-refractory elements. The other component was formed in a nebular region where the gaseous phase had an unfractionated refractory element pattern. These two components joined together later. Finally the entire inclusion was subjected to secondary alteration later to form the rim.

Data for two compound inclusions have been reported. Conard (1976) reported that the Allende inclusion B-32(dark) is a two-component system, the Allende matrix and a component enriched in Gd, Tb, Dy and Ho. Replotting her data according to their volatilities, I observe a peak of very-refractory elements terminating at Tm and superposed on a flat elemental pattern. B-32 is a high-Rb CAI (Gray et al., 1973). In Conard's work B-32 was separated into white and dark portions. B-32(white) is Ca-rich with a Group II pattern. B-32(dark) is Ca-poor. Kuehner and Grossman (1987) and Laughlin et al. (1988) reported another Allende compound inclusion, TS63F1, which

exhibits a Group II pattern. One component is a hibonite-spinel-rich region, the other is a vermicular-textured spinel-anorthite-diopside region, and both are surrounded by a spinel-diopside-rich outer mantle. Distinctive 10 um layers of anorthite and wollastonite are found where the two regions are in contact.

9. GROUP IV INCLUSIONS

Most of the studied inclusions are low in refractory elements. Twelve of them were randomly chosen for electron microprobe study. They are KI6, KI39, KI42, KI43, KI59, KI61, KI65, KI72, KI76, KI80, KI85 and KI96. All these twelve inclusions have relatively low Ca and Al abundances. They have unfractionated REE patterns with lower enrichments of refractory elements (1-5.5xCl). The average elemental abundances of these twelve inclusions are plotted in Fig. 9.1. The average enrichment for refractory lithophile elements is ~3.5xCl. The most volatile elements are depleted relative to Cl chondrite (0.6xCl). Siderophile elements have a similar pattern.

The microprobe study shows that their major minerals are olivine, pyroxene and/or diopside. Anorthite is present in some inclusions. Spinel is found only in one rounded nodule in KI72.

The element abundances of Allende Group IV inclusions have been compiled by Wark (1983). Our data agree well with Allende except that Allende Group IV inclusions contain higher Na and K and the abundances of volatile siderophile elements are more scattered. The unfractionated refractory element pattern suggests that these inclusions formed by the dilution of early formed unfractionated condensates by olivine, which condensed later at a lower temperature. It can be seen that Mg and Fe contents in Group IV inclusions are much higher than in Group III inclusions, consistent with the abundant olivine observed in microprobe study. Na and K are lower than in Allende, consistent with the lack of feldspathoid minerals in

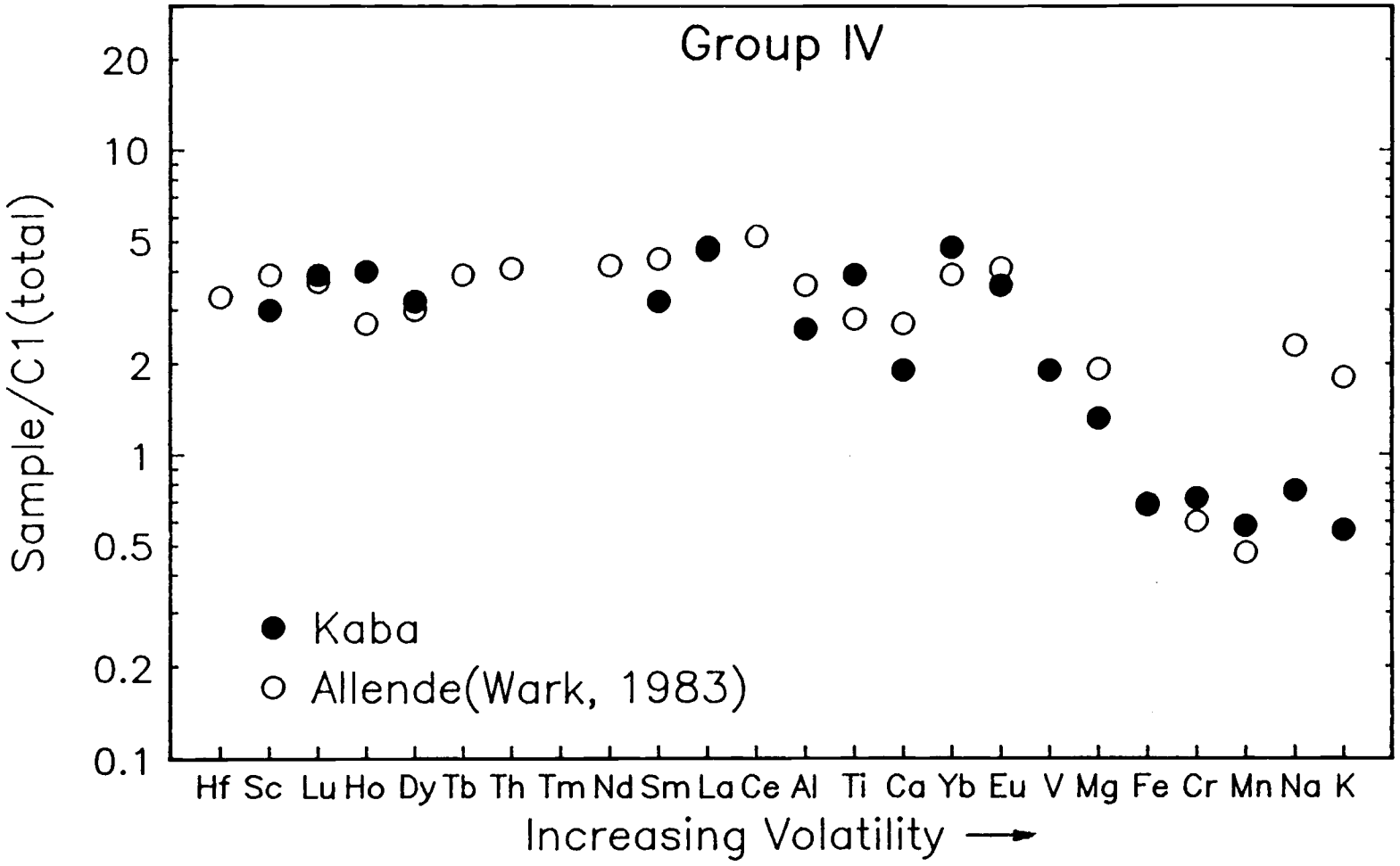

Figure 9.1 The C1-normalized abundances of lithophile elements for average Group IV inclusions. Allende data are from Wark (1983).

Kaba. This is an indication that Kaba inclusions were subjected to less alteration than was Allende.

Two representative olivine-rich inclusions are described here in some detail. KI6 (Fig. 9.2a) is composed of fragments broken from larger inclusions. These fragments are mainly composed of olivine. There are patches of diopside encased in olivine grains. Also it is common that a thin layer (<1 um thick) of diopside lining is observed on the fragment surface, around the cavities in the grains, around the anorthite grains, and along the cracks. The lining structure suggests that the diopside is the product of a solid-gas reaction that occurred on the surface, possibly the secondary alteration reaction of primary minerals with the parental nebular gas. Anorthite is present in some fragments. Fe inclusions (possibly as sulfide) exist. The EPMA data of these minerals are presented in Appendix Table VIII. Olivine anlyses show they are pure forsterite (<2.1% FeO). KI72 (Fig. 9.2b) is an aggregate of rounded and sub-rounded olivine-rich nodules and their fragments, with an overall size of ~1 mm. The diameter of nodules are ~150 um or less. The nodules are composed of olivine with fine-grained aluminous diopside. It is a commom feature that the nodular surfaces around the cavities and along the cracks are lined by a thin layer of diopside. Anorthite is present as a minor phase, usually surrounded by diopside. There is a spinel-rich nodule (right on Fig. 9.3a and Fig. 9.3b) which has a spinel core with aluminous diopside surrounded by a layer of coarser-grained diopside and finally an olivine layer. In the core spinel grains are surrounded by a thin layer (~1 um) of diopside. The

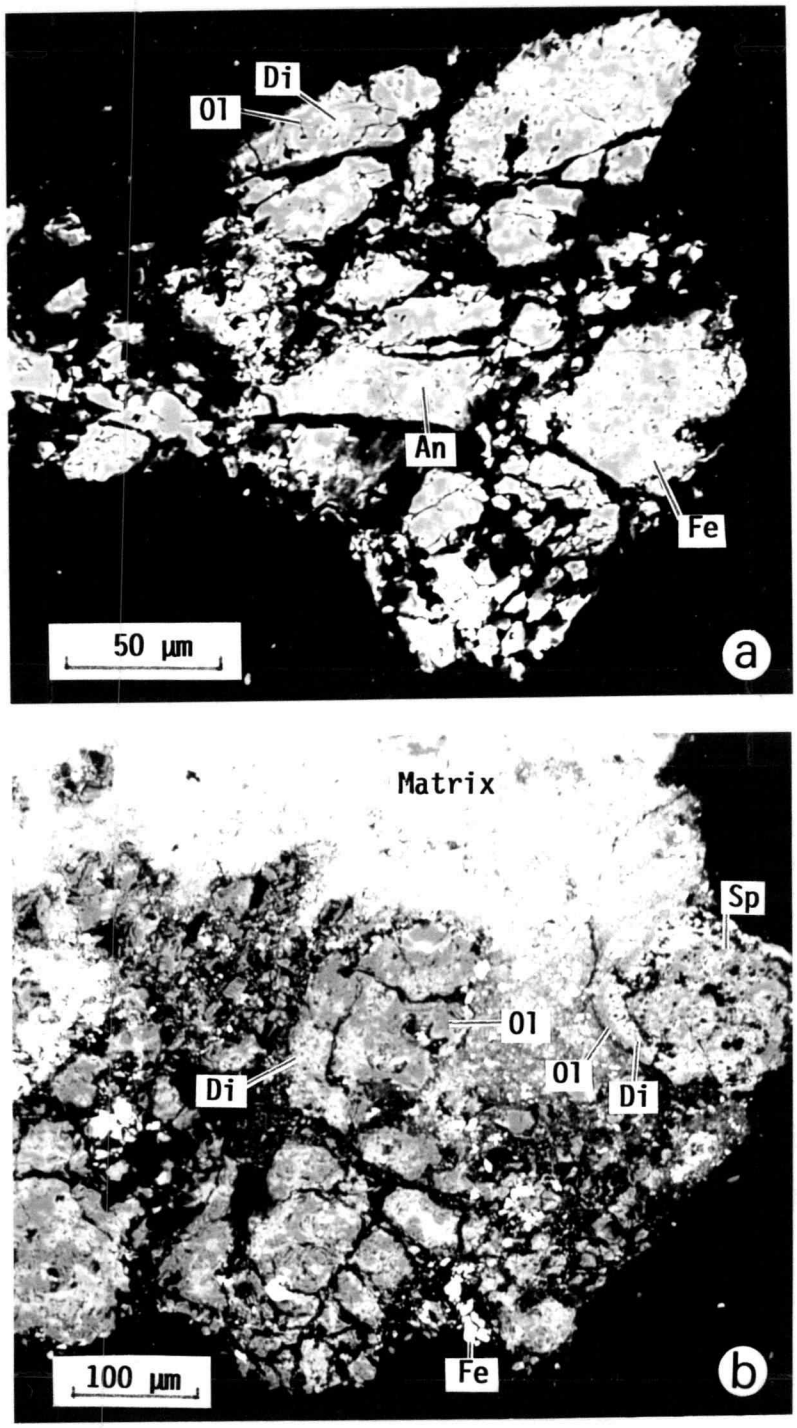

Figure 9.2 BSE images of KI6 (a) and KI72 (b). Abbreviations: Ol — olivine, Di — diopside, An — anorthite, Fe — Fe-rich phase, Sp — spinel.

texture suggests that the diopside is the alteration product of spinel. The EPMA data of minerals are shown in Appendix Table VIII.

The chemistry and mineralogy of Allende Group IV aggregates and chondrules have been studied by Mason and Martin (1977). They are characterized by high SiO_2 and MgO and low TiO_2 contents and consist largely of olivine with lesser amounts of clinoenstatite and glass. The amoeboid olivine aggregates in Allende have been studied by Grossman and Steele (1976) and Grossman et al. (1979). Spinel-rich assemblages have been found in Allende amoeboid olivine aggregates by Grossman and Steele (1976) and studied in detail by Hashimoto and Grossman (1987).

10. RIM STRUCTURE

Rim structure is a common feature in melilite-rich inclusions of this work as well as in spinel-rich inclusions in Kaba (Fegley and Post, 1985). It is also a commom feature in Allende, Mokoia, and other chondrites. Rims on Allende Type A inclusions were described in detail by Wark and Lovering (1977) as being composed of the following layers from innermost to outermost: Fe-rich spinel + perovskite, anorthite + feldspathoids + olivine + grossular + indeterminate Ca-Al-Mg-rich silicate phase, clinopyroxene which grades outward in composition to aluminous diopside, and finally, hedenbergite + andradite + wollastonite. The concentric objects of inclusions from Mokoia are always rimmed. Cohen et al. (1983) found that in fine-grained Mokoia CAIs (their Type C), a rim of high-Al phyllosilicate (HAP) usually surrounds the spinel core. HAP is found in Mokoia while feldspathoids are found in the Allende rim sequences. Surrounding HAP is a rim of diopside or Ti-Al-rich pyroxene. Type B Mokoia inclusions are surrounded by well-developed rim sequence. One Type B inclusion displays the following rim sequence from interior to exterior: anorthite + Fe-bearing fassaite, spinel, HAP, diopside, Fe-bearing diopside + pyrrhotite blebs, LAP, diopside and olivine. No Type A inclusions were sampled in their study. A fine-grained spinel-rich CAI in Kaba was studied by Fegley and Post (1985). The rim sequence (10-20 um thick) surrounding the spinel-rich cores is similar to the Wark-Lovering rims on Allende CAIs. From interior outward the rim sequence consists of Ti-Al-pyroxene, anorthite, diopside and hedenbergite. The composition of diopside layer grades from more

aluminous to less aluminous outward. Unidentified Mg-Al-Si-rich phases with 1-3 wt.% Na_2O and 0.2-0.7 wt.% K_2O are also present in BSE dark areas and pores near the inner edges of some rin sequences. These phases possibly are analogous to the HAP and LAP reported by Cohen et al. (1983).

There are basically four models that have been proposed for the formation of the banded mineral sequences that form rims on CAIs. (1) Rims are sequential condensates from the nebula (Wark and Lovering, 1977). The sequence corresponds to the sequence of the chemically-zoned nebular regimes the inclusion bodies passed through. (2) An igneous origin formed the crystallized minerals sequentially from thin films of melt (Bunch and Chang 1980, Wark 1981, Armstrong and Wasserburg 1981, Korina et al. 1982). (3) Rims are the alteration products formed by the reaction with nebular gas. MacPherson et al. (1981) suggested that rims were formed as by-products of the alteration process, prior to the accretion of the inclusions into the parental meteorite bodies. Inward diffusion of silica and alkalis from the surrounding nebular gas caused breakdown of melilite to anorthite, grossular and nepheline, releasing excess Ca which diffused outward and formed aluminous pyroxene, hedenbergite and andradite. (4) Rims are the refractory residue formed by flash heating of the CAI surface (Boynton 1988, Boynton and Wark 1987). Further discussion is in Chapter 11.

Rim structure is always related to a melilite-containing inclusion obejct and the alteration is largely due to melilite (MacPherson et al. 1981, Wark 1981). In the study of the alteration

of Al-rich inclusions in Allende, Hashimoto and Grossman (1987) demonstrated that melilite is the most susceptible to secondary alteration which converted it to anorthite, grossular and feldspathoids. In heavily altered inclusions anorthite was further altered to feldspathoids, and fassaite has been replaced by ragged material (a mixture of phyllosilicates). In very heavily altered inclusions spinel has reacted to form either phyllosilicates or a mixture of olivine + feldspathoids.

Our study shows that the Al/Ca ratio in HAP is relatively higher than that in melilite, the major constituent mineral in cores, while the Al/Ca ratio in Tpx-diopside layer is lower than that in melilite. By the time diopside was formed, essentially all Al and Ca had been condensed (Grossman, 1972). It also has been demonstrated that rims were formed before accretion (Blander and Fuchs 1975, Wark and Lovering 1977). It seems likely that Al and Ca could not come from the meteorite matrix. Al and Ca in rim layers can only be derived from the inclusion object itself. When the primary minerals, mainly melilite, reacted with nebular gas to form alteration products, Mg, Si, then Fe, and finally alkalis were added (Grossman, 1971). The Al-Mg-Si-rich phase (HAP) and Ti-Al-pyroxene or diopside were observed in this work. It is still not clear why the layered sequences were formed instead of intergrowing grains of these minerals. The layered structure requires that the excess Ca from the formation of HAP (or its precurssor minerals) move outward to form the Tpx-diopside layer. MacPherson et al. (1981) proposed a diffusion-controlled mechanism for the rim sequence formation. The inward diffusion of silica and

alkalis from the nebular gas caused breakdown of melilite, releasing excess Ca which diffused outward to form aluminous pyroxene, hedenbergite and andradite by a reaction with the incoming components from the nebular gas. Hashimoto and Wood (1986, 1987) showed theoretically and experimentally that at <1000°K Al and Ca are as volatile as Mg and Si because they form stable hydroxide vapors, so that the Ca migration during the alteration can be explained (see Chapter 11).

11. THE VOLATILITIES OF Al, Ti AND Ca

According to the 50% condensation temperature scenario (Wasson, 1985), Al is one of the ultra-refractory elements similar to Hf and Sc. Ti is approximately between the HREE and LREE, and the volatility of Ca is similar to Sm, La, and Ce. Therfore Al, Ti and Ca are expected to be equally enriched as other refractory elements down to and including Sm, La and Ce in Group III inclusions. But the enrichments of Al, Ti and Ca in Kaba Group III inclusions are lower than the enrichment of other refractory elements (Table 11.1 and Fig.11.1). The lower enrichments of Al, Ti and Ca relative to other refractory elements indicate they were not totally condensed at the temperature these inclusions were formed. Their lower enrichment can not be due to the partial removal of condensates because any removal of Al, Ti and Ca would also remove elements which are more refractory. This is inconsistent with the observation that the ultra-refractory elements are not depleted. The partial condensation of Al, Ti and Ca is not consistent with the classic condensation calculations.

A review of Allende inclusions reveals a similar situation. The abundances of Al, Ti, Ca and related elements for Allende inclusions (Mason and Martin, 1977; Mason and Taylor, 1982) relative to Cl as well as Kaba KI53 and Group III are listed in Table 11.1 and plotted in Fig.11.1. These Allende inclusion data were chosen because the major and trace element analyses are both available for the same individual inclusions. The average Allende Group III pattern on Fig.11.1 shows that Al and Ti are slightly lower than La and Ce, and

Table 11.1 The Cl-normalized abundances of Al, Ti, Ca and related elements in Kaba and Allende inclusions of various chemical groups

	Sm	La	Ce	Al	Ti	Ca	Yb	Eu
Kaba Group III								
KI60	38.3	47.9	39.0	18.7	8.3	10.9	7.5	11.6
KI62	40.9	50.4	37.3	19.8	11.0	11.0	14.5	14.8
KI73	30.9	36.4	30.8	14.7	8.7	10.7	8.8	9.6
KI74	28.9	33.5	32.5	15.1	6.4	8.9	8.2	9.3
KI75	36.9	40.3	40.6	17.7	7.1	11.7	8.9	11.6
KI86	20.1	22.5	13.8	11.7	5.1	10.1	9.4	7.1
KI92	11.9	15.3	9.4	7.8	6.2	3.9	4.4	4.6
Av.	29.5	35.2	29.2	15.4	7.8	9.3	8.8	8.9
Allende Group III[a]								
3593	20.8	24.6	24.4	21.3	13.2	8.2	11.9	6.4
4698	20.8	27.5	17.9	22.9	10.2	8.2	4.7	4.5
3529-0	27.7	31.8	31.5	19.2	32	16.4	28.4	19.5
3529-42	14.7	15.5	15.4	27.1	10.9	11.6	10.5	8.9
3529-41	22.5	22.0	23.4	19.7	22.5	13.7	21.7	13.8
3529-46	42.8	49.1	--	19.1	32.0	17.2	33.0	23.8
Av.	24.9	28.4	22.5	21.5	21.1	12.6	18.4	12.8
Kaba KI53	13.4	16.9	12.8	10.1	9.1	7.9	14.5	11.6
Allende Group II[a]								
3529-37	18.8	19.1	16.2	10.2	15.2	6.3	3.2	5.5
3598	22.1	28.4	26.0	20.3	13.0	9.6	5.3	3.2
3803	14.8	15.7	21.1	10.2	6.3	6.1	4.6	3.0
4691	41.6	55.1	50.3	23.3	15.2	17.2	10.1	11.1
4692	37.6	46.6	42.2	16.1	5.4	8.0	2.3	2.3
3529-40	51.1	61.9	62.0	27.7	7.9	4.8	0.09	5.2
5284	34.7	35.8	37.3	20.8	8.0	9.0	3.6	6.3
3655B	36.1	39.0	36.9	19.0	13.5	12.3	8.6	9.3
3529-43	36.3	36.9	37.5	22.1	8.0	5.5	2.3	7.1
4691	73.8	86.0	--	22.1	22.6	20.3	20.4	18.6
5242	15.4	14.0	20.8	12.6	9.1	10.0	6.9	6.3
Av.	34.8	39.9	35.0	18.6	11.3	9.9	6.1	7.1
Allende Group I(Av)[a]	14.8	17.4	17.4	17.4	17.0	21.3	15.8	18.3
Allende Group V(Av)[a]	21.3	21.8	20.4	19.0	20.2	20.9	21.8	19.8
Allende Group VI(Av)[a]	16.7	19.0	20.5	18.5	18.3	19.5	26.1	20.2

[a] Allende data are from Mason and Martin (1977) and Mason and Taylor (1982).

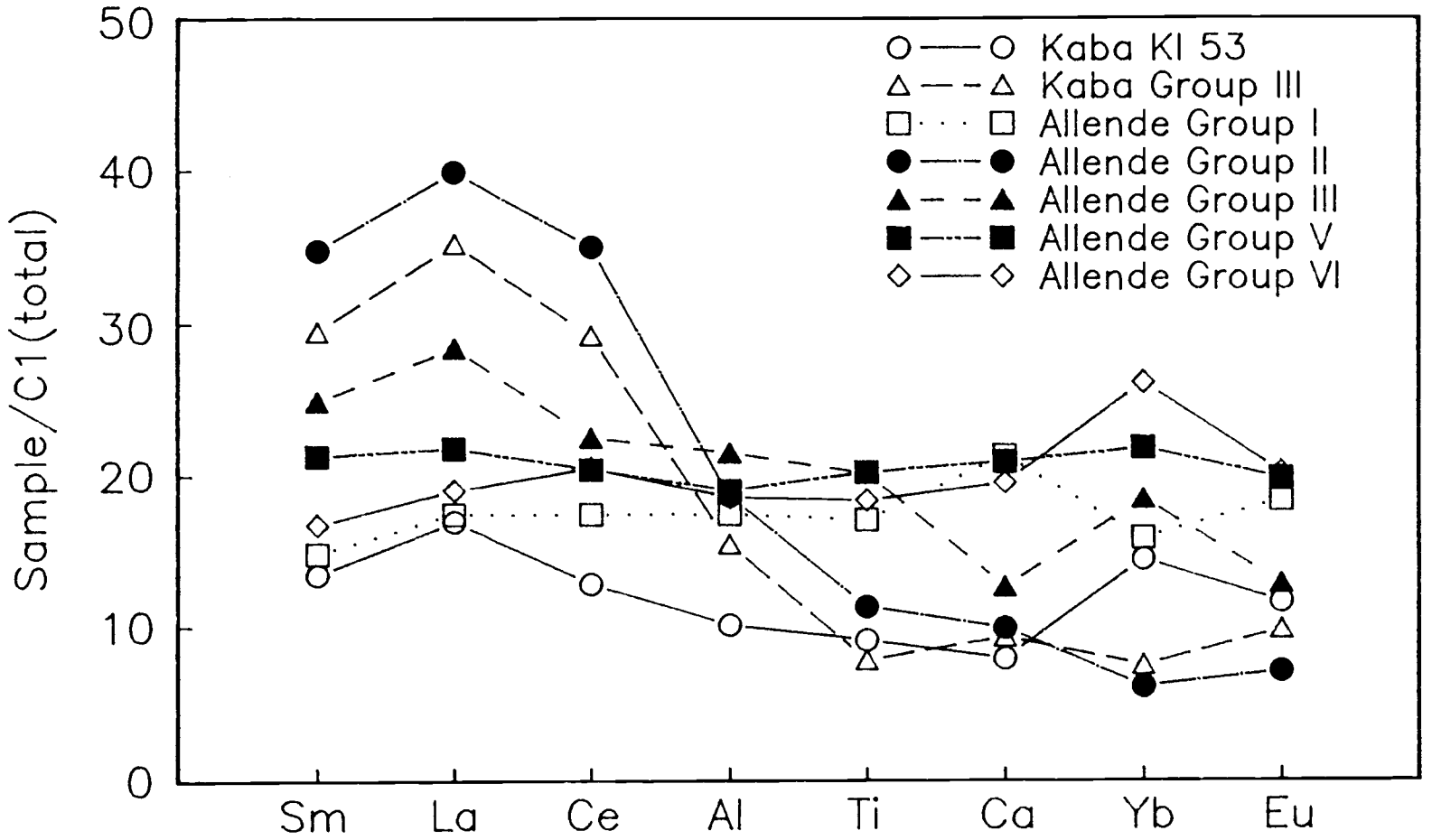

Figure 11.1 The Cl-normalized element abundances for various chemical groups in Kaba and Allende. Allende data are from Mason and Martin (1977) and Mason and Taylor (1982).

Ca is much lower and closer to Eu. Yb in this set of inclusions is somewhat higher than Eu. Examining individual inclusions in Table 11.1, I note that four of six Allende Group III inclusions have an enrichment factor lower than 25, in which Al is equally enriched while Ca is less enriched than are other refractory elements. In all Kaba Group III inclusions, Al is less enriched than are other refractory elements, and the enrichments of Ti and Ca are even lower and close to Yb and Eu. If Al, Ca and Ti are condensed as melilite, spinel and perovskite, then the total condensation of Al, Ca and Ti corresponds to ~4% of total condensable mass and would result in an enrichment of 25. The enrichment higher than 25 indicates partial condensation of Al+Ca+Ti. This is consistent in general with the observations of Kaba and Allende inclusions. The secondary alteration may reduce the enrichment by introducing more volatile elements such as Mg, Si, Fe, and Na.

For eleven Allende Group II inclusions, the enrichment factors in eight of them are higher than 25, and Al, Ti and Ca are less enriched than are the LREE. The enrichment of Al is higher than Ti in ten of eleven inclusions. This order is not consistent with the Group II formation mechanism if Al is a super-refractory element. A Group II pattern is presumed to be formed in a nebular volume where the gaseous phase has been depleted in the most-refractory elements, and Al has been depleted relative to Ti. The reversed enrichment order for Al and Ti is also observed in Allende Group II inclusions. The observed order is consistent with incomplete condensation of Al and Ti.

Group I, V and VI have basicaly unfractionated refractory element patterns. All Allende inclusions of these groups show equal enrichments of Al, Ti and Ca with other refractory elements. Enrichment factors are less than 25 except for one inclusion 3529-45 with 28xCl abundances.

From these observations, I suggest that the volatilities of Al, Ti and Ca are higher than expected from classic calculations. The observed order of increasing volatility is LREE, Al, Ti, Ca, Yb, Eu.

Hashimoto and Grossman(1987) have shown that the alteration of primary minerals in Ca-Al-rich inclusions involved element exchange between the inclusions and the gas phase. The inclusions lost Ca and gained Si, Fe, alkalis and in some cases Mg. Hashimoto and Wood(1986) pointed out that the key to this discrepancy may lie in local deviations of the nebular composition, specifically the H/O ratio, from the solar abundance pattern, and also in reactions that occur at lower temperatures. In a gas of solar composition, the alkaline earths evaporate at higher temperature via the dissociation of their oxides forming metal vapor. In a gas enriched in O (hence also H_2O), however, evaporation occurs via the formation of stable gaseous alkaline earth hydroxides. Their thermodynamic calculations show that the volatilities of alkaline earth elements are greatly enhanced in these circumstances. The uncertainties in the thermodynamic data prevent detailed conclusions from being drawn, but the calculations indicate that at $<1000^{\circ}K$ Ca and Al are as volatile as Mg and Si, even in a nebular volume having the solar elemental abundances. Experimental determination of $Ca(OH)_2$ vapor pressure (Hashimoto and

Wood, 1987) confirmed that Ca behaved as a volatile element when CAIs were being altered because it vaporized as $Ca(OH)_2(g)$ rather than as Ca(g). Ti has not yet been examined in the O-rich environment. From the observation in inclusions, the mechanism which causes less enrichment of Ti might be similar to Al and Ca.

Hashimoto and Wood's (1986) work provides a thermodynamic basis for understanding the relatively lower enrichments of Al and Ca relative to other refractory elements in inclusions. The only straightforward way to enhance O/H the ratio by orders of magnitude in the solar nebula is to concentrate dust and perhaps ice (both are rich in oxygen) locally relative to gas, and then postulate that a transient heating event vaporized a large fraction of the dust/ice releasing its oxygen into the gas phase (Wood, 1988). Silicate masses that remained unvaporized would be confined to an oxidizing gaseous environment. Gravitational settling of dust in the earliest evolving solar system would have concentrated dust near the nebular midplane.

The order of relative volatilities in Fig. 11.1 corresponds to the observed abundance order in Kaba and Allende CAIs. This order is attributed to vaporization or condensation in a high O/H environment. The condensation at higher temperature from solar composition gas phase should follow the order of classic calculation (Grossman, 1972).

In a series of papers, Boynton and Wark (1984, 1985, 1987), Wark and Boynton (1987), Wark et al. (1988), and Boynton (1988) demonstrated that REE patterns in CAI rims were identical to those in the underlying CAIs except that the concentrations of the REE were

higher in the rims by factors of 3-5, and that the most-volatile REE, Eu and sometimes Yb, were depleted. They suggested that the rims on the CAIs formed by a rapid heating process acting on a precursor CAI, leaving the rim as a refractory residue. The flash heating event formed a thin melt zone. After the melt quenched, the multiple, monomineralic layers were generated by solid-state metasomatism. They did not discuss how the major elements Al and Ca were evaporated by flash heating while the elements such as La, supposed to be more volatile than Al and Ca under classic solar nebular conditions, were not depleted.

From the above discussion, it seems that the transient heating is the key to understanding some of the above major observations. It is possible that the transient heating event caused the partial loss of the major elements Al, Ca, and possibly Ti in an oxidizing environment, thereby resulting in rim formation. The transient heating event also could have caused the depletion of both Yb and Eu relative to other REE, an important feature of both Group II and Group III patterns. The CAI precursor minerals likely formed at different nebular locations and conditions with resultant different element patterns. After the precursors had settled near or to the nebular midplane, a local transient heating event of unknown source created an oxygen-rich gas phase by evaporation of a large fraction of dust. In this oxidizing environment the volatilities of Al and Ca were enhanced and a fraction of them would be vaporized from the inclusions, resulting in the lesser enrichments of Al and Ca in the inclusions relative to other refractory elements. Also the rims were

likely formed as an evaporation residue. The transient heating event also caused the evaporization of the most-volatile REE Yb and Eu from the rims. The observed pattern of an inclusion would be the summation of at least two components, interior and rim (see two-component model of Group III pattern formation in Chapter 4). If Yb and Eu were strongly depleted yet in different degrees in the rim, and the interior has an unfractionated Yb and Eu pattern, then the observed pattern for the overall inclusion would show approximately equal Eu and Yb depletions, as observed in many Group II and Group III inclusions. If the inclusions have not experienced transient heating events or re-condensation occurred, the enrichment of these elements would remain unchanged. Group V and VI inclusions are such examples. This model accounts for rim formation and modification of the elemental pattern in a single event.

There are many unsolved problems. The transient heating source is unknown. It must have been very intense and of short duration. Boynton (1988) estimated that 300 watts/cm^2 are required to heat a CAI of 0.5 cm diameter to 1825°K in 1.2 seconds. The temperature required in this model is much lower for vaporizing Al, therefore the required power density of heating could be lower and the duration longer. Second, Boynton (1985) noted that Ce also tends to form a volatile oxide in an oxidizing environment, and that Ce depletions in most CAIs are not large enough to support more than a factor of 10-100 enhancement of O/H over cosmic. Third, Boynton and Wark (1987) have already demonstrated that REE patterns in rims are identical to those in the CAI interior except that REE in rims are more enriched

and Eu and Yb are depleted. These features are consistent with the two-component model. Detailed studies are needed to verify quantitatively this model.

Liu and schmitt (1988) interpreted the Eu and Yb depletions in Kaba Group III inclusions by the two-component model and the condensation in a highly reducing region in the solar nebula, and postulated that these Kaba inclusions were formed in a region with larger distance to the nebular midplane than was Allende. From the above considerations of the chemistries of Al, Ca, and REE, I prefer a two-component formation mechanism in an oxidizing environment.

12. COMPARISONS TO ALLENDE

Many important features are common for the CV3 chondrites Kaba and Allende. The whole-rock compositions are very similar with respect to major and trace elements, suggesting that Kaba and Allende mineral components were formed under similar conditions in the same general region in the primeval solar nebula. Also similar to Allende, a great variety of inclusions have been observed in Kaba. Many of these Kaba inclusions share the same common chemical patterns and petrographic features with Allende inclusions. The Kaba melilite-rich inclusions are composed of rounded or sub-rounded objects with sizes of 10-300 um, similar to the Allende "fluffy" Type A inclusions. The rim structure is another common feature. Olivine-rich inclusions are abundant in both Kaba and Allende. The similarities of spinel-rich inclusions in Kaba and Allende have been described by Fegley and Post (1985). The similarities for inclusions of many chemical groups and petrographic types in both Kaba and Allende suggest again that these two chondrites were formed in the same general solar nebular region.

However, differences exist between Kaba and Allende. In Kaba Group III inclusions, melilite contains a lower akermanite component than in Allende, indicating less interaction of gehlenite with the gas phase at a lower temperature. The Fe content is lower in Kaba spinels. An increase of Fe is only found in spinel at the outermost edge of a melilite-spinel core, suggesting that alteration took place between inclusion nodules and the gas phase before accretion. Another difference is that feldspathoids are found neither in the rims nor in the interiors of Kaba inclusions. Feldspathoids, forming a layer in

the rim of Allende inclusions (Wark and Lovering, 1977), are present as alteration products in the inclusions (MacPherson and Grossman, 1984) and in amoeboid olivine aggregates (Grossman and Steele, 1976). The Na and K contents are lower in Kaba Group III, KI53, and Group IV inclusions than are found in their Allende counterparts, which are consistent with the absence of feldspathoids. The absence of feldspathoids in Kaba suggests that the interaction of inclusions with the gas phase ceased before the feldspathoid formation temperature reached ~900°K (Grossman and Steele, 1976).

Kaba is less effected by metamorphism in the parent body as discussed in Chapter 1. Kaba is also less effected by secondary alteration with the gas phase before accretion compared to Allende.

13. SUMMARY

The Kaba CV3 chondrite is a collection of a great variety of inclusions as well as chondrules and matrix materials. In a 1.4 g specimen, the observed inclusions cover a wide range of chemical patterns, mineral assemblages and textures. The Cl-normalized elemental abundances in these inclusions show a smooth function with the volatilities of these elements, suggesting these inclusions were formed under the control of condensation/evaporization processes. The solar nebular conditions and locations for inclusion formation may be inferred from their chemical patterns and petrographic features. The great variety of inclusions in a small specimen indicates both strong nebular turbulence for mixing of inclusions formed at different locations and the complexity of local conditions.

Refractory elements, both lithophiles and siderophiles, in Group III inclusions are equally enriched (average 31xCl) with negative anomalies of Eu (average Eu/Eu^{*}=0.33) and Yb (average Yb/Yb^{*}=0.29). The depletions of Eu and Yb are of the same magnitude relative to other REE. This pattern is very similar to that observed in Allende Group III inclusions. Na is lower than in Allende fine-grained Group III inclusions. These Kaba Group III inclusions are irregular-shaped aggregates of rounded or sub-rounded nodules, except that KI60 consists of a single rounded body. These nodules are rich in gehlenitic melilite and spinel. Melilite has a limited compositional range, Ak2.5-14.3% with an average of 7.9%. Spinel is $MgAl_2O_4$ with 0-0.27% FeO in the nodule interior. The spinel at the outermost edge of the melilite-spinel core may contain higher Fe, ~1% FeO. Nodules in

most inclusions are rimmed by a sequence of thin and mineralogically distinct layers, consisting of, from interior outward, high-Al phase (HAP), Ti-Al pyroxene and/or diopside, and hedenbergite. The thickness of the entire rim sequence is 10-30 um. The sharply resolved BSE images, low Ak in melilite, low FeO content in spinel, and low Na in bulk inclusions all suggest that Kaba Group III inclusions are less altered than were their Allende counterparts.

The KI53 inclusion shows a strongly fractionated REE pattern which is similar to the typical Allende Group II pattern, but it differs in that KI53 shows no Eu and Yb negative anomalies. This pattern suggests that KI53 was formed at a lower temperature where Yb and Eu were equally condensed as were the other REE. KI53 is an irregular-shaped aggregate of rounded or sub-rounded nodules and their fragments. These nodules consist of melilite, spinel, high-Al phase and Ti-Al pyroxene in the core and surrounded by a band of Ti-Al pyroxene or diopside. They show different degrees of alteration.

KI77 and KI88 inclusions are unique in their mineral assemblage. They consist of anorthite, diopside, enstatite and a Si-rich phase in fine-grained areas. Spinel and melilite are absent. This mineralogy is found neither in known plagioclase-rich inclusions nor in the classic condensation sequence. Their REE patterns are similar to that of KI53. Their high Si and low Al contents and the REE pattern without Eu and Yb depletion suggest that these inclusions were condensed from a gas enriched in elements of moderate volatility probably as a liquid.

KI4 inclusion contains an ultra-refractory component. This component may be too small to be identified in petrographic study or it may have been altered mineralogically.

KI94 is a compound inclusion consisting of two components, one is a melilite-spinel spherule and the other contains melilite only. Chemically the refractory element pattern suggests a Group II-like pattern superposing on a Group VI pattern.

Most inclusions observed are olivine-rich exhibiting a Group IV pattern. The enrichments (1-5.5xCl) of refractory elements are lower than observed in CAIs. Their major constituent minerals are olivine and pyroxene. Anorthite is present in some inclusions.

Al, Ti and Ca are less enriched than other refractory elements in Kaba Group III inclusions, inconsistent with classic condensation calculations. The relatively lower enrichment of Al, Ti and Ca is also observed in Allende Group II and Group III inclusions. I suggest that the CAI precursors of these inclusions were formed at different nebular locations and conditions, acquiring different refractory element patterns. After they settled near the nebular midplane, a transient heating event created an oxygen-rich gas phase by evaporation of a large fraction of dust. In this oxidizing environment the volatilities of Al and Ca were enhanced and partially vaporized, resulting in the depletion of Al, Ca, and elements, such as Eu and Yb, which are more volatile than are Al and Ca. Ti may behave similarly to Al and Ca. As a result, rims were formed as the evaporization residue and the refractory element patterns were modified by the depletion of Al, Ti, Ca and the more volatile

elements, such as Eu and Yb. A two-component Group III pattern formation is proposed. One component is the CAI interior with an unfractionated pattern; the other is the residue rim with a similar pattern except for Eu and Yb that are strongly depleted in different degrees. The synthesized pattern of the whole CAI would show an unfractionated REE pattern with approximately equal depletions of Eu and Yb. This model combines rim formation and the modification of the refractory element pattern in the same event. The transient heating event plays a key role.

Several problems remain to be solved. The nature of the transient heating is unknown, the limit of enhanced O/H change which does not cause a significant Ce depletion needs to be further examined, and quantitative experimental data are needed to verify the two-component Group III pattern formation.

The similarities of Kaba and Allende in their whole-rock compositions and mineral assemblages and textures suggest they were formed in a same general region of the solar nebula. Yet differences do exist. Kaba inclusions are less altered by secondary reactions between inclusions and gas phase at a lower temperature than are Allende inclutions, therefore, informations of the early solar nebula conditions are better preserved in the Kaba CV3 meteorite.

BIBLIOGRAPHY

Allen J.M., Grossman L., Davis A.M. and Hutcheon I.D. (1978) Mineralogy, texture and mode of formation of a hibonite-bearing Allende inclusion. Proc. Lunar Planet. Sci. Conf. 9th, 1209-1233.

Armstrong J.T. and Wasserburg G.J. (1981) The Allende pink angel: its mineralogy, petrology, and the constraints of its genesis. Lunar Planet. Sci. XII, 25-27.

Blander M. and Fuchs L.H. (1975) Calcium-aluminum-rich inclusions in the Allende meteorite: Evidence for a liquid origin. Geochim. Cosmochim. Acta 39, 1605-1619.

Boynton W.V. (1975) Fractionation in the solar nebula: condensation of yttrium and the rare earth elements. Geochim. Cosmochim. Acta 39, 569-584.

Boynton W.V. (1983) Cosmochemistry of the rare earth elements: meteorite studies. in Rare Earth Element Geochemistry (ed. P. Henderson), 63-114. Elsvier.

Boynton W.V. (1985) Meteoritic evidence concerning conditions in the solar nebular. in Protostars and Planets II (eds. D.C. Black and M.S. Mathews), pp. 772-787. Tucson, Univ. Arizona Press.

Boynton W.V. (1988) Nebular processes associated with CAI rim formation. Met. 23, 259.

Boynton W.V. and Frazier R.M. (1980) Identification of an ultra-refractory component in the Muchison meteorite. Lunar Planet. Sci. XI, 103-105.

Boynton W.V. and Wark D.A. (1984) Trace element abundances in rim layers of an Allende type A coarse-grained, Ca, Al-rich inclusions. Met. 19, 195-197.

Boynton W.V. and Wark D.A. (1985) Refractory rims: evidence for high temperature events in the post-formation history of Ca, Al-rich inclusions. Met. 20, 613-614.

Boynton W.V. and Wark D.A. (1987) Origin of CAI rims: I. the evidence from the rare earth elements. Lunar Planet. Sci. XVIII, 117-118.

Boynton W.V., Frazier R.M. and Macdougall J.D. (1980) Identification of an ultra-refractory component in the Murchison meteorite. Lunar Planet. Sci. XI, 103-105.

Bunch T.E. and Chang S. (1980) An alternative origin for Allende CAI inclusion rims, or a correlation between the early solar system and a British steel furnace. Met. 15, 270-271.

Clarke R.S., Jr., Jarosewich E., Mason B., Nelen J., Gomez M. and Hyde J.R. (1970) The Allende Mexico meteorite shower. Smithson. Contrib. Earth Sci. No.5.

Cohen R.E., Kornacki A.S. and Wood J.A. (1983) Mineralogy and petrology of chondrules and inclusions in the Mokoia CV3 chondrite. Geochim. Cosmochim. Acta 47, 1739-1757.

Conard R. (1976) A study of the chemical composition of Ca-Al-rich inclusions from the Allende meteorite. M.S. Thesis, Oregon State University.

Davis A.M. and Grossman L. (1979) Condensation and fractionation of rare earths in the solar nebula. Geochim. Cosmochim. Acta 43, 1611-1632.

Ekambaram V., Kawabe I., Tanaka T., Davis A.M. and Grossman L. (1984) Chemical compositions of refractory inclusions in the Murchison C2 chondrite. Geochim. Cosmochim. Acta 48, 2089-2106.

El Goresy A., Ramdohr P. and Nagel K. (1980) A unique inclusion in Allende meteorite: A conglomerate of hundreds of various fragments and inclusions (abstract). Met. 15, 286-287.

Fegley B., Jr. and Palme H. (1985) Evidence for oxidizing conditions in the solar nebular from Mo and W depletion in refractory inclusions in carbonaceous chondrites. Earth Planet. Sci. Lett. 72, 311-326.

Fegley B., Jr. and Post J.E. (1985) A refractory inclusion in the Kaba CV3 chondrite: Some implications for the origin of spinel-rich objects in chondrites. Earth Planet. Sci. Letts. 75, 297-310.

Gray C.M., Papanastassiou D.A. and Wasserburg G.J. (1973) The identification of early condensates from the solar nebular. Icarus 20, 213-239.

Grossman L. (1972) Condensation in the primitive solar nebular. Geochim. Cosmochim. Acta 36, 597-619.

Grossman L. (1975) Petrography and mineral chemistry of Ca-rich inclusions in Allende meteorite. Geochim. Cosmochim. Acta 39, 433-454.

Grossman L. and Ganapathy R. (1976a) Trace elements in the Allende meteorite--I. coarse-grained, Ca-rich inclusions. Geochim. Cosmochim. Acta 40, 331-344.

Grossman L. and Ganapathy R. (1976b) Trace elements in Allende meteorite--II. fine-grained, Ca-rich inclusions. Geochim. Cosmochim. Acta 40, 967-977.

Grossman L. and Steele I.M. (1976) Amoeboid olivine aggregates in the Allende meteorite. Geochim. Cosmochim. Acta 40, 149-155.

Grossman L., Ganapathy R., Methot R.L. and Davis A.M. (1979) Trace in the Allende meteorite--IV. Amoeboid olivine aggregates. Geochim. Cosmochim. Acta 43, 817-829.

Hashimoto A. and Grossman L. (1987) Alteration of Al-rich inclusions inside amoeboid olivine aggregates in the Allende meteorite. Geochim. Cosmochim. Acta 51, 1685-1704.

Hashimoto A. and Wood J.A. (1987) Enhanced volatility of CaO in H_2O-rich gas environments as a factor in the alteration of Ca, Al-rich inclusions. Met. 21, 391-392.

Hashimoto A. and Wood J.A. (1988) Experimental determination of $Ca(OH)_2$ vapor pressure as a key to understanding the alteration of Ca, Al-rich inclusions. Met. 22, 405-406.

Jarosewich E., Clarke R.S., Jr. and Barrows J.N. (1987) The Allende meteorite reference sample. Smithson. Contrib. Earth Sci. No.27.

Kallemeyn G. W. and Wasson J.T. (1981) The compositional classification of chondrites--I. The carbonaceous chondrite groups. Geochim. Cosmochim. Acta 45, 1217-1230.

Korina M.I., Nazarov M.A. and Ulyyanov A.A. (1982) Efremovk CAI's: composition and origin of rims. Lunar Planet. Sci. XIII, 399-400.

Kornacki A.S., Cohen R.E. and Wood J.A. (1983) Petrography and classification of refractory inclusions in the Allende and Mokoia CV3 chondrites. Mem. Natl. Inst. Polar Res., Spec. Issue No.30, 45-60.

Kornacki A.S. and Fegley B., Jr. (1984) Origin of spinel-rich chondrules and inclusions in carbonaceous and ordinary chondrites. Proc. Lunar Planet. Sci. Conf. 14th, J. Geophy. Res. 89, Suppl. Part 2, B588-B596.

Kornacki A.S. and Fegley B., Jr. (1986) The abundance and relative volatility of refractory trace elements in Allende Ca, Al-rich inclusions: implications for chemical and physical processes in the solar nebula. Earth Planet. Sci. Lett. 79, 217-234.

Kornacki A.S. and Wood J.A. (1984) Petrography and classification of Ca, Al-rich and olivine-rich inclusions in the Allende CV3 chondrite. Proc. lunar Sci. Conf. 14th, J. Geophy. Res. 89, Suppl. Part 2, B573-B587.

Kring D.A. and Holmén B.A. (1988) Petrology of anorthite-rich chondrules in CV3 and CO3 chondrites. Met. 23, 282-283.

Kuehner S.M. and Grossman L. (1987) Petrography of a corundum-bearing compound Allende inclusion. Met. 22, 433-434.

Laughlin J.R., Davis A.M., Kuehner S.M. and Grossman L. (1988) Rare earth elements in a compound Group II Allende inclusion. Lunar Planet. Sci. XIX, 661-662.

Liu Y.-G. and Schmitt R.A. (1988) The relative locations for the formation of parental components in the CV3 chondrite Kaba, Mokoia and Allende. Lunar Planet. Sci. XIX, 684-685.

MacPherson G.J. and Grossman L. (1984) "Fluffy" type A Ca,-Al-rich inclusions in the Allende meteorite. Geochim. Cosmochim. Acta 48, 29-46.

MacPherson G.J., Grossman L. Allen J.M. and Beckett J.R. (1981) Origin of rims on coarse-grained inclusions in the Allende meteorite. Proc. Lunar Planet. Sci. 12B, 1079-1091.

Martin P.M. and Mason B. (1974) Major and trace elements in the Allende meteorite. Nature 249, 333-334.

Marvin U.B., Wood J.A. and Dickey J.S. Jr. (1970) Ca-Al-rich phases in the Allende meteorite. Earth Planet. Sci. Letts. 7, 346-350.

Mason B. and Martin P.M. (1974) Minor and trace element distribution in melilite and pyroxene from the Allende meteorite. Earth Planet. Sci. Lett. 22, 141-144.

Mason B. and Martin P.M. (1977) Geochemical differences among components of the Allende meteorite. Smithson. Contrib. Earth Sci. No.19, 84-95.

Mason B. and Taylor S.R. (1982) Inclusions in the Allende meteorite. Smithson. Contrib. Earth Sci. No.25.

McSween H.Y., Jr. (1977) Petrographic variations among carbonaceous chondrites of the Vigarano type. Geochim. Cosmochim. Acta 41, 1777-1790.

McSween H.Y., Jr. and Richardson S.M. (1977) The composition of carbonaceous chodrite matrix. Geochim. Cosmochim. Acta 41, 1145-1161.

Nagasawa H., Blanchard D.P., Jacobs J.W., Brannon J.C., Philpotts J.A. and Onuma N. (1977) Trace element distribution in mineral separates of the Allende inclusions and their genetic implications. Geochim. Cosmochim. Acta 41, 1587-1600.

Nagasawa H., Blanchard D.P., Shimizu H. and Masuda A. (1982) Trace element concentrations in the isotopically unique Allende inclusion, EK1-4-1. Geochim. Cosmochim. Acta 46, 1669-1673.

Osborn T.W., Warren R.G., Smith R.H and Wakita H., Zellmer D.L. and Schmitt R.A. (1974) Elemental composition of individual chondrules from carbonaceous chondrites, including Allende. Geochim. Cosmochim. Acta 38, 1359-1378.

Palme H., Wlotzka F., Nagel K. and El Goresy A. (1982) An ultra-refractory inclusion from the Ornans carbonaceous chondrite. Earth Planet. Sci. Lett. 61, 1-12.

Peck J.A. (1983) Chemistry of CV3 matrix minerals and Allende chondrule olivine. Met. 18, 373-374.

Peck J.A. (1984) Origin of the variation in properties of CV3 meteorite matrix and matrix clasts. Lunar Planet. Sci. XV, 635-636.

Schmitt R.A., Goles G.G., Smith R.H. and Osborn T.W. (1972) Elemental abundances in stone meteorites. Met. 7, 131-213.

Sheng Y.J., Hutcheon I.D. and Wasserburg G.J. (1988) Plagioclase-olivine inclusions in Allende. Lunar Planet. Sci. XIX, 1075-1076.

Sztrokáy K.I., Tolnay V. and Földvary-Vogl M. (1961) Mineralogical and chemical properties of the carbonaceous meteorite from Kaba, Hungary. Acta Geol. (Hungary) 7, 57-103.

Tanaka T. and Masuda A. (1973) Rare-earth elements in matrix, inclusions and chondrules of the Allende meteorite. Icarus 19, 523-530.

Tomeok K. and Buseck P.R. (1986) Phyllosilicates in the Mokoia CV3 carbonaceous chondrite: petrographic and transmission electron microscope observasions. Lunar Planet. Sci. XVII, 899-900.

Van Schmus W.R. (1969) Mineralogy, petrology and clasification of types 3 and 4 carbonaceous chondrites. In Meteorite Research (ed. P.M. Milman), 480-491.

Van Schmus W.R. and Hayes J.M. (1974) Chemical and petrographic correlations among carbonaceous chondrites. Geochim. Cosmochim. Acta 38, 47-64.

von Torok J. (1858) Ueber den Kaba-Debreczin-Meteorit. Ann. Phys. Chem. Poggendorff, Ser. IV, 15, 329-334.

Wai C.M. and Wasson J.T. (1977) Nebular condensation of moderately volatile elements and their abundances in ordinary chondrites. Earth Plant. Sci. Lett. 36, 1-13.

Wark D.A. (1981) Alteration and metasomatism of Allende Ca-Al-rich materials. Lunar Planet. Sci. XII, 1145-1147.

Wark D.A. (1984) The Allende meteorite: information from Ca-Al-rich inclusions on the formation and early evolution of the solar system. Ph.D. Thesis, University of Melbourne, Australia.

Wark D.A. (1985) Combined chemical/petrological classification of Ca-Al-rich inclusions. Lunar planet. Sci. XVI 887-888.

Wark D.A. (1986) Evidence for succesive episodes of condensation at high temperature in a part of the solar nebula. Earth Planet. Sci. Lett. 77, 129-148.

Wark D.A. (1987) Palgioclase-rich inclusions in carbonaceous chondrite meteorites: Liquid condensation? Geochim. Cosmochim. Acta 51, 221-242.

Wark D.A. and Boynton W.V. (1984) The relationship between size and composition of Allende CAI's. Lunar Planet. Sci. XV, 888-889.

Wark D.A. and Boynton W.V. (1987) Origin of CAI rims--II: The evidence from refractory metals, major elements and mineralogy. Lunar Planet. Sci. XVIII, 1054-1055.

Wark D.A. and Lovering J.F. (1977) Marker events in the early evolusion of the solar system: evidence from rims on Ca-Al-rich inclusions in carbonaceous chondrites. Proc. Lunar Sci. Conf. 8th, 95-112.

Wark D.A., Spettel B., Palme H. and El Goresy A. (1988) Rim formation by flash heating and metasomatism: evidence from Vigarano CAI VI-1. Lunar Planet. Sci. XIX, 1230-1231.

Wasson J.T. (1985) Meteorites: Their Record of Early Solar System History. Appendix G. W. H. Freeman and Co.

Wood J.A. (1988) Chondritic meteorites and the solar nebular. Ann. Rev. Earth Planet. Sci. 16, 53-72.

Wood J.A. and Hashimoto A. (1988) The condensation sequence under non-classic conditions ($P<10^{-3}$atm, non-cosmic composition). Lunar Planet. Sci. XIX, 1292-1293.

APPENDIX

Appendix Table I. Elemental analyses of whole rock and matrix of Kaba and Mokoia, and the matrix of Allende[a]

Sample	KW1	KW2	KM2	KM3	MW1	MW2	MM1	MM2	AM1	AM2	AM3	Uncertainty (%)
Weight (mg)	132.6	129.8	2.22	2.85	200.1	111.0	2.582	1.984	3.52	0.675	2.94	
Ti (%)	0.072	0.108	0.062	0.053	0.060	0.114	0.083	0.075	0.066	0.034	0.060	10-25
Al	1.31	1.54	1.18	1.21	1.40	1.58	1.19	1.56	1.39	1.14	1.42	2-5
Fe	21.4	24.9	25.0	25.8	22.8	23.7	25.3	22.7	26.2	27.8	27.2	2-5
Mg	13.5	13.0	11.1	14.4	12.5	13.0	9.7	9.8	12.8	12.3	11.5	2-5
Ca	1.46	1.58	1.14	1.33	1.50	1.66	1.27	1.60	1.59	1.36	1.62	3-6
Na	0.34	0.36	0.33	0.39	0.35	0.40	0.36	0.34	0.137	0.145	0.24	2-5
K (%)	0.030	0.031	0.030	0.038	0.030	0.033	0.029	0.029	0.011	0.017	0.027	10-15
Sc (ppm)	7.7	9.8	7.6	7.5	9.1	9.9	7.5	8.8	7.9	7.9	10.5	2-5
V	74	76	63	59	76	86	65	85	73	61	72	3-6
Cr	2810	3210	3220	3260	2860	3070	3270	3170	2740	2690	2690	3-6
Mn	1330	1390	1560	1520	1310	1360	1480	1390	1580	1690	1410	2-5
La	0.40	0.47	0.35	0.35	0.49	0.80	0.35	0.41	0.54	0.75	0.76	10-20
Ce	1.2	1.3	-	-	1.3	1.1	0.9	1.1	-	-	-	20-30
Sm	0.223	0.246	0.215	0.207	0.247	0.265	0.230	0.266	0.237	0.210	0.334	3-6
Eu	0.101	0.095	0.095	0.093	0.104	0.112	0.103	0.131	0.084	0.142	0.096	5-10
Dy	0.34	0.57	0.39	0.35	0.50	0.57	0.35	0.35	0.34	0.35	0.24	20-30
Ho	-	-	0.068	0.075	0.068	-	0.067	0.056	-	-	-	20-30
Yb	0.32	0.27	0.24	0.29	0.34	0.31	0.26	0.23	0.38	0.34	0.46	20-30
Lu	0.023	0.029	0.033	0.027	0.033	0.026	0.048	0.023	0.020	0.029	0.022	20-30
Hf	0.20	0.15	0.13	0.12	0.16	0.15	-	-	-	-	-	20-30
Co	580	670	600	620	610	640	650	600	650	630	600	2-5
Ni	12700	14500	12900	14400	13200	13900	16900	15300	13200	13300	12700	2-5
Zn	150	130	150	150	180	150	150	150	120	220	190	10-25
Ga	5.8	6.9	6.3	7.3	5.9	6.6	7.5	7.5	6.3	6.2	6.3	5-10
As	2.1	2.0	2.0	1.9	2.0	2.3	2.5	1.8	2.1	1.7	1.7	10-20
Se	9.4	13.0	6.1	9.8	8.6	11.0	14	13	10.6	7.5	9.8	10-25
Br	1.8	1.7	1.9	1.7	1.6	2.6	1.7	1.7	2.7	4.3	1.3	10-20
Ru	0.74	0.80	0.5	1.1	0.83	1.00	0.90	0.50	0.57	0.55	0.59	15-30
Sb	0.13	0.13	0.067	0.075	0.12	0.085	0.051	0.088	0.22	0.18	0.063	15-30
Re	0.040	0.049	-	-	0.060	0.066	0.032	0.028	0.061	0.070	0.054	15-30
Os	0.48	0.58	0.37	0.45	0.56	0.65	0.64	0.51	0.75	0.73	0.87	15-25
Ir	0.47	0.53	0.40	0.37	0.48	0.65	0.59	0.60	0.55	0.56	0.51	2-5
Au (ppm)	0.178	0.172	0.126	0.144	0.153	0.146	0.152	0.153	0.138	0.27	0.116	2-5

a. KW - Kaba whole rock, KM - Kaba matrix, MW - Mokoia whole rock, MM - Mokoia matrix, AM - Allende matrix.

Appendix Table II. Elemental analyses of Kaba inclusions

Sample	KI60	KI62	KI73	KI74	KI75	KI86	KI92	KI31	KI53	KI77	KI88	KI4	KI94	KI6	KI39	KI42	KI43	KI59
Weight (mg)	0.203	0.097	0.312	0.339	0.151	0.188	0.72	0.056	0.156	0.184	0.182	0.143	0.695	0.207	0.036	0.084	0.684	0.263
Ti (%)	0.36	0.48	0.38	0.28	0.31	0.22	0.27	0.29	0.40	0.34	-	0.34	1.0	0.14	0.41	0.17	0.08	0.22
Al	18.2	19.8	13.1	12.3	15.8	9.0	5.5	7.0	8.8	9.6	-	3.9	12.6	2.8	5.0	1.51	1.23	1.82
Fe	4.1	3.3	7.0	9.6	6.5	12.5	19.2	12.6	10.6	0.81	12.0	9.2	3.3	4.4	16.1	1.8	26.3	11.3
Mg	7.7	7.5	6.9	8.2	7.7	7.4	11.7	13.6	10.2	6.6	-	16.7	3.9	21.6	14.9	31.7	15.8	4.9
Ca	10.6	11.0	9.5	7.4	10.5	7.8	3.1	6.1	7.3	8.8	-	0.82	19.6	2.6	3.4	0.79	0.32	1.3
Na	0.29	0.52	0.37	0.51	0.49	0.34	0.38	0.41	0.72	0.47	0.38	0.75	0.31	0.185	0.64	0.21	0.13	0.74
K (%)	0.031	0.038	0.032	0.063	0.043	-	0.036	0.059	0.076	-	-	0.096	-	0.019	0.017	0.010	0.011	0.094
Sc (ppm)	228	259	160	136	265	98	91	12.3	14.7	16.9	10.9	78	171	17.2	29.8	8.9	7.9	27.3
V	1340	1420	920	870	1120	630	410	410	500	250	-	70	310	129	250	112	77	79
Cr	320	410	480	850	290	1170	1930	2000	1220	3100	3300	4100	330	1360	1530	1440	3500	1720
Mn	450	510	840	970	650	1430	1620	1080	1030	1080	930	1350	230	1220	1350	370	730	1630
La	11.3	11.9	8.6	7.9	9.5	5.3	3.6	3.0	4.0	2.8	-	1.2	3.4	0.69	-	-	-	0.94
Ce	24	23	19	20	25	8.5	5.8	-	7.9	7.9	-	3.5	10	-	-	-	-	-
Nd	18	20	17	15	22	-	6.3	-	7.3	-	-	-	6.5	-	-	-	-	-
Sm	5.7	6.1	4.6	4.3	5.5	3.0	1.77	1.66	2.00	1.82	0.71	1.1	2.5	0.47	0.75	0.17	0.20	0.77
Eu	0.65	0.83	0.54	0.52	0.65	0.40	0.26	0.44	0.65	0.68	0.22	0.28	1.4	0.23	0.41	0.06	0.08	0.32
Tb	-	-	0.85	-	-	0.86	0.44	-	-	-	-	-	1.9	-	-	-	-	-
Dy	8.5	11.6	7.6	7.1	8.2	5.8	5.8	0.88	1.1	1.2	0.63	3.1	10.5	1.0	1.4	0.44	0.42	1.2
Ho	1.9	2.7	2.1	2.2	2.2	0.63	0.72	0.44	0.15	0.20	-	0.70	0.85	-	-	-	-	0.19
Tm	-	-	-	-	-	0.58	-	0.38	0.40	0.19	-	-	1.1	-	-	-	-	-
Yb	1.2	2.3	1.4	1.3	1.4	1.5	0.70	1.7	2.3	2.6	0.93	0.91	4.5	-	0.80	-	-	1.2
Lu	0.68	0.90	0.56	0.42	0.74	0.43	0.36	0.22	0.10	0.11	-	0.27	0.31	-	-	-	-	0.090
Hf	3.0	5.0	4.4	3.5	3.0	2.3	2.4	-	0.36	-	-	-	1.3	-	-	-	-	-
Th	1.5		1.8	0.99	1.8	-	-	-	-	-	-	-	1.9	-	-	-	-	-
Co	80	50	130	200	90	270	480	230	170	19	390	220	68	154	210	45	620	150
Ni	2470	1610	7930	13140	1820	6730	10290	5500	4230	290	9020	5400	1790	3400	4300	800	16570	3550
Zn	95	210	170	320	250		240	360	280	105		120	130	-	-	-	-	220
Ga	2.5	0.4	2.7	4.6	2.0	6.2	4.8	4.6	3.4	0.58	3.7	0.9	1.9	1.5	0.50	10.2	3.0	3.3
As	0.8	1.7	1.3	1.8	1.5	2.9	1.8	3.2	1.0	-	1.3	0.94	0.90	0.29	1.9	2.6	2.0	0.40
Se	-	-	-	-	-	-	-	-	-	-	-	-	-	-	-	-	-	15
Br	3.1	-	4.9	6.9	11	-	4.8	-	-	-	-	2.5	5.2	-	-	-	-	3.1
Ru	21	25	18	14	14	10.8	7.5	-	-	-	-	-	8.1	-	-	-	-	-
Re	1.17	2.3	1.45	0.51	1.62	0.42	0.24	-	-	-	-	-	0.22	-	-	-	-	0.093
Os	22	31	45	14	20	5.5	4.0	-	-	-	-	0.44	2.8	0.70	-	-	-	1.6
Ir	27	29	26	16	28	8.0	5.7	0.25	0.17	-	0.49	0.32	3.7	1.02	2.2	0.062	0.47	2.5
Au (ppm)	0.035	0.084	0.047	0.142	0.064	0.036	0.040	0.034	0.024	-	-	0.039	0.021	0.014	0.038	-	0.051	0.041

Appendix Table II. Elemental analyses of Kaba inclusions (continued)

Sample	KI61	KI65	KI72	KI76	KI80	KI85	KI96	KI2	KI7	KI8	KI9	KI10	KI13	KI33	KI34	KI35	KI36	KI37
Weight (mg)	0.243	0.092	1.500	0.357	0.662	0.297	0.454	0.277	0.056	0.075	0.038	0.022	0.043	0.126	0.076	0.057	0.043	0.113
Ti (%)	0.16	0.26	0.046	0.12	0.054	0.33	0.05	0.14	0.18	-	-	-	-	0.11	0.25	-	-	-
Al	3.1	2.00	1.34	2.4	1.37	3.0	0.87	1.69	1.32	-	-	-	-	1.62	5.6	-	-	-
Fe	7.6	11.2	11.9	10.0	17.1	8.0	26.0	4.8	7.4	4.6	4.9	5.4	13.7	9.5	19.9	25.7	24.6	2.5
Mg	18.8	21.4	16.5	20.1	14.5	17.4	12.5	25.6	20.0	-	-	-	-	20.6	9.5	-	-	-
Ca	4.0	1.7	1.41	-	1.89	1.8	1.2	1.13	-	-	-	-	-	0.89	5.6	-	-	-
Na	0.21	0.61	0.22	0.083	0.36	0.151	0.41	0.273	0.134	0.069	0.113	0.158	0.20	0.22	0.46	0.26	0.21	0.171
K (%)	0.024	0.049	0.022	-	0.028	0.021	0.025	0.045	0.017	0.012	0.041	0.091	0.049	0.029	0.063	0.028	0.030	0.022
Sc (ppm)	22.1	22.1	9.5	16.8	8.9	20.6	5.6	14.5	10.3	5.7	11.6	14.6	14.9	11.1	10.4	5.5	5.3	10.0
V	119	62	61	98	69	104	50	61	60	-	-	-	-	67	300	-	-	-
Cr	1040	1750	1930	1440	2200	1440	2800	2200	1820	1180	1380	1700	1820	2700	1680	1430	810	1870
Mn	540	1560	930	530	1590	830	1660	830	1440	810	740	2600	2200	730	1500	1700	2310	540
La	0.78	1.2	-	-	-	-	-	0.60	0.75	-	-	-	-	-	-	-	-	-
Ce	-	-	-	-	-	-	-	-	-	-	-	-	-	-	-	-	-	-
Nd	-	-	-	-	-	-	-	-	-	-	-	-	-	-	-	-	-	-
Sm	0.65	0.58	0.24	0.52	0.29	0.47	0.15	0.39	0.28	0.15	0.35	0.38	0.48	0.23	1.02	0.17	0.20	0.17
Eu	0.27	0.24	0.12	0.27	0.11	0.16	0.089	0.13	0.17	0.11	0.13	0.17	0.18	0.12	0.40	0.14	0.096	0.083
Tb	-	-	-	-	-	-	-	-	-	-	-	-	-	-	-	-	-	-
Oy	1.0	1.1	0.46	0.79	0.43	0.80	0.44	0.72	0.53	0.23	0.47	0.65	0.80	0.36	1.0	0.40	0.57	-
Ho	0.21	-	-	0.20	-	0.30	-	-	-	-	-	-	-	-	0.35	-	-	-
Tm	-	-	-	-	-	-	-	-	-	-	-	-	-	-	-	-	-	-
Yb	0.79	0.60	-	-	-	0.59	0.28	-	-	-	-	-	-	-	0.90	-	-	-
Lu	0.15	0.11	-	-	-	0.054	0.048	-	-	-	-	-	-	-	-	-	-	-
Hf	-	-	-	-	-	-	-	-	-	-	-	-	-	-	-	-	-	-
Th	-	-	-	-	-	-	-	-	-	-	-	-	-	-	-	-	-	-
Co	270	220	300	440	410	210	560	119	213	178	160	220	300	260	340	540	440	39
Ni	6000	5440	7810	9020	9860	4770	12720	2950	5460	4130	3600	5100	6900	6290	9310	12820	9760	830
Zn	67	-	66	-	83	-	96	-	-	-	-	-	-	-	300	-	-	-
Ga	0.42	4.0	4.8	1.4	7.1	1.8	9.4	3.1	2.9	1.4	0.75	-	2.4	3.6	4.1	3.2	4.7	1.0
As	0.55	3.6	1.8	0.8	2.2	1.2	2.4	0.46	-	-	-	-	0.74	2.0	3.8	2.7	1.9	1.0
Se	-	-	-	15	25	-	13	16	-	-	-	-	-	-	-	-	-	-
Br	2.4	-	0.86	1.1	1.1	-	-	0.90	1.2	-	-	-	-	-	-	-	-	-
Ru	-	-	-	2.7	-	-	-	-	-	-	-	-	-	-	-	-	-	-
Re	-	-	-	0.051	0.055	-	-	-	-	-	-	-	-	-	-	-	-	-
Os	2.0	1.9	0.60	2.0	-	1.1	-	-	-	-	-	-	-	-	-	-	-	-
Ir	2.4	2.2	1.06	1.36	0.64	1.16	0.46	0.068	0.52	0.31	0.88	1.11	0.98	0.25	0.28	0.45	0.39	0.10
Au (ppm)	0.043	0.072	0.189	0.025	0.29	0.024	0.055	0.011	0.097	0.034	0.023	0.017	0.087	0.089	0.036	0.054	0.027	0.039

Appendix Table II. Elemental analyses of Kaba inclusions (continued)

Sample	KI40	KI44	KI51	KI52	KI54	KI56	KI58	KI63	KI67	KI68	KI69	KI70	KI71	KI78	KI79	KI81	KI82	KI83
Weight (mg)	0.029	0.179	0.148	0.094	0.101	0.125	0.081	0.163	0.079	0.159	0.927	0.725	0.646	0.250	0.149	0.356	0.531	1.222
Ti (%)	-	-	-	-	-	-	-	-	-	-	-	-	-	-	-	0.17	-	-
Al	-	-	-	-	-	-	-	-	-	-	-	-	-	-	-	2.7	-	-
Fe	16.4	19.4	6.4	10.0	24.6	16.6	12.0	16.1	8.9	4.5	14.3	9.9	6.6	21.0	13.6	16.5	8.3	20.5
Mg	-	-	-	-	-	-	-	-	-	-	-	-	-	-	-	5.3	-	-
Ca	-	-	-	-	-	-	-	-	-	-	-	-	-	-	-	2.2	-	-
Na	0.130	0.33	0.33	0.29	0.46	0.34	0.094	0.120	0.187	0.122	0.27	0.142	0.158	0.28	0.164	0.98	0.194	0.44
K (%)	0.083	0.037	0.039	-	0.058	0.025	-	0.014	0.024	-	0.026	0.0068	0.019	0.26	-	0.054	0.020	0.026
Sc (ppm)	3.8	10.0	10.4	17.7	7.5	27.8	6.0	12.6	8.4	13.5	9.4	13.6	19.3	6.0	7.7	30.3	14.5	8.1
V	-	-	-	-	-	-	-	-	-	-	-	-	-	-	-	165	-	-
Cr	330	3200	4200	4600	2200	1780	1480	2000	1430	810	1860	1450	1410	2400	2000	2200	1540	2500
Mn	1370	960	2400	1340	1410	1230	1090	1180	1480	370	1770	710	770	1400	1160	1870	850	1490
La	-	0.52	-	0.98	0.51	1.3	-	-	-	-	-	-	0.71	-	-	-	-	-
Ce	-	-	-	-	-	-	-	-	-	-	-	-	-	-	-	-	-	-
Nd	-	-	-	-	-	-	-	-	-	-	-	-	-	-	-	-	-	-
Sm	0.15	0.34	0.23	0.57	0.51	0.77	0.17	0.32	0.24	0.41	0.23	0.38	0.54	0.19	0.20	0.85	0.39	0.20
Eu	0.11	0.14	0.082	0.23	0.16	0.32	0.089	0.17	0.084	0.20	0.12	0.16	0.20	0.089	0.15	0.30	0.21	0.092
Tb	-	-	-	-	-	-	-	-	-	-	-	-	-	-	-	-	-	-
Dy	0.32	0.75	0.34	1.1	0.36	1.4	0.36	0.75	0.37	0.54	0.47	0.69	0.89	0.30	0.38	0.80	0.61	0.34
Ho	-	-	-	-	-	-	-	0.19	-	-	-	-	0.26	-	-	-	-	-
Tm	-	-	-	-	-	-	-	-	-	-	-	-	-	-	-	-	-	-
Yb	-	-	-	-	-	1.1	-	-	-	-	-	-	0.46	-	-	1.1	-	-
Lu	-	-	-	-	-	0.16	-	-	-	-	-	-	0.091	-	-	0.12	0.052	-
Hf	-	-	-	-	-	-	-	-	-	-	-	-	-	-	-	-	-	-
Th	-	-	-	-	-	-	-	-	-	-	-	-	-	-	-	-	-	-
Co	230	440	120	380	570	390	260	320	190	170	310	360	150	550	290	310	210	480
Ni	4440	11990	2270	7430	13690	10360	6260	6180	5680	3800	8660	9020	3840	11770	6180	6830	4640	10640
Zn	-	120	-	-	-	-	-	-	-	-	94	-	62	-	-	160	-	83
Ga	6.2	6.4	4.7	1.5	8.8	4.0	2.0	2.9	2.7	-	3.7	2.0	1.3	6.7	2.4	6.7	1.5	7.5
As	2.9	1.3	1.3	0.70	2.5	2.0	0.87	1.4	0.90	0.73	1.4	1.0	0.86	2.2	2.2	1.8	1.1	2.3
Se	-	19	11	-	-	-	-	-	-	-	15	-	-	-	-	-	-	8.3
Br	-	2.2	-	-	4.2	2.6	-	-	-	-	1.3	-	-	-	0.8	2.2	-	2.7
Ru	-	-	-	-	-	-	-	-	-	-	2.0	-	-	-	-	2.5	-	-
Re	-	-	-	-	-	-	-	-	-	-	-	-	-	-	-	0.12	-	-
Os	-	-	-	-	-	-	-	-	-	-	1.5	-	-	-	-	1.7	1.2	0.6
Ir	0.36	0.64	0.082	1.33	0.32	2.1	0.67	1.31	0.66	1.36	0.84	1.37	1.89	0.44	0.60	2.1	1.48	0.54
Au (ppm)	0.046	0.107	0.026	0.062	0.22	0.047	0.017	0.51	0.031	0.015	0.124	0.023	0.045	0.15	0.030	0.41	0.020	0.117

Appendix Table II. Elemental analyses of Kaba inclusions (continued)

Sample	KI84	KI87	KI89	KI90	KI91	KI93	KI95	KI97	KI98	KC1	KC2	KC3	KC4	Uncertainty (%)
Weight (mg)	0.511	0.372	0.333	0.103	0.248	0.044	0.213	0.294	0.246	0.793	0.125	0.387	7.35	
Ti (%)	-	-	-	-	-	-	-	-	-	-	0.20	0.13	-	10-25
Al	-	-	-	-	-	-	-	-	-	-	3.0	1.50	-	2-5
Fe	12.4	9.4	22.6	15.4	11.9	20.3	18.9	21.7	5.0	4.4	3.5	11.8	13.7	2-5
Mg	-	-	-	-	-	-	-	-	-	-	23.5	23.3	-	2-5
Ca	-	-	-	-	-	-	-	-	-	-	2.3	1.37	-	3-6
Na	0.21	0.180	0.29	0.38	0.056	0.39	0.22	0.49	0.33	0.168	0.52	0.159	0.39	2-5
K (%)	0.021	0.035	0.033	0.051		0.047	0.029	0.051	0.041	0.011	0.077	0.013	0.016	10-15
Sc (ppm)	11.0	11.6	7.9	11.7	9.4	8.2	6.1	8.6	22.7	9.6	20.9	10.7	15.4	2-5
V	-	-	-	-	-	-	-	-	-	-	64	113	-	3-6
Cr	1770	1630	2600	2100	1580	2100	2300	2300	1290	1800	3600	3300	4300	3-6
Mn	1090	1020	1430	1660	550	1730	1350	1760	680	310	1200	820	970	2-5
La	-	-	-	-	-	-	-	-	-	0.46	1.2	0.67	0.68	10-20
Ce	-	-	-	-	-	-	-	-	-	-	-	-	-	20-30
Nd	-	-	-	-	-	-	-	-	-	-	-	-	-	20-30
Sm	0.33	0.27	0.21	0.36	0.27	0.19	0.17	0.26	0.71	0.24	0.72	0.34	0.40	3-6
Eu	0.14	0.12	0.082	0.10	0.11	0.10	0.066	0.083	0.22	0.10	0.31	0.13	0.14	5-10
Tb	-	-	-	-	-	-	-	-	-	-	-	-	-	20-30
Dy	0.42	0.52	0.44	0.65	0.44	0.45	0.51	0.37	1.1	0.44	1.1	0.57	0.76	20-30
Ho	-	-	-	-	-	-	-	-	-	0.10	-	-	-	20-30
Tm	-	-	-	-	-	-	-	-	-	-	-	-	-	20-30
Yb	0.30	0.28	0.24	-	-	-	-	-	0.72	0.28	1.1	0.44	0.53	20-30
Lu	0.039	-	0.037	-	-	-	-	-	-	0.055	-	-	-	20-30
Hf	-	-	-	-	-	-	-	-	-	-	-	-	0.027	20-30
Th	-	-	-	-	-	-	-	-	-	-	-	-	-	20-30
Co	270	200	580	490	510	370	440	500	110	140	53	390	350	2-5
Ni	5820	4490	13420	12950	11800	6660	10480	12530	2230	2980	1260	8910	7850	2-5
Zn	140	-	140	-	-	-	240	-	-	-	-	110	78	10-25
Ga	4.3	4.0	7.1	6.8	1.4	7.3	4.7	7.5	1.5	1.6	2.2	1.8	3.0	5-10
As	1.8	1.7	2.1	2.5	1.0	2.7	2.1	1.8	1.2	0.50		0.72	1.4	10-20
Se	-	-	-	-	-	-	-	-	-	-	-	-	9.7	10-25
Br	-	-	1.4	-	-	-	-	-	-	-	-	1.0	2.3	10-20
Ru	-	-	-	-	-	-	-	-	-	-	-	-	-	15-30
Re	-	-	-	-	-	-	-	-	-	-	-	-	-	15-30
Os	-	1.5	-	-	-	-	-	-	2.4	-	-	0.90	0.65	15-25
Ir	0.82	0.98	0.58	0.95	0.58	0.58	0.60	0.24	2.4	0.11	0.091	0.25	0.91	2-5
Au (ppm)	0.024	0.068	0.20	0.103	0.019	0.20	0.035	0.048	0.26	0.0044	0.011	0.035	0.11	2-5

Appendix Table III. EPMA data of minerals in Kaba Group III inclusions (wt. %)

Mineral	No.	Inclusion	SiO_2	MgO	Al_2O_3	CaO	FeO	TiO_2	Na_2O	K_2O	V_2O_3	Cr_2O_3	MnO	NiO	ZnO	Total
Melilite	1	KI60	25.08	1.62	34.17	39.00	0.00	0.02	0.01	0.01	0.09	0.02	0.00	0.00	0.10	100.03
	2		23.69	0.42	36.78	39.58	0.04	0.08	0.01	0.00	0.03	0.00	0.00	0.07	0.00	100.70
	3		23.78	0.60	35.85	39.13	0.08	0.04	0.03	0.00	0.10	0.02	0.01	0.00	0.00	99.64
	4	KI62	23.19	0.46	37.29	40.75	0.03	0.06	0.00	0.00	0.02	0.04	0.00	0.08	0.00	101.92
	5		23.46	0.79	36.79	39.86	0.03	0.05	0.02	0.02	0.09	0.00	0.00	0.00	0.04	101.06
	6		23.53	1.14	34.01	41.36	0.00	0.01	0.00	0.02	0.03	0.08	0.12	0.00	0.06	100.36
	7	KI73	24.93	1.55	32.68	42.48	0.13	0.00	0.01	0.00	0.05	0.03	0.00	0.00	0.00	101.86
	8		25.05	1.63	31.89	42.09	0.04	0.04	0.03	0.02	0.09	0.00	0.03	0.18	0.05	101.10
	9	KI74	23.80	1.34	33.79	41.88	0.00	0.00	0.02	0.03	0.11	0.00	0.00	0.13	0.00	101.10
	10		22.56	0.75	34.10	41.42	0.07	0.04	0.01	0.00	0.08	0.02	0.07	0.19	0.03	99.30
	11	KI75	23.46	0.96	33.57	42.18	0.04	0.04	0.04	0.00	0.05	0.02	0.00	0.21	0.31	100.89
	12		24.13	1.21	33.57	41.42	0.09	0.05	0.00	0.03	0.08	0.05	0.06	0.00	0.00	100.69
	13	KI86	22.93	0.75	35.22	43.17	0.11	0.06	0.00	0.00	0.06	0.00	0.04	0.00	0.00	102.35
	14		22.75	0.86	34.74	41.95	0.12	0.03	0.00	0.00	0.02	0.00	0.02	0.04	0.08	100.58
	15	KI92	22.41	0.96	33.52	41.78	0.13	0.07	0.02	0.00	0.05	0.07	0.00	0.00	0.11	99.11
	16		24.67	1.63	32.14	41.50	0.25	0.06	0.00	0.01	0.03	0.00	0.00	0.00	0.04	100.33
Spinel Interior	1	KI60	0.10	27.79	72.69	0.08	0.00	0.33	0.00	0.02	0.54	0.10	0.02	0.00	0.06	101.73
	2		0.04	27.92	70.82	0.17	0.05	0.26	0.00	0.02	0.56	0.06	0.04	0.13	0.10	100.17
	3	KI62	0.10	28.20	71.22	0.18	0.01	0.29	0.03	0.00	0.60	0.11	0.01	0.00	0.14	100.89
	4		1.44	26.08	72.39	0.21	0.14	0.80	0.00	0.01	0.55	0.10	0.01	0.00	0.00	101.72
	5	KI73	0.02	28.09	70.79	0.12	0.09	0.32	0.00	0.00	0.61	0.10	0.00	0.08	0.09	100.32
	6		0.02	28.24	71.00	0.19	0.14	0.26	0.00	0.02	0.57	0.13	0.04	0.00	0.06	100.65
	7	KI74	0.04	28.08	71.09	0.20	0.02	0.24	0.01	0.00	0.56	0.06	0.03	0.07	0.00	100.40
	8		0.02	28.06	72.04	0.12	0.00	0.26	0.00	0.00	0.57	0.10	0.00	0.00	0.00	101.17
	9	KI75	0.08	28.88	71.79	0.20	0.09	0.27	0.00	0.00	0.58	0.01	0.02	0.13	0.03	102.07
	10		0.06	28.13	70.01	0.22	0.09	0.25	0.00	0.02	0.55	0.12	0.00	0.12	0.05	99.60
	11	KI86	0.00	28.19	71.57	0.20	0.11	0.25	0.01	0.00	0.56	0.04	0.00	0.08	0.03	101.03
	12		0.08	27.47	70.52	0.27	0.22	0.25	0.00	0.01	0.57	0.07	0.01	0.17	0.11	99.75
	13	KI92	0.00	27.01	71.48	0.09	0.24	0.26	0.01	0.01	0.59	0.15	0.00	0.06	0.00	99.91
	14		0.08	27.66	73.25	0.19	0.27	0.31	0.02	0.01	0.61	0.01	0.02	0.12	0.03	102.56
Edge	15	KI60	0.36	25.32	71.49	0.30	1.05	0.19	0.01	0.02	0.40	0.16	0.04	0.05	0.00	99.39
	16	KI62	0.11	26.29	69.04	0.08	1.16	0.29	0.00	0.00	0.60	0.07	0.02	0.00	0.00	97.64
	17	KI86	1.92	25.42	70.55	2.98	0.97	0.26	0.02	0.00	0.51	0.01	0.02	0.00	0.10	102.76
Anorthite	1	KI86	41.20	3.01	37.32	16.45	0.90	0.02	1.03	0.04	0.06	0.01	0.00	0.04	0.13	100.21

Appendix Table III. EPMA data of minerals in Kaba Group III inclusions (continued)

Mineral	No.	Inclusion	SiO_2	MgO	Al_2O_3	CaO	FeO	TiO_2	Na_2O	K_2O	V_2O_3	Cr_2O_3	MnO	NiO	ZnO	Total
High-Al phase	1	KI60	12.98	18.83	40.95	1.09	3.42	0.12	0.09	0.12	0.46	0.04	0.00	0.02	0.03	78.15
	2	KI62	28.58	15.25	36.16	7.92	5.03	4.32	1.70	0.32	0.46	0.07	0.05	0.00	0.15	100.02
	3		22.82	15.86	44.00	4.77	5.56	2.18	1.18	0.29	0.35	0.03	0.10	0.02	0.00	97.16
	4		21.44	12.66	31.30	4.39	4.74	1.24	1.06	0.33	0.17	0.03	0.04	0.02	0.14	77.58
	5		20.65	12.95	41.32	1.76	6.48	0.09	0.80	0.38	0.09	0.00	0.02	0.00	0.15	84.70
	6		18.72	16.67	48.41	2.90	6.17	1.08	0.50	0.16	0.40	0.05	0.05	0.00	0.25	95.36
	7		25.34	4.85	44.71	4.88	3.91	0.07	1.52	0.37	0.08	0.01	0.09	0.06	0.27	86.15
	8	KI86	17.36	18.12	49.00	2.45	5.48	0.10	0.62	0.13	0.22	0.07	0.00	0.06	0.00	93.59
	9		24.13	16.45	41.50	5.76	2.81	1.34	1.14	0.28	0.26	0.06	0.02	0.25	0.01	94.10
Ti-Al-pyroxene	1	KI60	30.85	10.45	22.21	23.76	1.43	6.85	0.04	0.03	0.46	0.29	0.04	0.00	0.00	96.41
	2		35.84	12.60	18.26	25.64	0.32	5.48	0.02	0.01	0.30	0.38	0.02	0.12	0.00	98.99
	3	KI62	42.17	12.49	9.88	24.39	2.28	3.69	0.09	0.02	0.21	0.11	0.08	0.00	0.14	95.55
	4	KI86	37.48	12.57	16.98	23.88	2.12	8.65	0.08	0.00	0.51	0.39	0.09	0.08	0.04	102.89
	5		46.52	12.59	6.04	23.94	9.12	1.12	0.21	0.00	0.09	0.00	0.16	0.14	0.00	99.93
Hedenbergite	1	KI60	47.22	4.81	0.13	24.34	22.72	0.09	0.07	0.00	0.07	0.00	0.28	0.00	0.12	99.85
	2		44.01	0.81	0.71	24.81	28.03	0.11	0.00	0.00	0.05	0.02	0.58	0.00	0.07	99.20
	3	KI86	47.11	0.66	0.23	22.93	27.73	0.10	0.06	0.00	0.06	0.07	0.31	0.04	0.08	99.37
	4		42.16	9.80	0.67	19.17	25.13	0.07	0.13	0.00	0.07	0.07	0.38	0.12	0.07	97.82
	5		49.91	3.25	0.99	22.35	25.35	0.10	0.04	0.00	0.08	0.00	0.38	0.25	0.12	102.82

Appendix Table IV. EPMA data of minerals in KI53 (wt. %)

Mineral	No.	SiO_2	MgO	Al_2O_3	CaO	FeO	TiO_2	Na_2O	K_2O	V_2O_3	Cr_2O_3	MnO	NiO	ZnO	Total
Melilite and its alteration product	1	23.12	1.32	32.78	42.18	0.50	0.07	0.06	0.01	0.09	0.02	0.11	0.02	0.00	100.27
	2	27.26	14.46	36.51	21.19	0.31	0.79	0.04	0.00	0.11	0.12	0.03	0.00	0.00	100.92
	3	20.95	17.89	43.84	14.51	0.31	2.43	0.02	0.01	0.28	0.15	0.02	0.06	0.07	100.54
spinel	1	1.33	25.17	71.21	0.59	1.44	0.16	0.03	0.00	0.34	0.19	0.00	0.00	0.00	100.44
	2	0.21	27.86	72.33	0.18	1.16	0.12	0.01	0.00	0.36	0.17	0.08	0.14	0.05	102.66
	3	1.02	26.25	71.50	0.56	2.24	0.36	0.01	0.00	0.37	0.03	0.01	0.00	0.00	102.34
High-Al phase	1	25.81	9.87	18.65	2.60	4.64	0.05	1.00	0.67	0.03	0.00	0.06	0.01	0.08	63.46
	2	28.86	11.60	26.02	1.50	3.49	0.02	1.17	0.76	0.07	0.02	0.00	0.05	0.00	73.56
	3	25.07	16.61	38.32	3.98	5.35	0.48	2.77	0.33	0.14	0.04	0.00	0.00	0.00	93.07
	4	26.24	8.31	38.16	18.63	2.67	0.04	0.77	0.63	0.03	0.01	0.01	0.02	0.14	95.64
	5	24.76	13.35	32.29	5.09	5.16	1.52	0.26	0.34	0.23	0.07	0.06	0.17	0.07	83.36
	6	31.51	12.76	30.53	2.10	5.27	0.08	0.61	0.81	0.07	0.04	0.04	0.05	0.00	83.84
Ti-Al-pyroxene and Al-diopside	1	40.13	15.08	16.06	21.40	0.90	5.15	0.14	0.06	0.35	0.04	0.01	0.20	0.07	99.59
	2	43.62	16.96	13.55	20.44	1.67	0.58	0.21	0.08	0.08	0.09	0.02	0.16	0.03	97.46
	3	46.16	15.49	12.31	21.52	0.47	3.05	0.01	0.02	0.22	0.08	0.06	0.01	0.07	99.47
	4	47.07	16.86	11.18	22.18	0.72	1.73	0.08	0.06	0.25	0.00	0.00	0.05	0.15	100.33
	5	51.25	18.24	8.92	19.72	0.79	0.32	0.34	0.17	0.06	0.06	0.00	0.17	0.09	100.13
	6	52.01	17.57	6.61	22.26	0.62	0.93	0.10	0.06	0.17	0.03	0.00	0.04	0.00	100.40
Hedenbergite	1	50.67	1.84	0.29	24.95	23.03	0.02	0.04	0.00	0.07	0.00	0.55	0.08	0.12	101.64
	2	47.83	1.96	0.67	22.65	26.88	0.05	0.11	0.00	0.06	0.00	0.67	0.06	0.18	101.12
	3	45.01	3.14	1.08	22.47	26.43	0.00	0.15	0.00	0.05	0.05	0.77	0.02	0.00	99.17

Appendix Table V. EPMA data of minerals in inclusions KI77 and KI78 (wt. %)

Mineral	No.	Inclusion	SiO_2	MgO	Al_2O_3	CaO	FeO	TiO_2	Na_2O	K_2O	V_2O_3	Cr_2O_3	MnO	NiO	ZnO	Total
Anorthite	1	KI77	45.52	0.65	33.86	20.30	0.07	0.04	0.52	0.01	0.05	0.05	0.04	0.15	0.13	101.38
	2		45.07	0.48	34.33	20.49	0.08	0.05	0.47	0.01	0.06	0.00	0.02	0.14	0.00	101.19
	3		45.47	0.66	34.47	19.24	0.05	0.08	0.45	0.03	0.03	0.06	0.00	0.00	0.00	100.54
	4		50.25	0.91	30.75	16.14	0.06	0.09	1.51	0.01	0.05	0.03	0.07	0.00	0.02	99.89
	5		46.59	0.67	33.33	18.43	0.08	0.04	0.84	0.03	0.04	0.00	0.01	0.18	0.13	100.37
	6	KI88	45.64	0.54	35.33	19.96	0.00	0.05	0.36	0.01	0.05	0.04	0.06	0.00	0.00	102.05
	7		45.31	1.17	34.89	19.93	0.09	0.07	0.37	0.00	0.03	0.04	0.00	0.01	0.00	101.89
	8		46.49	0.72	33.79	18.29	0.08	0.05	0.91	0.00	0.06	0.01	0.00	0.00	0.13	100.53
	9		47.29	2.06	29.94	18.17	0.51	0.50	0.60	0.04	0.03	0.17	0.07	0.00	0.02	99.42
	10		44.49	0.49	34.94	19.54	0.10	0.01	0.39	0.00	0.08	0.00	0.00	0.12	0.00	100.16
Enstatite	1	KI77	57.33	38.13	2.57	1.70	0.56	0.37	0.01	0.03	0.15	0.89	0.18	0.17	0.10	102.19
	2		56.34	35.94	1.92	2.36	0.64	0.38	0.01	0.00	0.14	0.86	0.20	0.00	0.00	98.79
	3		59.54	36.66	1.16	2.75	0.76	0.36	0.00	0.00	0.14	1.04	0.30	0.00	0.07	102.77
	4	KI88	56.57	36.14	3.23	1.51	0.51	0.35	0.00	0.00	0.16	0.62	0.16	0.01	0.11	99.37
	5		58.48	36.99	2.24	1.85	0.54	0.40	0.01	0.00	0.12	0.85	0.16	0.17	0.01	101.81
	6		59.02	37.35	1.57	1.62	0.54	0.24	0.00	0.00	0.13	0.63	0.20	0.01	0.08	101.40
Diopside	1	KI77	54.81	21.73	2.16	20.81	0.40	1.00	0.00	0.02	0.17	0.78	0.22	0.07	0.00	102.18
	2		51.72	18.52	4.13	20.86	0.54	2.19	0.04	0.00	0.14	1.25	0.29	0.03	0.00	99.71
	3		52.65	21.67	3.87	15.34	1.42	1.71	0.05	0.00	0.10	2.15	0.69	0.00	0.01	99.66
	4		54.19	20.64	2.66	21.13	0.48	1.42	0.03	0.00	0.22	0.71	0.24	0.06	0.06	101.85
	5	KI88	53.72	19.52	3.28	21.53	0.55	2.08	0.02	0.02	0.16	1.09	0.29	0.00	0.06	102.32
	6		55.32	22.14	1.27	18.46	0.67	0.81	0.01	0.00	0.11	0.75	0.26	0.18	0.06	100.04
Si-rich phase	1	KI77	74.81	0.33	15.23	8.01	0.34	0.30	0.60	0.02	0.03	0.05	0.00	0.13	0.11	99.97
	2		71.86	0.77	17.48	9.86	1.01	0.37	0.46	0.00	0.02	0.07	0.08	0.00	0.00	101.99

Appendix Table VI. EPMA data of minerals in KI4 (wt. %)

Mineral	No.	SiO_2	MgO	Al_2O_3	CaO	FeO	TiO_2	Na_2O	K_2O	V_2O_3	Cr_2O_3	MnO	NiO	ZnO	Total
Enstatite	1	60.61	36.70	1.22	0.55	0.55	0.22	0.00	0.00	0.04	0.43	0.03	0.00	0.00	100.35
	2	53.97	34.16	6.04	0.63	1.88	2.14	0.00	0.01	0.12	2.75	1.27	0.00	0.00	102.97
	3	51.73	31.28	7.58	0.69	1.98	1.97	0.01	0.00	0.12	2.90	1.07	0.05	0.04	99.42
Anorthite	1	50.86	0.43	31.79	16.71	0.32	0.07	1.64	0.08	0.06	0.04	0.07	0.00	0.00	102.07
	2	50.74	0.64	31.86	14.95	0.25	0.03	1.30	0.07	0.01	0.02	0.07	0.07	0.08	100.09
	3	50.88	0.45	33.43	15.97	0.29	0.06	1.32	0.05	0.06	0.05	0.10	0.05	0.00	102.70
Diopside	1	48.82	13.84	4.70	25.94	6.35	0.45	0.05	0.00	0.10	0.03	0.23	0.14	0.05	100.07
	2	48.63	11.10	4.34	25.47	10.71	0.44	0.08	0.00	0.05	0.03	0.47	0.02	0.12	101.45
	3	50.13	13.45	4.77	25.68	6.47	0.41	0.15	0.00	0.08	0.00	0.19	0.23	0.00	101.55
High-Al phase	1	37.09	11.83	23.46	5.57	3.39	0.07	0.64	0.51	0.04	0.01	0.03	0.20	0.01	83.03
	2	30.65	17.14	33.59	3.82	5.31	0.06	2.72	0.36	0.03	0.04	0.14	0.00	0.04	93.91
	3	36.82	15.73	16.45	0.70	7.38	0.28	0.25	0.77	0.06	0.03	0.01	0.11	0.13	78.69
Olivine	1	31.03	4.92	1.56	0.43	60.66	0.87	0.11	0.00	0.09	0.24	0.69	0.06	0.01	100.63

Appendix Table VII. EPMA data of minerals in KI94 (wt. %)

Mineral	No.	SiO_2	MgO	Al_2O_3	CaO	FeO	TiO_2	Na_2O	K_2O	V_2O_3	Cr_2O_3	MnO	NiO	ZnO	Total
Melilite															
in spherule	1	23.56	1.70	31.46	42.75	0.02	0.02	0.03	0.02	0.08	0.00	0.00	0.03	0.00	99.69
	2	25.69	2.61	30.00	43.47	0.05	0.04	0.01	0.01	0.11	0.03	0.02	0.03	0.00	102.06
	3	26.18	3.57	28.16	43.85	0.06	0.05	0.02	0.02	0.04	0.00	0.03	0.05	0.05	102.08
	4	24.24	1.69	33.20	42.84	0.03	0.04	0.00	0.00	0.05	0.00	0.00	0.14	0.00	102.23
	5	23.87	1.76	32.92	41.88	0.00	0.08	0.01	0.00	0.00	0.00	0.00	0.07	0.18	100.77
	6	22.77	1.36	33.84	41.55	0.00	0.15	0.00	0.00	0.04	0.00	0.00	0.24	0.07	100.02
	7	23.37	1.19	34.41	41.55	0.00	0.10	0.00	0.00	0.10	0.09	0.00	0.15	0.00	100.96
Outside	8	22.70	1.21	33.34	43.37	0.06	0.09	0.01	0.00	0.01	0.05	0.01	0.01	0.10	100.95
spherule	9	24.73	2.29	31.16	42.99	0.23	0.03	0.06	0.00	0.10	0.00	0.07	0.15	0.14	101.95
	10	23.49	1.48	32.82	41.92	0.00	0.05	0.05	0.00	0.04	0.03	0.00	0.08	0.12	100.08
	11	24.27	1.84	32.88	41.00	0.02	0.04	0.01	0.00	0.03	0.00	0.04	0.09	0.11	100.33
	12	24.78	2.18	33.04	42.33	0.06	0.02	0.00	0.00	0.01	0.05	0.03	0.17	0.08	102.73
Spinel															
Interior	1	0.05	28.98	71.54	0.23	0.04	0.16	0.03	0.01	0.59	0.10	0.00	0.10	0.01	101.92
	2	0.05	28.23	70.63	0.23	0.01	0.19	0.01	0.00	0.57	0.08	0.00	0.00	0.07	100.07
	3	0.04	28.28	69.70	0.26	0.05	0.22	0.03	0.01	0.49	0.12	0.00	0.00	0.13	99.33
	4	0.06	28.45	72.33	0.27	0.06	0.24	0.00	0.01	0.48	0.11	0.00	0.15	0.00	102.16
	5	0.05	28.06	71.86	0.21	0.03	0.28	0.01	0.00	0.55	0.07	0.06	0.00	0.08	101.26
	6	0.10	27.53	71.40	0.22	0.09	0.29	0.00	0.00	0.43	0.10	0.00	0.06	0.00	100.22
	7	0.07	28.70	70.34	0.18	0.08	0.08	0.01	0.00	0.48	0.16	0.04	0.11	0.00	100.25
	8	0.08	28.77	71.72	0.24	0.00	0.24	0.00	0.00	0.30	0.16	0.01	0.00	0.01	101.50
along	9	1.45	26.81	67.24	2.67	0.56	0.10	0.02	0.00	0.44	0.13	0.00	0.00	0.00	99.42
rim	10	0.15	29.07	68.00	0.14	1.32	0.11	0.01	0.00	0.37	0.21	0.03	0.00	0.02	99.43
	11	1.31	27.39	67.53	0.93	1.40	0.35	0.01	0.00	0.52	0.18	0.02	0.08	0.00	99.72
	12	0.09	27.23	70.33	0.14	0.78	0.07	0.00	0.00	0.43	0.31	0.01	0.00	0.06	99.45
	13	0.39	27.07	70.63	0.31	0.96	0.06	0.02	0.00	0.41	0.22	0.00	0.02	0.00	100.09

Appendix Table VII. EPMA data of minerals in KI94 (continued)

Mineral	No.	SiO_2	MgO	Al_2O_3	CaO	FeO	TiO_2	Na_2O	K_2O	V_2O_3	Cr_2O_3	MnO	NiO	ZnO	Total
High-Al phase	1	20.26	16.75	25.72	2.10	6.60	0.12	2.56	0.43	0.09	0.06	0.04	0.25	0.21	75.19
	2	24.06	15.54	22.43	4.81	4.33	0.44	2.09	0.32	0.10	0.04	0.03	0.00	0.20	74.38
	3	23.14	14.77	26.57	1.81	5.51	0.03	2.13	0.55	0.09	0.00	0.06	0.12	0.14	74.90
	4	21.71	14.48	21.51	2.26	7.48	0.09	2.28	0.34	0.01	0.00	0.03	0.06	0.00	70.25
	5	26.12	9.48	24.32	2.58	4.14	0.00	0.96	0.67	0.04	0.01	0.02	0.19	0.00	68.51
	6	24.69	13.61	28.97	1.66	4.56	0.06	0.69	0.41	0.06	0.00	0.05	0.02	0.14	74.52
	7	19.15	13.70	27.09	4.50	5.66	0.26	1.40	0.50	0.11	0.00	0.00	0.19	0.22	72.78
	8	22.16	14.49	24.33	2.26	5.31	0.41	1.02	0.49	0.09	0.02	0.07	0.07	0.08	70.80
Ti-Al-pyroxene and diopside	1	40.92	10.78	13.51	24.72	2.95	3.46	0.07	0.00	0.46	0.05	0.03	0.01	0.00	96.95
	2	38.18	11.68	18.35	24.42	1.07	6.90	0.04	0.01	0.47	0.03	0.00	0.18	0.00	101.33
	3	42.98	12.78	13.21	24.91	0.79	0.61	0.18	0.07	0.13	0.10	0.00	0.00	0.08	95.85
	4	48.97	16.85	2.20	20.53	11.47	0.13	0.19	0.00	0.08	0.07	0.14	0.00	0.19	100.82
	5	47.17	14.42	6.31	26.54	0.37	0.19	0.01	0.01	0.09	0.00	0.00	0.15	0.06	95.32
	6	50.04	19.31	3.28	23.97	1.53	0.31	0.02	0.01	0.11	0.04	0.00	0.07	0.00	98.69

Appendix Table VIII. EPMA data of minerals in KI6 and KI72 (wt. %)

Mineral	No.	Inclusion	SiO_2	MgO	Al_2O_3	CaO	FeO	TiO_2	Na_2O	K_2O	V_2O_3	Cr_2O_3	MnO	NiO	ZnO	Total
Olivine	1	KI6	43.19	56.17	0.04	0.12	2.04	0.07	0.00	0.00	0.09	0.18	0.05	0.13	0.03	102.10
	2		42.97	56.01	0.06	0.07	0.31	0.04	0.00	0.00	0.07	0.14	0.08	0.05	0.19	99.99
	3		43.18	56.99	0.02	0.10	0.79	0.00	0.00	0.00	0.03	0.10	0.06	0.00	0.00	101.27
	4	KI72	41.04	57.50	0.03	0.10	0.48	0.05	0.02	0.00	0.05	0.22	0.11	0.07	0.07	99.72
	5		41.65	58.45	0.02	0.08	0.78	0.04	0.01	0.00	0.04	0.16	0.10	0.22	0.01	101.56
	6		41.64	56.56	0.00	0.14	1.04	0.03	0.00	0.00	0.06	0.00	0.05	0.05	0.20	99.76
	7		41.38	55.76	0.16	0.37	2.61	0.05	0.00	0.00	0.05	0.00	0.04	0.00	0.01	100.42
Ti-Al-pyroxene and diopside	1	KI6	51.82	17.05	7.53	24.01	0.60	0.82	0.04	0.01	0.07	0.05	0.00	0.00	0.01	101.99
	2		52.28	19.36	3.78	25.00	0.26	0.14	0.00	0.00	0.07	0.04	0.03	0.13	0.07	101.16
	3	KI72	47.45	15.65	7.09	26.54	0.28	2.42	0.03	0.01	0.16	0.07	0.00	0.01	0.12	99.81
	4		43.38	5.77	26.03	23.24	0.31	1.03	0.04	0.00	0.09	0.07	0.00	0.00	0.00	99.96
	5		53.10	19.21	1.60	26.75	0.40	0.26	0.01	0.01	0.07	0.03	0.00	0.01	0.00	101.44
Anorthite	1	KI6	44.44	4.60	31.41	20.13	0.47	0.12	0.04	0.00	0.04	0.06	0.00	0.10	0.01	101.41
	2	KI72	40.72	0.42	36.35	21.02	0.25	0.02	0.04	0.02	0.06	0.00	0.03	0.19	0.00	99.13
	3		40.70	1.59	37.11	19.78	0.26	0.07	0.05	0.02	0.05	0.11	0.02	0.01	0.02	99.79
Spinel	1	KI72	0.09	27.55	70.11	0.07	1.99	0.29	0.02	0.00	0.14	0.41	0.03	0.00	0.23	100.93
	2		0.05	28.12	70.72	0.08	0.63	0.47	0.01	0.00	0.17	0.31	0.00	0.00	0.00	100.55